LECTURE NOTES MPRI 2.38.1
GEOMETRIC GRAPHS, TRIANGULATIONS AND POLYTOPES

VINCENT PILAUD

These lecture notes on "Geometric Graphs, Triangulations and Polytopes" cover (more than) the material presented for my part of the MPRI Master Course 2.38.1 entitled "Algorithmique et combinatoire des graphes géométriques". The course contains two other parts, one on "Planar graphs and their embeddings" taught by Luca Castelli Aleardi, and another one on "Graphs on surfaces" taught by Arnaud de Mesmay. Announcements and further informations on the course are available online:

https://wikimpri.dptinfo.ens-cachan.fr/doku.php?id=cours:c-2-38-1

Comments and questions are welcome by email: vincent.pilaud@lix.polytechnique.fr.

These lecture notes focus on combinatorial and structural properties of geometric graphs and triangulations. The aim is to give both an overview on classical theories, results and methods, and an entry to recent research on these topics. The course decomposes into the following 6 interconnected chapters:

(i) Chapter 1 introduces planar, topological and geometric graphs. It first reviews combinatorial properties of planar graphs, essentially applications of Euler's formula. It then presents considerations on topological and rectilinear crossing numbers.

(ii) Chapter 2 presents the structure of Schnyder woods on 3-connected planar graphs and their applications to graph embedding, orthogonal surfaces and geometric spanners.

(iii) Chapter 3 introduces the theory of polytopes needed later in the notes. It tackles in particular the equivalence between $\mathcal{V}$- and $\mathcal{H}$-descriptions, faces and f- and h-vectors, the Upper and Lower Bound Theorems for polytopes, and properties of graphs of polytopes.

(iv) Chapter 4 is devoted to triangulations of planar point sets. It first discusses upper and lower bounds on the number of triangulations of a point set, and then introduces regular triangulations (with a particular highlight on the Delaunay triangulation) and their polytopal structure.

(v) Chapter 5 focuses on triangulations of a convex polygon and the associahedron. The goal is to present Loday's construction and its connection to the permutahedron.

(vi) Chapter 6 explores combinatorial and geometric properties of further flip graphs with a more combinatorial flavor. It first presents the interpretation of triangulations, pseudotriangulations and multitriangulations in terms of pseudoline arrangements on a sorting network. Finally, it constructs brick polytopes and discusses their combinatorial structure.

Most of the material presented here is largely inspired from classical textbook presentations. We recommend in particular the book of Felsner [Fel04] on geometric graphs and arrangements (in particular for Sections 1 and 2), the book of De Loera, Rambau and Santos [DRS10] on triangulations (Section 4 and its extension to higher dimension), and the book of Ziegler [Zie95] for an introduction to polytope theory (Section 3). The last two chapters present more recent research from [Lod04, PP12, PS12]. Original papers are not always carefully referenced along the text, but precise references can be found in the textbooks and articles mentioned above.

Contents

1. Introduction to planar, topological, and geometric graphs

This section gives a short introduction to planar, topological, and geometric graphs. It focusses on combinatorial properties of planar graphs (essentially from Euler's relation), and topological and geometric graph drawings and embeddings (in particular considerations on the topological and rectilinear crossing number). This material is classical, see *e.g.* [Fel04, Chap. 1, 3, 4].

1.1. **Graph drawings and embeddings.** A *graph* G is given by a set $V = V(G)$ of vertices and a set $E = E(G)$ of edges connecting two vertices. We use the following definition for graph drawings and embeddings.

Definition 1. A *drawing* of a graph $G = (V, E)$ in the plane is given by an injective map $\phi_V : V \to \mathbb{R}^2$ and a continuous map $\phi_e : [0, 1] \to \mathbb{R}^2$ for each $e \in R$ such that

(i) $\phi_e(0) = u$ and $\phi_e(1) = v$ for any edge $e = (u, v)$,
(ii) $\phi_e(]0, 1[) \cap \phi_V(V) = \varnothing$ for any $e \in E$,

The drawing is a *topological drawing* if

- no edge has a self-intersection,
- two edges with a common endpoint do not cross,
- two edges cross at most once.

Finally, the drawing is an *embedding* if $\phi_e(x) \neq \phi_{e'}(x')$ for any $e, e' \in E$ and $x, x' \in]0, 1[$ such that $(e, x) \neq (e', x')$.

Exercice 2. Show that a drawing of a graph in the plane can be modified to get a topological drawing with at most as many crossings.

1.2. **Planar graphs and Euler's formula.** A graph is *planar* if it admits an embedding in the plane. The connected components of the complement of this embedding are called *faces* of the graph. Planar graphs will be a central subject in these lecture notes.

Proposition 3 (Euler's formula)**.** *If a connected planar graph has n vertices, m edges and p faces, then $n - m + p = 2$.*

Proof. The formula is valid for a tree (n vertices, $n-1$ edges and 1 face). If the graph is not a tree, we delete an edge from a cycle. This edge is incident to two distinct faces (Jordan's Theorem), so that the flip preserves the value of $n - m + p$. We conclude by induction on $m - n$. □

Corollary 4. *A simple planar graph with $n \geq 3$ vertices has at most $3n - 6$ edges. A simple planar graph with $n \geq 3$ vertices and no triangular face has at most $2n - 4$ edges. In general, a planar graph with $n \geq 3$ vertices and no face of degree smaller or equal to k has at most $\frac{k+1}{k-1}(n-2)$ edges.*

Proof. Assume that all faces have degree strictly greater than k. By double counting of the edge-face incidences, and using Euler's relation, we get

$$2m \geq (k + 1)p = (k + 1)m - (k + 1)(n - 2),$$

which yields

$$m \leq \frac{(k + 1)(n - 2)}{k - 1}.$$

□

Corollary 5. *The complete graph K_5 and the complete bipartite graph $K_{3,3}$ (see Figure 1) are not planar.*

Proof. Both would contradict the previous statement: the complete graph K_5 has 5 vertices and 10 edges, and the complete bipartite graph $K_{3,3}$ has 6 vertices, 9 edges, but no triangle. □

Exercice 6. Show that the Petersen graph is not planar (see Figure 1).

A *subdivision* of a graph G is any other graph obtained by replacing some edges of G by paths of edges. This operation clearly preserves planarity and non-planarity. Therefore, Corollary 5 tells that all subdivisions of K_5 and $K_{3,3}$ are non-planar. In fact, this turns out to be a characterization of planar graphs, known as Kuratowski's theorem.

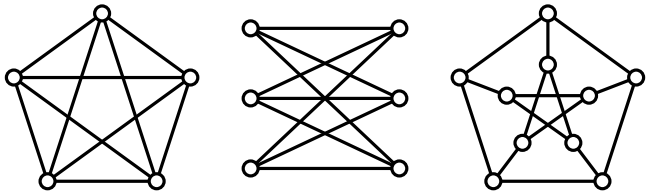

FIGURE 1. The complete graph K_5 (left), the complete bipartite graph $K_{3,3}$ (middle), and the Petersen graph (right) are not planar.

Theorem 7 (Kuratowski [Kur30]). *A graph is planar if and only if it contains no subdivision of K_5 and $K_{3,3}$.*

This characterization is not algorithmic: testing naively whether a graph G contains a subdivision of K_5 or $K_{3,3}$ is exponential in the number of vertices of G. However, it turns out that there exist efficient algorithms for planarity testing: planarity can be tested in linear time.

Exercice 8 (Colorability of planar graphs). (1) Prove that all planar graphs are 6-colorable. (Hint: delete a vertex of degree at most 5 and apply induction).

(2) Prove that all planar graphs are 5-colorable. (Hint: immediate by induction if there is a vertex of degree strictly less than 5. Otherwise, consider a vertex u of degree 5 with neighbors $v_1, \dots, v_5$ cyclically around u. Construct by induction a 5-coloring of the graph where v is deleted. If all 5 colors appear on $v_1, \dots, v_5$, consider the subgraph induced by the vertices colored as v_1 or v_3. If this subgraph is disconnected, exchange the two colors in the connected component of v_1 and conclude. Otherwise, observe that the subgraph induced by the vertices colored as v_2 or v_4 is disconnected and conclude).

In fact, the *four color theorem* ensures that all planar graphs are 4-colorable (see *e.g.* [RSST97]).

Exercice 9 (Sylvester-Gallai theorem). For any set of $n \geq 3$ points in the plane, not all on one line, there is always a line that contains exactly two points. (Hint: By duality, the statement is equivalent to showing that for any set of $n \geq 3$ lines in the plane, not all through one point, there is always a point contained in exactly two of them. This is clear since a planar graph has at least one vertex of degree at most 5).

Exercice 10 (Monochromatic line in a bicolored point set). Show that in a planar graph whose edges have been colored black and white, there is always a vertex with at most two color changes in the cyclic order around it. (Hint: show that the number c of bicolored corners is bounded by $c \leq 2f_3 + 4f_4 + 4f_5 + 6f_6 + 6f_7 + \dots \leq 4m - 4p = 4n - 8$). Derive from this result that for any configuration of black and white points, there is always a monochromatic line.

1.3. **Topological graphs and the crossing lemma.** The *crossing number* of a graph G is the minimal number $\mathrm{cr}(G)$ of crossings in a drawing of G. We start with an upper bound on the crossing number of the complete graph K_n.

Exercice 11 (On the crossing number of the complete graph). The goal of this exercice is to obtain a non-trivial upper bound on the crossing number $\mathrm{cr}(K_n)$ of the complete graph K_n.

(1) Consider n points in convex position and connect any two of them by the straight segment between them. How many crossings appear?

(2) Assume that $n = 2\nu$ is even and consider a prism over a ν-gon. Label the vertices of the two bases of this prism by $a_1, \dots, a_\nu$ and $b_1, \dots, b_\nu$ respectively. Draw the complete graph K_n on this prism as follows:
   - any two vertices of the same base are connected by the straight segment in this base,
   - for any $i, j \in [\nu]$, vertex a_i is connected to vertex b_j by the clockwise geodesic on the surface of the prism not crossing the edge $[a_i, b_i]$. Denote by E_i the set of edges from a_i to the vertices $\{b_1, \dots, b_\nu\}$.

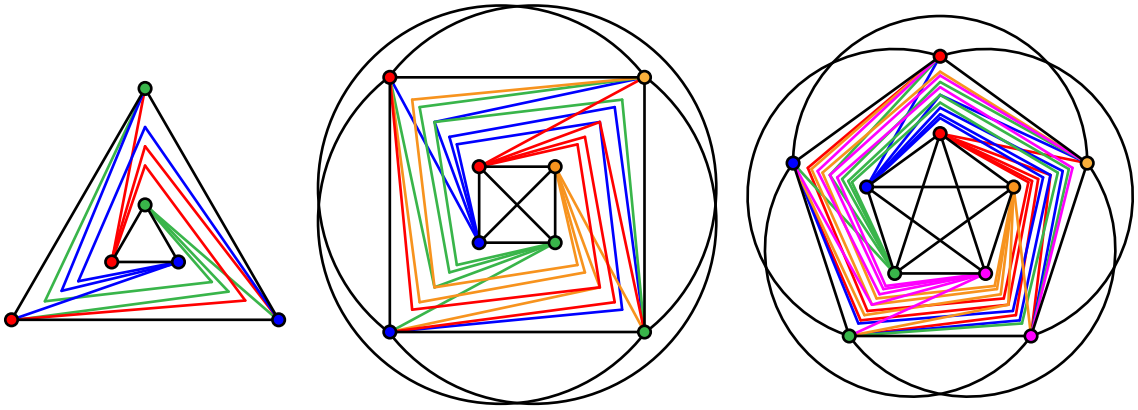

FIGURE 2. Drawings of the complete graphs K_6 (left), K_8 (middle), and K_{10} (right).

This drawing is illustrated on Figure 2 for K_6, K_8 and K_{10}, where the prism has been projected to the plane. For each $i \in [\nu]$, we have colored the vertices a_i, b_i and the edge set E_i with the same color.

(i) Show that for any $i \neq j$, the edge sets E_i and E_j have

$$\frac{(|i-j|-1)|i-j|}{2} + \frac{(\nu-|i-j|-1)(\nu-|i-j|)}{2}$$

crossings.

(ii) Deduce that E_i has $\nu(\nu-1)(\nu-2)/3$ crossings for any $i \in [\nu]$.

(iii) Deduce that the total number of crossings of this drawing of K_n is

$$\frac{\nu(\nu-1)^2(\nu-2)}{4} \simeq \frac{n^4}{64} \simeq \frac{3}{8}\binom{n}{4}.$$

(3) Using a similar construction, show that the crossing number of the complete graph on $n = 2\nu+1$ vertices is at most

$$\frac{\nu^2(\nu-1)^2}{4} \simeq \frac{\nu^4}{64} \simeq \frac{3}{8}\binom{n}{4}.$$

(4) Conclude that

$$\mathrm{cr}(K_n) \leq \frac{1}{4}\left\lfloor \frac{n}{2} \right\rfloor \left\lfloor \frac{n-1}{2} \right\rfloor \left\lfloor \frac{n-2}{2} \right\rfloor \left\lfloor \frac{n-3}{2} \right\rfloor.$$

This bound was conjectured to be tight for all values of n by Guy [Guy60].

We now consider a simple graph G with n vertices and m edges, and give lower bounds on the crossing number $\mathrm{cr}(G)$ in terms of n and m, as well as applications to incidence problems in geometry.

Proposition 12. $\mathrm{cr}(G) \geq m - 3n + 6$.

Proof. Let H be a maximal planar subgraph of G. All edges in $G \setminus H$ create at least one crossing. Conclude by Euler relation on H. □

Exercice 13. Prove that $\mathrm{cr}(G) \geq r\sum_{i=1}^{\lfloor m/r \rfloor} i$, where $r \leq 3n-6$ denotes the number of edges in a maximal planar subgraph of G. (Hint: delete successive maximal planar subgraphs of G). Derive a lower bound on the crossing number $\mathrm{cr}(G)$ of order $m^2/6n$.

The following theorem gives the right order of magnitude for the crossing number $\mathrm{cr}(G)$, as conjectured by Erdős and Guy [EG73].

Theorem 14 (Crossing lemma)**.** *If G as n vertices and $m \geq 4n$ edges, then* $\mathrm{cr}(G) \geq m^3/64\,n^2$.

Proof. Consider an optimal drawing of G, and let H be the random induced subgraph of G obtained by picking independently each vertex of G with probability p. The expected number of vertices, edges, and crossings of H are respectively

$$\mathbb{E}(n(H)) = p \cdot n(G), \qquad \mathbb{E}(m(H)) = p^2 \cdot m(G), \qquad \text{and} \qquad \mathbb{E}(\mathrm{cr}(H)) = p^4 \cdot \mathrm{cr}(G).$$

We conclude using the trivial bound of Proposition 12 on the graph H and setting the probability $p = 4n/m$ (thus needing the assumption $m \geq 4n$). □

Remark 15. The previous bound is tight up to a constant. Indeed, for any $n \in \mathbb{N}$, the complete graph K_n has by Exercice 11

$$n(K_n) = n, \qquad m(K_n) = \binom{n}{2}, \qquad \text{and} \qquad \mathrm{cr}(K_n) \leq \frac{3}{8}\binom{n}{4} \simeq \frac{m^3}{8\,n^2}$$

However, the constant $1/64$ of Theorem 14 can be slightly improved as discussed in the next proposition and exercice.

Proposition 16. *If G as n vertices and $m \geq 21\,n/4$ edges, then*

$$\mathrm{cr}(G) \geq 32\,m^3/1323\,n^2 \simeq m^3/41.34\,n^2.$$

Proof. Call a graph *k-restricted* if it admits a drawing where each edge has at most k crossings. *E.g.* a planar graph is 0-restricted. We claim that a k-restricted graph has at most $(k+3)(n-2)$ edges for $k \in \{0, 1\}$. We show this claim at the end of this proof. Consider for now an arbitrary graph G, and let $G_2 = G$, let G_1 be a maximal 1-restricted subgraph of G and G_0 a maximal planar subgraph of G_1. By maximality, all edges in $G_i \smallsetminus G_{i-1}$ have at least i crossings. We therefore obtain using our claim that

$$\begin{aligned}
\mathrm{cr}(G) &\geq 2\big(|E(G_2)| - |E(G_1)|\big) + \big(|E(G_1)| - |E(G_0)|\big) \\
&\geq 2m - |E(G_1)| - |E(G_0)| \\
&\geq 2m - 4(n-2) - 3(n-2) \\
&\geq 2m - 7n.
\end{aligned}$$

We then use this inequality instead of the trivial bound of Proposition 12 as in the proof of Theorem 14.

We still have to show our claim. It is clear for $k = 0$ (Corollary 4). For $k = 1$, consider a 1-restricted drawing of a graph G with n vertices maximizing the number of edges in such a graph, and let H be a maximal planar subgraph of G. For any edge $e = (u, v) \in G \smallsetminus H$, there exists an edge $e' = (u', v')$ such that u, u', v' and v, u', v' are triangular faces of H. We say that these triangular faces *witness* e. Since any edge in $G \smallsetminus H$ is witnessed by two triangular faces of H, and any triangular face can witness at most one edge of $G \smallsetminus H$, we obtain that $|G \smallsetminus H| \leq n - 2$ and thus $m(G) \leq 4(n-2)$. □

Exercice 17. In fact, one can prove [PT97] that a k-restricted graph with n vertices has at most $(k+3)(n-2)$ edges for any $k \leq 4$. Deduce from this statement that $\mathrm{cr}(G) \geq m^3/33.75\,n^2$ as soon as $m \geq 7.5\,n$.

We close this section with some applications to incidence problems in geometry. The *incidences* between a point set $\mathbf{P}$ and a line set $\mathbf{L}$ are all pairs $(\mathbf{p}, \mathbf{l})$ with $\mathbf{p} \in \mathbf{P}$, $\mathbf{l} \in \mathbf{L}$ and $\mathbf{p} \in \mathbf{l}$. Incidence problems deal with counting (or estimating the number of) incidences between arbitrary point and line sets of given sizes. Points and lines can also be replaced by other elementary geometric objects, such as circles, squares, etc. Although other (rather complicated) proofs were known for the results below, Szekely [Szé97] noticed that they can be obtained as direct applications of the crossing lemma.

Theorem 18 (Szemerédi and Trotter [ST83, Szé97])**.** *The maximum number*

$$I(p, \ell) := \max_{|\mathbf{P}|=p, |\mathbf{L}|=\ell} |\,\{(\mathbf{p}, \mathbf{l}) \mid \mathbf{p} \in \mathbf{P},\ \mathbf{l} \in \mathbf{L},\ \mathbf{p} \in \mathbf{l}\}\,|$$

of incidences between p points and ℓ lines in the plane is bounded by

$$I(p,\ell) \leq 3.2\, p^{2/3}\ell^{2/3} + 4p + 2\ell.$$

Proof. Consider the graph G whose vertices are given by the points and edges by the segments between two consecutive points. This graph has $n(G) = p$ vertices, $m(G) = I - \ell$ edges, and since any two lines intersect at most once, we get

$$\frac{\ell^2}{2} > \binom{\ell}{2} \geq \mathrm{cr}(G) \geq (I-\ell)^3/64\, p^2,$$

as soon as $I - \ell > 4p$. We therefore obtain that $I < 3.2\, p^{2/3}\ell^{2/3} + \ell$ or $I < 4p + \ell$, and the sum of these two bounds give the announced bound. □

Exercice 19 (Unit distances in a point set)**.** Prove that the maximum number

$$U(p) := \max_{|\mathbf{P}|=p} \left| \left\{ (\mathbf{p},\mathbf{q}) \in \mathbf{P}^2 \;\middle|\; \|p-q\| = 1 \right\} \right|$$

of unit distances between p points in the plane is bounded by

$$U(p) \leq 4\, p^{4/3}.$$

(Hint: Let $\mathbf{P}$ be a maximizing point set. Apply the crossing lemma to the graph with vertices given by the points of $\mathbf{P}$ and edges given by the arcs between two points of $\mathbf{P}$ of the unit circles centered at points of $\mathbf{P}$, after deletion of duplicated edges).

1.4. **Geometric graphs and the rectilinear crossing number.** A *geometric drawing* of a graph is a drawing where vertices are points in the plane and edges are straight segments between these points. We always assume general position, *i.e.* no three points are colinear. The *rectilinear crossing number* of a graph G is the minimal number $\overline{\mathrm{cr}}(G)$ of crossings of a geometric drawing of G. We discuss here the rectilinear crossing number of the complete graph K_n. For small values of n, the rectilinear crossing number is given by

n	4	5	6	7	8	9	10	11	12	13	14	15	16	17	18	19
$\overline{\mathrm{cr}}(K_n)$	0	1	3	9	19	36	62	102	153	229	324	447	603	798	1029	1318

and crossing minimizing rectilinear drawings of K_n for $4 \leq n \leq 9$ are represented on Figure 3.

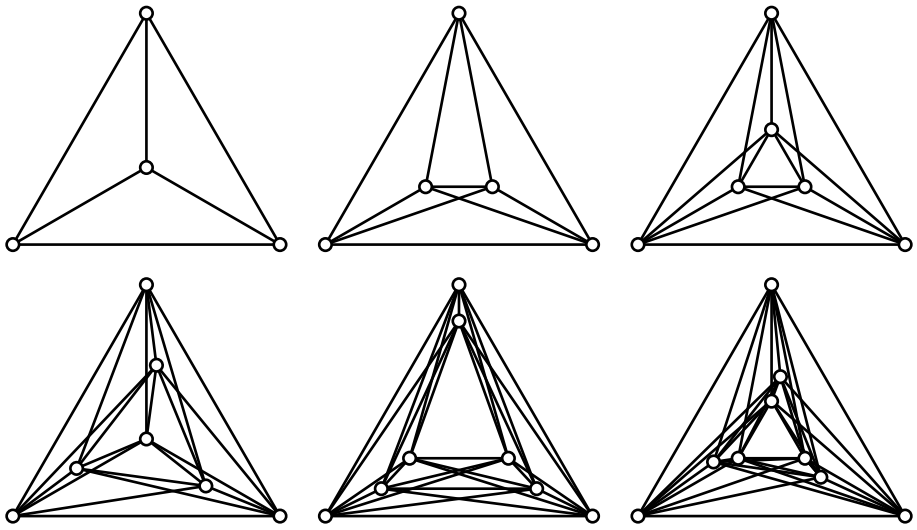

FIGURE 3. Optimal rectilinear drawings of the complete graphs K_n for $4 \leq n \leq 9$.

Under the general position assumption, the convex hull of any four points is either a quadrangle or a triangle. Fix a point set $\mathbf{P}$ and denote by $\square(\mathbf{P})$ (resp. $\triangle(\mathbf{P})$) the number of quadruples of points in $\mathbf{P}$ with 4 (resp. 3) points on the convex hull. Note that the number of crossings in

the geometric drawing of the complete graph determined by $\mathbf{P}$ is precisely $\square(\mathbf{P})$ and that $\binom{n}{4} = \square(\mathbf{P}) + \triangle(\mathbf{P})$.

Exercice 20. Show that any 5 points in general position determine a convex quadrilateral. Derive from this observation that

$$\frac{1}{5}\binom{n}{4} \le \overline{\mathrm{cr}}(K_n) \le \binom{n}{4}.$$

Is the upper bound tight?

Our goal is to improve the trivial lower bound. For this, we connect the rectilinear crossing number of $\mathbf{P}$ to the k-edges of $\mathbf{P}$. A *k-edge* of $\mathbf{P}$ is a directed edge between two points of $\mathbf{P}$ such that exactly k points of $\mathbf{P}$ lie on the left side of the directed line supporting that edge. For example, 0-edges are convex hull edges. We denote by $e_k(\mathbf{P})$ the number of k-edges of $\mathbf{P}$ and $E_k(\mathbf{P})$ the number of $(\le k)$-edges of $\mathbf{P}$.

Proposition 21. *The numbers $\square(\mathbf{P})$ of convex quadrilaterals in $\mathbf{P}$ and $e_k(\mathbf{P})$ of k-edges of $\mathbf{P}$ are connected by*

$$\square(\mathbf{P}) = \sum_{k=0}^{\frac{n}{2}-1} (n/2-k-1)^2\, e_k(\mathbf{P}) - \frac{3}{4}\binom{n}{3}.$$

Proof. We double-count the number Z of (ordered) quadruples $(\mathbf{p},\mathbf{q},\mathbf{r},\mathbf{s})$ of $\mathbf{P}$ such that the points $\mathbf{r}$ and $\mathbf{s}$ lie respectively on the right and left side of the directed line from $\mathbf{p}$ to $\mathbf{q}$. On the one hand, a quadruple in convex position contributes 4 to Z, while a quadruple in non-convex position contributes 6. Therefore,

$$Z = 6\,\triangle(\mathbf{P}) + 4\,\square(\mathbf{P}) = 6\binom{n}{4} - 2\,\square(\mathbf{P}).$$

On the other hand, a k-edge defines $k(n-2-k)$ such quadruples, so that

$$Z = \sum_{k=0}^{n-2} k(n-2-k)\, e_k(\mathbf{P}).$$

Since $\sum_k e_k = n(n-1)$, we therefore obtain

$$\begin{aligned}
\square(\mathbf{P}) + \frac{3}{4}\binom{n}{3} &= \frac{n(n-1)(n-2)^2}{8} - \frac{Z}{2} \\
&= \frac{1}{2}\sum_{k=0}^{n-2}\left(\frac{(n-2)^2}{4} - k(n-2-k)\right) e_k(\mathbf{P}) \\
&= \sum_{k=0}^{\frac{n}{2}-1}\left(\frac{n}{2}-1-k\right) e_k(\mathbf{P}).
\end{aligned}$$

□

Corollary 22. *The numbers $\square(\mathbf{P})$ of convex quadrilaterals in $\mathbf{P}$ and $E_k(\mathbf{P})$ of $(\le k)$-edges of $\mathbf{P}$ are connected by*

$$\square(\mathbf{P}) = \sum_{k=0}^{\frac{n}{2}-1} (n-2k-3)\, E_k(\mathbf{P}) + O(n^3).$$

Proof. Replace $e_k(\mathbf{P})$ by $E_k(\mathbf{P}) - E_{k-1}(\mathbf{P})$ in Proposition 21 and simplify using the equality $(n/2-k-1)^2 - (n/2-k-2)^2 = n-2k-3$. □

Theorem 23. *For any point set $\mathbf{P}$ in general position in the plane, $\square(\mathbf{P}) \ge \frac{1}{4}\binom{n}{4}$.*

Proof. The proof uses the dual pseudoline arrangement $\mathbf{P}^*$ of the point set $\mathbf{P}$, which is described later in Section 6.4. Observe that:

(i) The k-edges in $\mathbf{P}$ correspond to the crossings of $\mathbf{P}^*$ at level $k+1$ or $n-1-k$. Therefore, $E_k(\mathbf{P})$ is the number of crossings in the first and last k levels of $\mathbf{P}^*$.

(ii) For $j \leq k$ or $n-k \leq j$, the jth pseudoline has at least $2(k-j)$ such crossings. However, we might count each such crossing twice this way.

It follows that

$$E_k(\mathbf{P}) \geq 2\sum_{j\leq k}(k-j) = k(k+1).$$

Using Corollary 22, we derive

$$\square(\mathbf{P}) \geq \sum_{k<n/2-1}(n-2k-3)\cdot k(k+1) \geq \frac{n^4}{96} \geq \frac{1}{4}\binom{n}{4}. \qquad \square$$

Remark 24. Using slightly more sophisticated arguments, one can bound the number of crossings counted twice in the previous proof, and derive that the number of $(\leq k)$-edges is bounded by

$$E_k(\mathbf{P}) \geq 3\binom{k+2}{2}.$$

Using Corollary 22, this bound yields the following lower bound on the rectilinear crossing number:

$$\overline{\mathrm{cr}}(K_n) \geq \frac{3}{8}\binom{n}{4}.$$

This bound can even be improved to reach

$$\overline{\mathrm{cr}}(K_n) \geq \left(\frac{3}{8}+\varepsilon\right)\binom{n}{4},$$

which is strictly bigger than the upper bound on the topological crossing number of K_n obtained in Exercice 11. The first value of n for which $\mathrm{cr}(K_n) < \overline{\mathrm{cr}}(K_n)$ is $n=8$ for which

$$18 = \mathrm{cr}(K_8) < \overline{\mathrm{cr}}(K_8) = 19.$$

This approach is due to [LVWW04] and is nicely presented in [Fel04, p. 64–65].

2. Schnyder woods and planar drawings

This section presents a very relevant structure on planar maps: Schnyder woods and their application to graph embedding, orthogonal surfaces, and geometric spanners. This structure was introduced by Schnyder in [Sch89] for planar triangulations in connection to order dimension and graph embedding. It was later extended to arbitrary 3-connected planar maps independently by Felsner [Fel04, Chap. 2], Di Battista, Tamassia and Vismara [DBTV99], and Miller [Mil02]. We follow here the presentation in [Fel04, Chap. 2].

2.1. Schnyder labelings and Schnyder woods.

Let M be a planar map (*i.e.* an embedded connected planar graph) with three distinguished vertices v_1, v_2, v_3 in clockwise order on the outer face, where a half-edge is pending in the outer face. See Figure 5 (left).

Definition 25. A *Schnyder labeling* of M is a labeling of the angles of M with labels $\{1, 2, 3\}$ satisfying the following rules (see Figure 4):

(L1) The two angles at the half-edge of v_i are labeled by $i+1$ and $i-1$ in clockwise order.
(L2) The labels of the angles clockwise around a vertex form non-empty intervals of 1's, 2's and 3's.
(L3) The labels of the angles clockwise around a face form non-empty intervals of 1's, 2's and 3's.

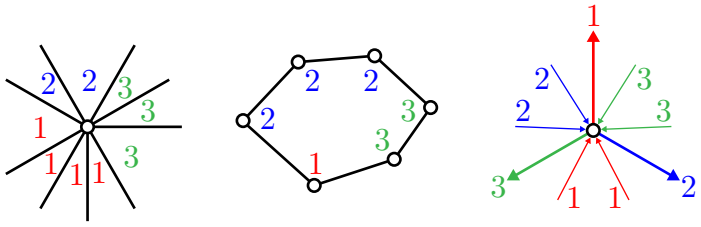

Figure 4. Rules (L2), (L3), and (W3).

Definition 26. A *Schnyder wood* of M is an orientation and coloring of the edges of M with colors $\{1, 2, 3\}$ satisfying the following rules:

(W1) Each edge is oriented in one or two directions. Bioriented edges get two distinct colors.
(W2) The half-edge at v_i is directed outwards and colored i.
(W3) Each vertex v has outdegree one in each label. The edges are arranged as in Figure 4 (right).
(W4) There is no interior face whose boundary is a directed cycle in one color.

Figure 5 illustrates an example of a map with a Schnyder labeling and a Schnyder wood.

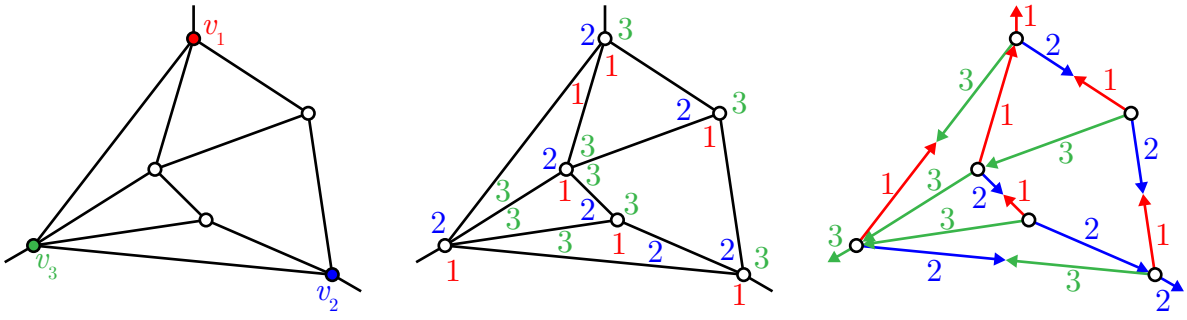

Figure 5. A map (left), a Schnyder labeling (middle), and a Schnyder wood (right).

Lemma 27. *In a Schnyder labeling, the three labels $\{1, 2, 3\}$ appear among the four angles surrounding any edge.*

Proof. By Rules (L2) and (L3), there are precisely three label changes around each vertex and around each face. The total number of label changes is thus $3|V|+3|F| = 3|E|+6$ by Euler relation. Since each half-edge contribute to two label changes, the average number of label changes per edge is three. Since each edge can have either zero or three label changes, it follows that each edge has precisely three label changes. □

This lemma leads to the following theorem, illustrated on Figure 5.

Theorem 28. *The transformation given by*

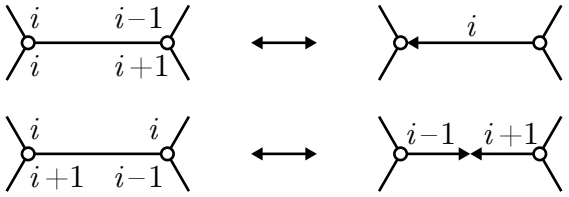

is a bijection from Schnyder labelings to Schnyder woods.

Proof. Exercice. The only difficulty is to show that Rule (L3) holds when we construct a Schnyder labeling from a Schnyder wood. Use an argument similar to that of the proof of Lemma 27. □

Remark 29. If the map M is a triangulation, then the bottom situation in the previous picture cannot happen, except for the three external edges. It follows that all internal edges are oriented in a unique direction. This is the usual context for Schnyder woods, as defined by Schnyder in [Sch89]. The double orientation is required to treat arbitrary 3-connected maps [Fel04, Chap. 2].

2.2. **Regions, coordinates, and straightline embedding.** Consider a planar map M with a Schnyder wood, and let T_i denote the directed graph formed by the edges colored by i. The digraphs T_1, T_2, T_3 form three trees, which justifies the name Schnyder woods. In general, the bioriented edges are shared by two of the trees T_1, T_2, T_3. However, if the map is a triangulation, and if we forget about the external edges, then the trees T_1, T_2, T_3 are edge disjoint spanning trees.

Proposition 30. *For $i \in [3]$, the digraph T_i is a directed tree rooted at v_i.*

Proof. Since any vertex except v_i has outdegree one in T_i, it is sufficient to prove that T_i is acyclic. In fact, even the digraph $D_i := T_i \cup T_{i-1}^{\text{rev}} \cup T_{i+1}^{\text{rev}}$ is acyclic (where G^{rev} denotes the digraph obtained by reversing all edges of G), if we ignore bidirected edges or paths. Assume for contradiction that D_i has a cycle and consider an area minimal cycle Z. We observe that

- Z bounds a single face F: it cannot have a chord, and a vertex inside the bounded surface could be connected to Z by a path in T_i and in T_{i-1}, thus creating a shorter path.
- If Z is clockwise (resp. counterclockwise), then no angle of F has label $i+1$ (resp. $i-1$).

We get a contradiction. □

For a vertex v of M, we denote

- by $P_i(v)$ the directed path in T_i to the root v_i;
- by $R_i(v)$ the region bounded by the two paths $P_{i-1}(v)$ and $P_{i+1}(v)$;
- by $r_i(v)$ the number of faces in region $R_i(v)$.

For example, Figure 6 shows the three regions $R_1(v)$, $R_2(v)$, and $R_3(v)$ of a vertex v in the Schnyder wood of Figure 5.

Lemma 31. *Let u, v be two adjacent vertices in the map M. Then*
(R1) if there is a unidirected edge colored i from u to v, then

$$R_i(u) \subsetneq R_i(v), \qquad R_{i-1}(u) \supsetneq R_{i-1}(v), \qquad \text{and} \qquad R_{i+1}(u) \supsetneq R_{i+1}(v),$$

(R2) if there is a bidirected edge colored $i+1$ from u to v and colored $i-1$ from v to u, then

$$R_i(u) = R_i(v), \qquad R_{i-1}(u) \supsetneq R_{i-1}(v), \qquad \text{and} \qquad R_{i+1}(u) \subsetneq R_{i+1}(v).$$

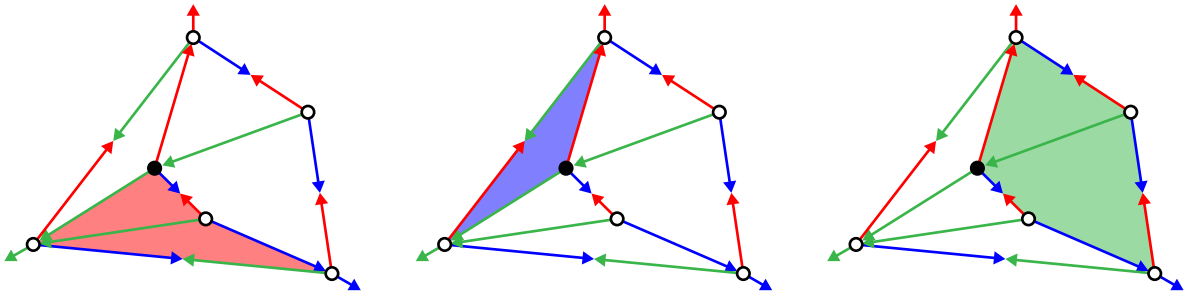

FIGURE 6. The three Schnyder regions $R_1(v)$, $R_2(v)$, and $R_3(v)$ of the black vertex v.

Proof. The two situations are schematized below:

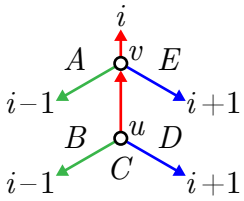

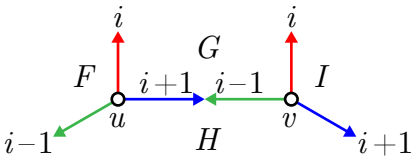

$$\begin{array}{rcl} R_i(u) = C & \subsetneq & B \cup C \cup D = R_i(v) \\ R_{i-1}(u) = D \cup E & \supsetneq & E = R_{i-1}(v) \\ R_{i+1}(u) = A \cup B & \supsetneq & A = R_{i+1}(v) \end{array} \qquad \begin{array}{rcl} R_i(u) = H & = & R_i(v) \\ R_{i-1}(u) = G \cup I & \supsetneq & I = R_{i-1}(v) \\ R_{i+1}(u) = F & \subsetneq & F \cup G = R_{i+1}(v) \end{array}$$

□

The next section is devoted to the proof of the following statement, due to Schnyder in the context of triangulations [Sch89] and extended by Felsner in this setting, see [Fel04, Chap. 2].

Theorem 32. *Let M be a planar map with f faces (including the unbounded one), and with a Schnyder wood. Let $\mathbf{p}_1, \mathbf{p}_2, \mathbf{p}_3$ be three arbitrary non-colinear points in the plane. Then the map*

$$\mu : v \mapsto \frac{1}{f-1}\big(r_1(v) \cdot \mathbf{p}_1 + r_2(v) \cdot \mathbf{p}_2 + r_3(v) \cdot \mathbf{p}_3\big)$$

defines a straightline embedding of M in the plane where all faces are convex.

Up to the existence of Schnyder woods which will be established for 3-connected planar maps in Section 2.4, we obtain the following statement by choosing $\mathbf{p}_1 = (f-1, 0)$, $\mathbf{p}_2 = (0, f-1)$ and $\mathbf{p}_3 = (0, 0)$.

Corollary 33. *Every 3-connected planar map with f faces admits a convex drawing on the $(f-1) \times (f-1)$ grid.*

2.3. **Geodesic maps on orthogonal surfaces.** Dominance (or componentwise) order in $\mathbb{R}^3$ is defined by $\mathbf{u} \le \mathbf{v}$ iff $u_i \le v_i$ for $i \in [3]$. We denote by $\mathbf{u} \vee \mathbf{v}$ and $\mathbf{u} \wedge \mathbf{v}$ the *join* (componentwise maximum) and *meet* (componentwise minimum) of $\mathbf{u}, \mathbf{v} \in \mathbb{R}^3$. For $\mathbf{y} \in \mathbb{R}^3$, we denote by $\Delta_{\mathbf{y}} := \{\mathbf{z} \in \mathbb{R}^3 \mid \mathbf{y} \le \mathbf{z}\}$ the cone dominating $\mathbf{y}$ and by $\nabla_{\mathbf{y}} := \{\mathbf{x} \in \mathbb{R}^3 \mid \mathbf{x} \le \mathbf{y}\}$ the cone dominated by $\mathbf{y}$. For an antichain $\mathbf{V} \subset \mathbb{Z}^3$, consider the filter

$$\langle \mathbf{V} \rangle := \{\mathbf{z} \in \mathbb{R}^3 \mid \mathbf{v} \le \mathbf{z} \text{ for some } \mathbf{v} \in \mathbf{V}\} = \bigcup_{\mathbf{v} \in \mathbf{V}} \Delta_{\mathbf{v}}$$

of $\mathbf{V}$ under dominance order. The boundary $\mathcal{S}_{\mathbf{V}}$ of this set is the *orthogonal surface* generated by $\mathbf{V}$. Note that the following conditions are equivalent for $\mathbf{x} \in \mathbb{R}^3$:

- $\mathbf{x}$ belongs to $\mathcal{S}_{\mathbf{V}}$,
- for all $\mathbf{v} \in \mathbf{V}$, there exists $i \in [3]$ such that $x_i \le v_i$, but there exists $\mathbf{v} \in \mathbf{V}$ and $i \in [3]$ such that $x_i = v_i$,
- $\mathring{\nabla}_{\mathbf{x}} \cap \mathbf{V} = \varnothing$ and $\partial\nabla_{\mathbf{x}} \cap \mathbf{V} \neq \varnothing$ (where $\mathring{\nabla}_{\mathbf{x}}$ is the interior and $\partial\nabla_{\mathbf{x}}$ the boundary of $\nabla_{\mathbf{x}}$).

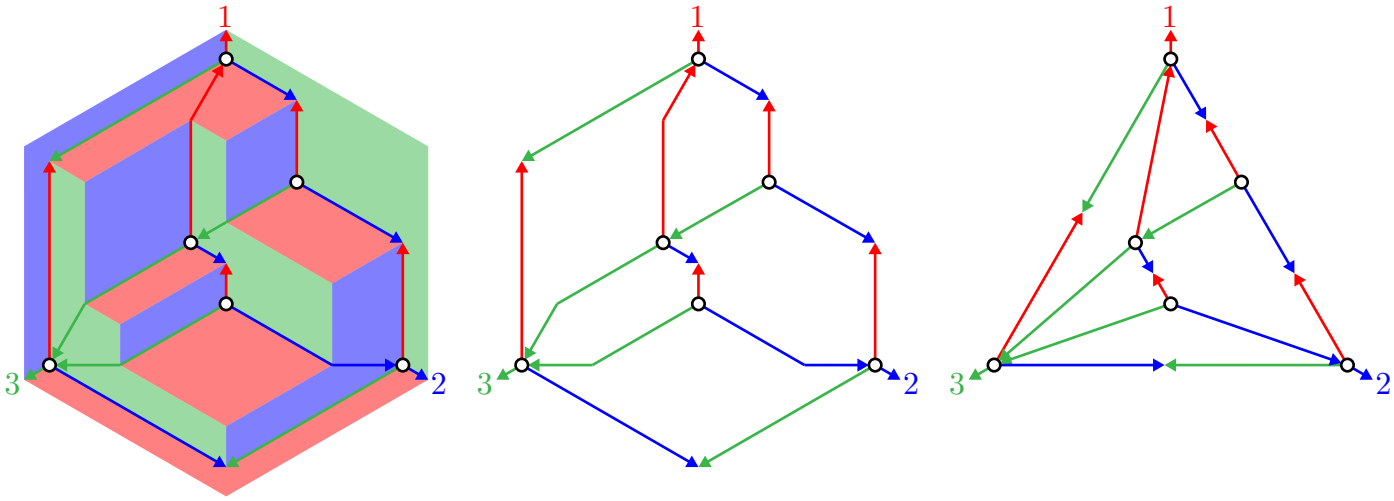

FIGURE 7. Embedding a map on an orthogonal surface, and the resulting Schnyder embedding.

On this surface, we call

- *elbow geodesic* the union of the two segments connecting points $\mathbf{u}, \mathbf{v} \in \mathbf{V}$ to their meet $\mathbf{u} \vee \mathbf{v}$;
- *coordinate arcs* the (not always bounded) segments from a point in $\mathbf{V}$ in the direction of an axis.

The antichain $\mathbf{V}$ is called *axial* if there are only three unbounded coordinate arcs, one in each direction.

Definition 34. A *geodesic embedding* of a map M on the orthogonal surface $\mathcal{S}_{\mathbf{V}}$ generated by an antichain $\mathbf{V}$ is a drawing of M on $\mathcal{S}_{\mathbf{V}}$ such that

(G1) There is a bijection between $\mathbf{V}$ and the vertices of M.
(G2) Every edge of M is an elbow geodesic in $\mathcal{S}_{\mathbf{V}}$ and every bounded coordinate arc is part of an edge of M.
(G3) The drawing is crossing-free.

An example is illustrated on Figure 7 (left).

Theorem 35. *If $\mathbf{V}$ is an axial antichain, then a geodesic embedding of a map M on $\mathcal{S}_{\mathbf{V}}$ induces a Schnyder wood on M. Conversely, given a Schnyder wood W on a planar map M, the region vectors of the vertices of M with respect to W form an axial antichain $\mathbf{V}$ inducing a geodesic embedding of M on $\mathcal{S}_{\mathbf{V}}$.*

Proof. Consider an axial antichain $\mathbf{V}$ and a geodesic embedding of a map M on $\mathcal{S}_{\mathbf{V}}$. There are two ways to see a Schnyder structure on M:

(i) Orient and color the edges according to the three axis. An elbow geodesic can get one or two colors depending on whether it contains one or two bounded coordinate arcs.
(ii) label the angles according to the color of the flat region containing it.

Proving that these colorings yield Schnyder woods and Schnyder labelings is left as an exercice.

Conversely, consider a Schnyder wood on a planar map M. The set $\mathbf{V}$ of region vectors of the vertices of M live in the hyperplane $v_1+v_2+v_3 = f-1$, so that $\mathbf{V}$ is an antichain in dominance order and we get automatically (G1). For any edge $e = \{u, v\}$ of M and any vertex w of M distinct from u, v, the edge e is contained in a certain region $R_i(w)$. This implies that $r_i(u) \leq r_i(w)$ and $r_i(v) \leq r_i(w)$ and thus that the elbow geodesic connecting u to v lies on the surface $\mathcal{S}_{\mathbf{V}}$. Moreover the elbow geodesic corresponding to the three outgoing edges at v will contain the three coordinate arcs at its region vector $\mathbf{v}$. This yields (G2). The only difficulty is thus to prove that the resulting drawing of M is crossing-free. Assume that two elbow geodesics $\{u, v\}$ and $\{x, y\}$

cross. Since an elbow geodesic cannot transversally intersect a coordinate arc, we can assume up to symmetry that the crossing between $\{u, v\}$ and $\{x, y\}$ looks like

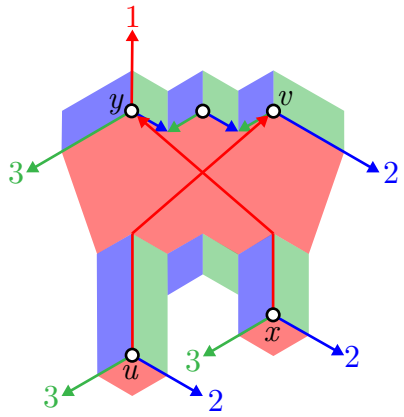

In other words, we can assume that $v_1 = y_1$, $u_2 < x_2$, $v_2 > y_2$, $u_3 > x_3$, and $v_3 < y_3$. Since there is a path P between v and y consisting of orthogonal paths only, (G2) ensures that y is on the path $P_3(v)$. Let w denote the first vertex common to $P_3(u)$ and $P_3(v)$. This vertex w cannot lie on P, since otherwise uvw would define a cycle in $T_1 \cup T_2^{\text{rev}} \cup T_3^{\text{rev}}$. Hence, w lies on $P_3(y)$ and $w \neq y$. This shows that y lies in the interior of the region $R_2(u)$, and thus that x lies in $R_2(u)$ since $\{x, y\}$ is an edge. This contradicts our assumption that $u_2 < x_2$. □

We need the following technical lemma. Remind that we have denoted by $\nabla_{\mathbf{y}} := \{\mathbf{x} \in \mathbb{R}^3 \mid \mathbf{x} \leq \mathbf{y}\}$ the cone of $\mathbb{R}^3$ dominated by $\mathbf{y}$.

Lemma 36. *Consider the orthogonal surface $\mathcal{S}_{\mathbf{V}}$, where $\mathbf{V}$ is the set of region vectors of a map M with respect to an arbitrary Schnyder wood. Then*

(i) For any edge $\{u, v\}$ of M, the region vectors $\mathbf{u}$ and $\mathbf{v}$ of u and v lie on the boundary of $\nabla_{\mathbf{u}\vee\mathbf{v}}$ and there is no other point of $\mathbf{V}$ in $\nabla_{\mathbf{u}\vee\mathbf{v}}$.

(ii) For any face F of M, the join $\vee F := \mathbf{v}_1 \vee \cdots \vee \mathbf{v}_p$ of the region vectors of the vertices $v_1, \dots, v_p$ of F is a maximum of the surface $\mathcal{S}_{\mathbf{V}}$. Moreover, all region vectors of the vertices of F lie on the boundary of $\nabla_{\vee F}$ and there is no other point of $\mathbf{V}$ in $\nabla_{\vee F}$.

Proof. We have already shown that if $\{u, v\}$ is an edge of M, then the elbow geodesic between u and v lies on the surface $\mathcal{S}_{\mathbf{V}}$. In particular, $\mathbf{u} \vee \mathbf{v} \in \mathcal{S}_{\mathbf{V}}$, which implies (i).

For (ii), consider any vertex w of M, and let $i \in [3]$ be such that F lies in region $R_i(w)$. Hence, for any vertex v of the face F, we have $r_i(v) \leq r_i(w)$, and thus $(\vee F)_i \leq r_i(w)$. Moreover, for any vertex v of F, we have $r_i(v) = (\vee F)_i$ while $r_{i-1}(v) > (\vee F)_{i-1}$ and $r_{i+1}(v) > (\vee F)_{i+1}$ for the color $i \in [3]$ such that F lies in region $R_i(v)$. Finally, for each $i \in [3]$, there is a vertex v of F such that F lies in region $R_i(v)$. It follows that $\vee F$ is a maximum of the surface $\mathcal{S}_{\mathbf{V}}$, that all region vectors of the vertices of F lie on the boundary of $\nabla_{\vee F}$ and that there is no other point of $\mathbf{V}$ in $\nabla_{\vee F}$. □

Using this result, one can then derive the proof of Theorem 32. It is illustrated on Figure 7.

Proof of Theorem 32. The projection of the geodesic embedding given by Theorem 35 onto the plane $v_1 + v_2 + v_3 = f - 1$ gives a planar drawing of M whose edges are bended segments. See Figure 7 (middle). Replacing them by straight segments preserves the non-crossing-freeness (because of Lemma 36 (i)) and leads to convex faces (applying Lemma 36 (ii), the vertices of a face F lie on the triangle obtained as the intersection of $\nabla_{\vee F}$ with the plane $v_1 + v_2 + v_3 = f - 1$). See Figure 7 (right). □

Remark 37. The dual map of M can also be visualized on the orthogonal surface. It is illustrated on Figure 8 (right). It corresponds to the duality between the dominance order and its reverse order. More details can be found in [Fel04, Sect. 2.4].

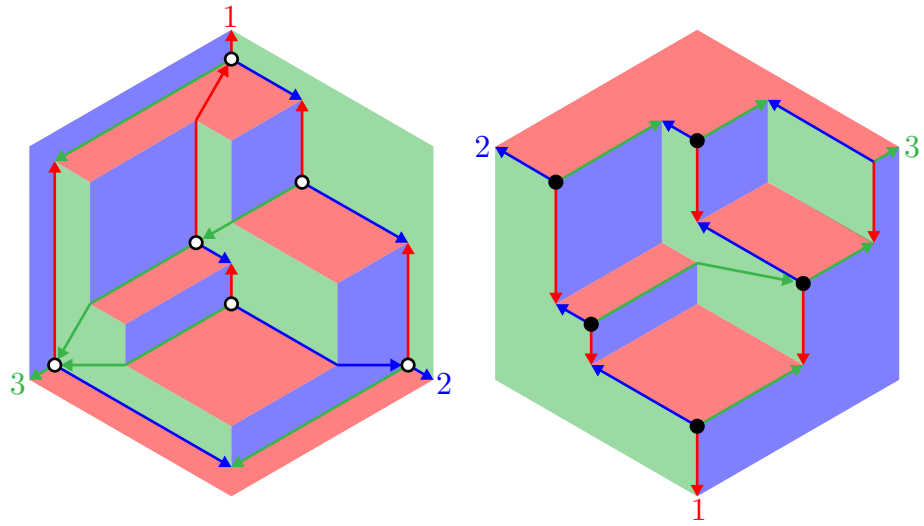

FIGURE 8. Embedding a map and its dual on an orthogonal surface.

2.4. **Existence of Schnyder labelings.** A graph G is *k-connected* if we need to delete k vertices of G to disconnect it. In this section, we prove the existence of Schnyder woods for sufficiently connected maps:

Proposition 38. *Any 3-connected planar map admits a Schnyder wood.*

Different proofs of this statement are possible. The original proof of Schnyder [Sch89] for triangulations and of Felsner [Fel04, Sect. 2.6] for 3-connected planar maps is based on edge contractions. The idea is to choose an edge e of M, construct recursively a Schnyder labeling of M/e, and expand this labeling of M/e to a Schnyder labeling of M. The realization of this idea is however not immediate since contracting an edge in a 3-connected map does not always produces a 3-connected map. The details are carefully written in [Fel04, Sect. 2.6].

In these notes, we prefer an alternative proof based on certain canonical orderings of the vertex set of the map. We start with the special situation when M is a triangulation.

Proposition 39. *Let M be a triangulated planar map, and v_1, v_2 be two distinguished vertices on its outer face. Then there exists an ordering $v_1, \dots, v_n$ of the vertices of M such that for each $k \geq 3$, the submap M_k of M induced by $\{v_1, \dots, v_k\}$ satisfies the following properties:*

(i) M_k is connected and its boundary is a simple cycle,
(ii) M_k is triangulated,
(iii) v_{k+1} is in the outer face of M_k.

We use these canonical orderings to obtain a Schnyder wood on M. Namely, we start from the edge v_1v_2, add points one by one in the order given by the canonical ordering, and color and orient at each step the edges incident to the new point as illustrated in Figure 9

For general 3-connected maps, similar canonical orderings exists and a similar construction can be performed. The proof of the following statement can be found in [Kan96].

Proposition 40. *Let M be a 3-connected planar map, and v_1v_2 be a distinguished edge on its outer face. Then there exists an ordered partition $V_1, \dots, V_N$ of the vertices of M such that $V_1 = \{v_1, v_2\}$ and for each $k \geq 2$, the submap M_k of M induced by $V_1 \cup \cdots \cup V_k$ satisfies the following properties:*

(i) M_k is 2-connected, internally 3-connected, and its boundary is a simple cycle,
(ii) either of the following happens:
- *V_k is a singleton $\{v\}$, v belongs to the boundary of M_k, and has at least one neighbor in $M \setminus M_k$;*

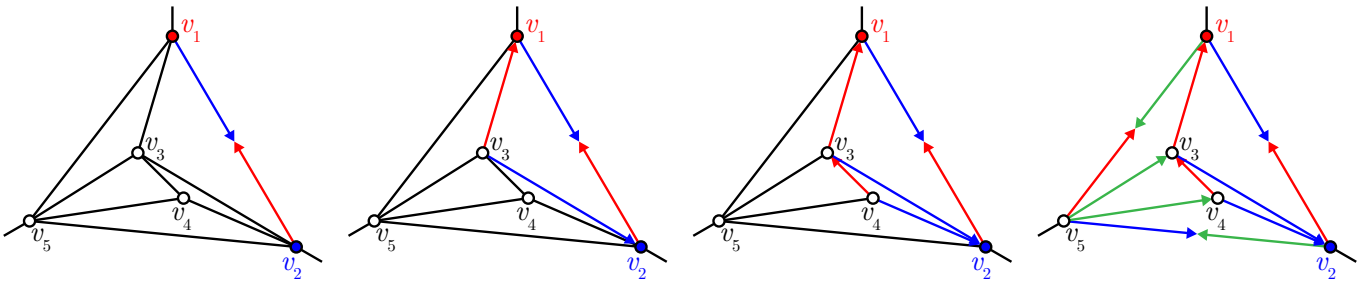

FIGURE 9. A canonical ordering of a triangulation (left), and the resulting Schnyder wood (right).

- *V_k is a chain $v_1, \dots, v_p$, where each v_i has at least one neighbor in $M \smallsetminus M_k$, and where both v_1 and v_p have one neighbor in the boundary of M_{k-1}, and these are the only two neighbors of V_k in M_{k-1}.*

Again, we can use these canonical orderings to construct a Schnyder wood on M. Namely, we start from the edge v_1v_2, add points one by one in the order given by the canonical ordering, and color and orient at each step the edges incident to the new point as follows:

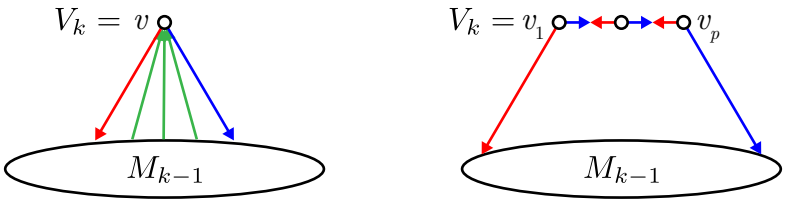

2.5. **Connection to TD-Voronoi and TD-Delaunay diagrams.** We remind in Section 4.4 the definition of Voronoi diagram and Delaunay triangulation of a point set in the Euclidean plane. The reader unfamiliar with these classical notions is invited to take a break to see the definitions in Section 4.4. An intuitive way to think of the Voronoi diagram of a point set $\mathbf{P}$ is as follows: consider circles centered at the points of $\mathbf{P}$ that grow simultaneously. They start from the points themself and end by covering the entire plane. The Voronoi diagram is the partition of the plane where a point $\mathbf{q}$ is colored according to which circle first reached $\mathbf{q}$. If we represent the time in an additional direction z, we can therefore see the Voronoi diagram of a point set $\mathbf{P}$ as the projection down to the plane $z = 0$ of the lower envelope of the union of the cones $C(\mathbf{p}) := \{(\mathbf{q}, z) \in \mathbb{R}^3 \mid \|\mathbf{p} - \mathbf{q}\| \le z\}$ for all points $\mathbf{p} \in \mathbf{P}$. This is illustrated on Figure 10.

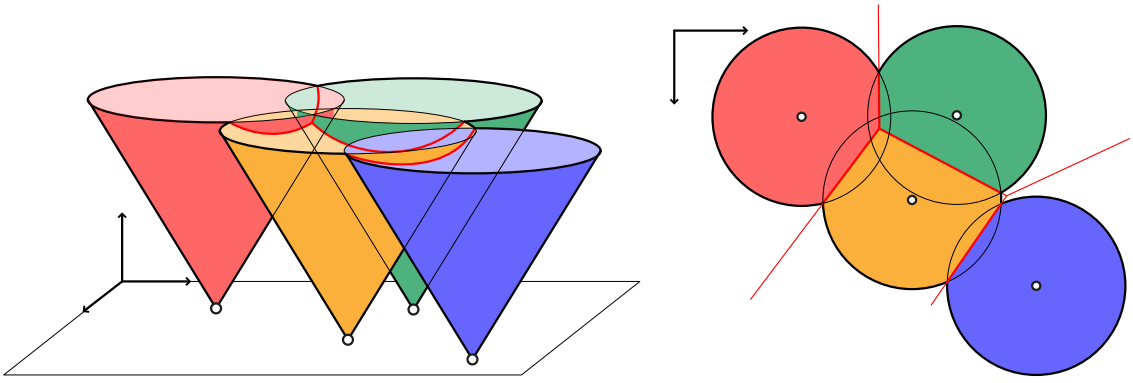

FIGURE 10. The Voronoi diagram of $\mathbf{P}$ (right) obtained as the projection of the lower envelope of the union of the cones $C(\mathbf{p})$ for $\mathbf{p} \in \mathbf{P}$.

In this section, we relate Schnyder woods and orthogonal surfaces to Voronoi and Delaunay diagrams for a different notion of distance. Namely, we define the *triangular distance* on the plane $H := \{\mathbf{x} \in \mathbb{R}^3 \mid x_1 + x_2 + x_3 = c\}$ to be the quasi-metric TD whose ball is the equilateral triangle $\triangle := \text{conv}(c\mathbf{e}_1, c\mathbf{e}_2, c\mathbf{e}_3)$. In other words, for any points $\mathbf{v}, \mathbf{w} \in H$,

$$\text{TD}(\mathbf{v}, \mathbf{w}) := \min\{\lambda \in \mathbb{R}_{\geq 0} \mid \mathbf{v} \in \mathbf{w} + \lambda(\triangle - c\mathbb{1}/3)\}.$$

Observe that this quasi-metric is not a metric as it is not symmetric. Given a point set $\mathbf{V}$ in H, the TD-*Voronoi region* of a point $\mathbf{v} \in \mathbf{V}$ is the region

$$\text{Vor}_{\text{TD}}(\mathbf{v}, \mathbf{V}) := \{\mathbf{x} \in H \mid \text{TD}(\mathbf{v}, \mathbf{x}) \leq \text{TD}(\mathbf{w}, \mathbf{x}) \text{ for all } \mathbf{w} \in \mathbf{V}\}$$

of all points closer to $\mathbf{v}$ than to any other site of $\mathbf{V}$ for the triangular distance. The TD-*Voronoi diagram* $\text{Vor}_{\text{TD}}(\mathbf{V})$ of $\mathbf{V}$ is the diagram formed by the TD-Voronoi regions $\text{Vor}_{\text{TD}}(\mathbf{v}, \mathbf{V})$ for all $\mathbf{v} \in \mathbf{V}$. As in the Euclidean case, we can interpret it using a dynamic process: let homothetic copies of the triangle $\triangle$ grow simultaneously around the points of $\mathbf{V}$, starting from the points themself and growing until they cover the entire plane H. The TD-Voronoi diagram is the partition of the plane H where a point $\mathbf{w}$ is colored according to which triangle first reached $\mathbf{w}$. Thus, it can as well be seen as the projection of the lower envelope of the union of the cones $C_{\text{TD}}(\mathbf{v}) := \{\mathbf{w} + t\mathbb{1} \mid \text{TD}(\mathbf{v}, \mathbf{w}) \leq t\} = \mathbf{v} + (\mathbb{R}_{\geq 0})^3$ for all points $\mathbf{v} \in \mathbf{V}$. It should be clear that this lower envelope coincides with the orthogonal surface $\mathcal{S}_{\mathbf{V}}$. See Figure 11.

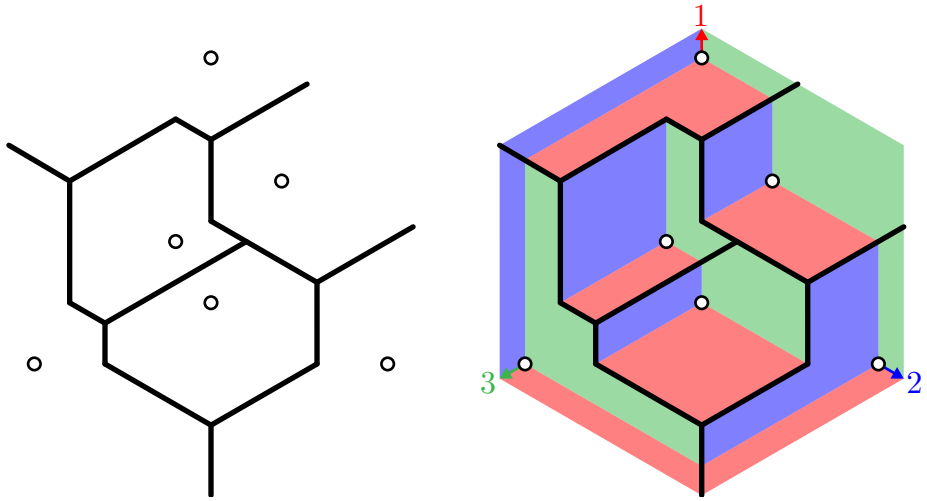

FIGURE 11. The TD-Voronoi diagram of $\mathbf{V}$ (left) is the projection of the lower envelope of the union of the cones $C_{\text{TD}}(\mathbf{v})$ for $\mathbf{v} \in \mathbf{V}$ (right).

The TD-*Delaunay diagram* $\text{Del}_{\text{TD}}(\mathbf{V})$ of $\mathbf{V}$ is the dual of the TD-Voronoi diagram $\text{Vor}_{\text{TD}}(\mathbf{V})$: its vertex set is the point set $\mathbf{V}$ and its edges connect two points $\mathbf{v}, \mathbf{w} \in \mathbf{V}$ if the TD-Voronoi regions $\text{Vor}_{\text{TD}}(\mathbf{v}, \mathbf{V})$ and $\text{Vor}_{\text{TD}}(\mathbf{w}, \mathbf{V})$ intersect. We can even orient and color the edges of $\text{Del}_{\text{TD}}(\mathbf{V})$: for any two neighbors $\mathbf{v}, \mathbf{w}$ in $\text{Del}_{\text{TD}}(\mathbf{V})$, consider the moment when the two growing homothetic copies of $\triangle$ around $\mathbf{v}$ and $\mathbf{w}$ meet. We then orient and color the edge of $\text{Del}_{\text{TD}}(\mathbf{V})$ between $\mathbf{v}$ and $\mathbf{w}$ according to which triangle "pins" the other and in which direction. We obtain the following statement.

Proposition 41. *Consider a Schnyder wood W on a planar map M, and let $\mathbf{V}$ denote the set of region vectors of the vertices of M with respect to W. Then the oriented and colored* TD-*Delaunay diagram of $\mathbf{V}$ coincides with the Schnyder wood W.*

Finally, as in the Euclidean case (see Section 4.4), one can characterize the edges and the triangles in the Delaunay diagram by "empty witnesses". An *empty reverse triangle* is an homothetic copy of the reverse triangle $\triangledown := -\triangle$ whose interior contains no point of $\mathbf{V}$. The following statement is similar to Proposition 108.

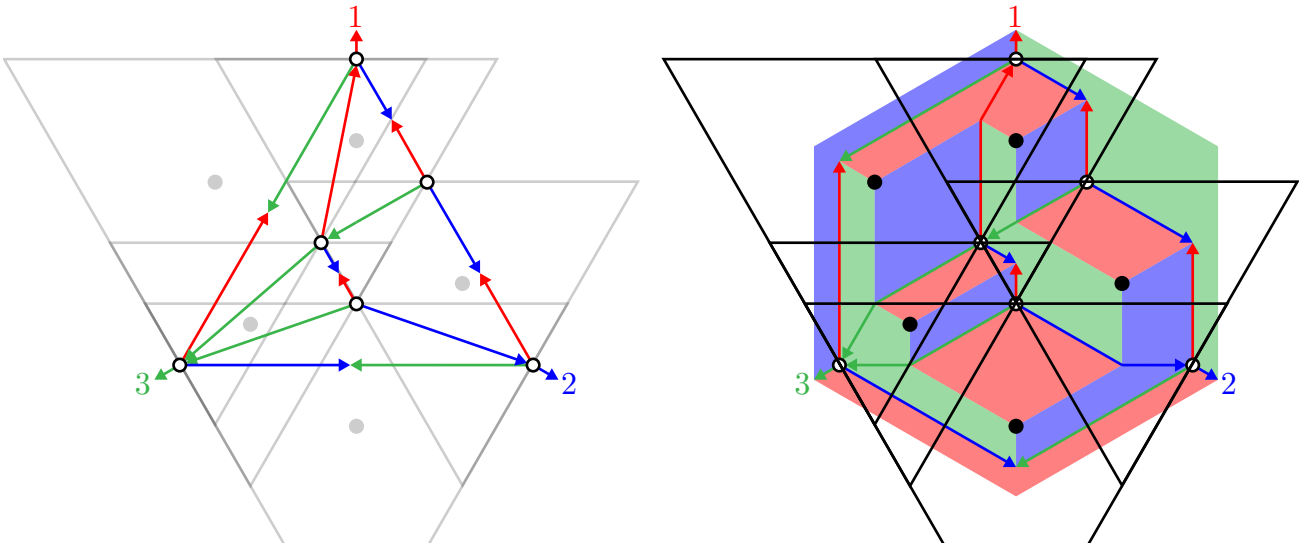

FIGURE 12. The TD-Delaunay diagram of $\mathbf{V}$ (left) with its witness empty reverse triangles. These triangles are centered at projections of maximums of $\mathcal{S}_{\mathbf{V}}$ (right).

Proposition 42. *Let* $\mathbf{u}, \mathbf{v}$ *be points of* $\mathbf{V}$*, and* $\mathbf{W} \subseteq \mathbf{V}$*.*

(i) $\mathbf{vw}$ *is a* TD*-Delaunay edge iff there exists an empty reverse triangle passing through* $\mathbf{v}$ *and* $\mathbf{w}$*.*
(ii) $\mathbf{W}$ *belongs to a* TD*-Delaunay face iff its circumscribed reversed triangle is empty.*

Proof. Exercice. (Hint: see Lemma 36). □

Exercice 43 (TD-Delaunay realizations of stacked triangulations)**.** We say that a triangulation T is *stacked* if

- either T is reduced to a triangle,
- or T is obtained from a stacked triangulation refining a triangle $\mathbf{pqr}$ into three triangles $\mathbf{pqt}$, $\mathbf{qrt}$, and $\mathbf{prt}$ (one can imagine that we stacked a flat tetrahedron $\mathbf{pqrt}$ on the triangle $\mathbf{pqr}$).

The *construction tree* of T is the tree whose nodes correspond to triangles of T and where the children of triangle $\mathbf{pqr}$ are the three triangles $\mathbf{pqt}$, $\mathbf{qrt}$, $\mathbf{prt}$ refining it. Note the color code for the letters and edges in the construction tree of T in Figure 13.

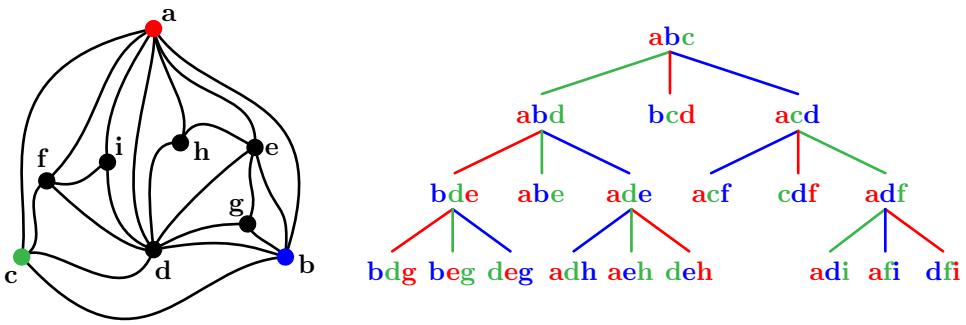

FIGURE 13. A stacked triangulation (left) and its construction tree (right).

(1) Show that a stacked triangulation admits a unique Schnyder labeling and a unique Schnyder wood. Describe them both explicitely.
(2) Describe explicit coordinates for a TD-Delaunay triangulation realizing a stacked triangulation in terms of its construction tree. Illustrate on the triangulation of Figure 13 (left).

In contrast, Exercice 112 shows that not all stacked triangulations can be realized as Euclidean Delaunay triangulations. Exercice 113 characterizes precisely the stacked triangulations that can. Stacked triangulations are also related to stacked polytopes (see Section 3.4.2).

Exercice 44 (Voronoi diagrams and Delaunay triangulations for quasi-distances)**.** Consider a quasi-metric δ on a set Q, *i.e.* a function $\delta : Q^2 \to \mathbb{R}_{\geq 0}$ which

(i) vanishes exactly on the diagonal: $\delta(p,q) = 0 \iff p = q$ for all $p, q \in Q$ and
(ii) satisfies the triangular inequality: $\delta(p,r) \leq \delta(p,q) + \delta(q,r)$ for all $p, q, r \in Q$.

Define the *δ-Voronoi diagram* $\mathrm{Vor}_\delta(P)$ of a subset P of Q as the partition of Q formed by the δ-Voronoi regions

$$\mathrm{Vor}_\delta(p,P) := \{r \in Q \mid \delta(p,r) \leq \delta(q,r) \text{ for all } q \in Q\}$$

of all sites $p \in P$. Define the *δ-Delaunay* $\mathrm{Del}_\delta(P)$ complex of P as the intersection complex of the δ-Voronoi diagram of P:

$$\mathrm{Del}_\delta(P) := \left\{ X \subseteq P \;\middle|\; \bigcap_{p \in X} \mathrm{Vor}_\delta(p,P) \neq \varnothing \right\} \subseteq 2^P.$$

Show that

(i) The δ-Voronoi diagram $\mathrm{Vor}_\delta(P)$ is the projection of the lower envelope of the union of cones

$$\bigcup_{p \in P} \{(q,t) \in Q \times \mathbb{R}_{\geq 0} \mid \delta(p,q) \leq t\}.$$

(ii) A subset X of P belongs to the δ-Delaunay complex of P iff there exists $q \in Q$ and $z \in \mathbb{R}_{\geq 0}$ such that intersection of the reversed cone $\{(r,t) \in Q \times \mathbb{R}_{\geq 0} \mid \delta(r,q) \leq z - t\}$ with $P \times \{0\}$ is precisely $X \times \{0\}$.

Assume that $Q = \mathbb{R}^d$ and δ is invariant by translation, *i.e.* $\delta(\mathbf{p},\mathbf{q}) = \delta(\mathbf{0},\mathbf{q}-\mathbf{p})$ for all $\mathbf{p}, \mathbf{q} \in \mathbb{R}^d$. Interpret the previous statements in terms of the cones

$$C_\delta^+ := \left\{(\mathbf{p},t) \in \mathbb{R}^d \times \mathbb{R}_{\geq 0} \;\middle|\; \delta(\mathbf{0},\mathbf{p}) \leq t\right\},$$
$$\text{and} \quad C_\delta^- := -C_\delta^+ = \left\{(\mathbf{p},t) \in \mathbb{R}^d \times \mathbb{R}_{\leq 0} \;\middle|\; \delta(\mathbf{p},\mathbf{0}) \leq -t\right\}.$$

2.6. **Geometric spanners.** Let G be an edge weighted graph. The distance between two vertices of G is the minimal weight of a path between them. Here, the graph G will be a geometric graph and the weight of an edge $\{u,v\}$ is the Euclidean distance $|uv|$. A subgraph H of a graph G is a *t-spanner* of G if the quotient of distances in H and in G between any two vertices is at most t. The smallest possible constant t is called the *stretch factor*. A *geometric spanner* of a point set $\mathbf{P}$ is a spanner of the complete geometric graph with vertices $\mathbf{P}$. For example, it is known that the Euclidean Delaunay triangulation is a geometric spanner, but the precise value of its stretch factor is unknown: it is upper bounded by $1.998 < 2$ (see [Xia13] and [KG92]) and lower bounded by $1.5846 > \pi/2$ (see [BDL+11]). The stretch factor of the TD-Delaunay triangulation is given by the following statement.

Theorem 45 (Chew [Che89])**.** *The TD-Delaunay triangulation of a planar point set is a geometric 2-spanner.*

Proof. The proof of [Che89] is rather technical and we prefer a proof based on Schnyder woods, using ideas of [BGHP10]. Consider a point set $\mathbf{P}$ and its TD-Delaunay triangulation $\mathrm{Del}_{\mathrm{TD}}(\mathbf{P})$. Color and orient this triangulation with the Schnyder wood described in Section 2.5. Consider two distinct points $\mathbf{p}, \mathbf{q} \in \mathbf{P}$, and let $\bigtriangledown$ denote the smallest reversed triangle passing through $\mathbf{p}$ and $\mathbf{q}$. Without loss of generality, we assume that $\mathbf{p}$ is at the bottom vertex, while $\mathbf{q}$ lies on the top edge of $\bigtriangledown$ (the other cases are similar). Then the path $P_1(\mathbf{p})$ has to cross one of the paths $P_2(\mathbf{q})$ and $P_3(\mathbf{q})$. Assume by symmetry that $P_1(\mathbf{p})$ crosses $P_2(\mathbf{q})$. This situation is illustrated in Figure 14. In this picture, the Euclidean length of the path from $\mathbf{p}$ to $\mathbf{q}$ in $\mathrm{Del}_{\mathrm{TD}}(\mathbf{P})$ is bounded by the Euclidean length of the orange path, which projects to the boundary of the triangle $\bigtriangledown$. It is now easy to see that the ratio of the Euclidean length of the path from $\mathbf{p}$ to $\mathbf{q}$ in $\mathrm{Del}_{\mathrm{TD}}(\mathbf{P})$ by the Euclidean distance between $\mathbf{p}$ and $\mathbf{q}$ is at most 2. □

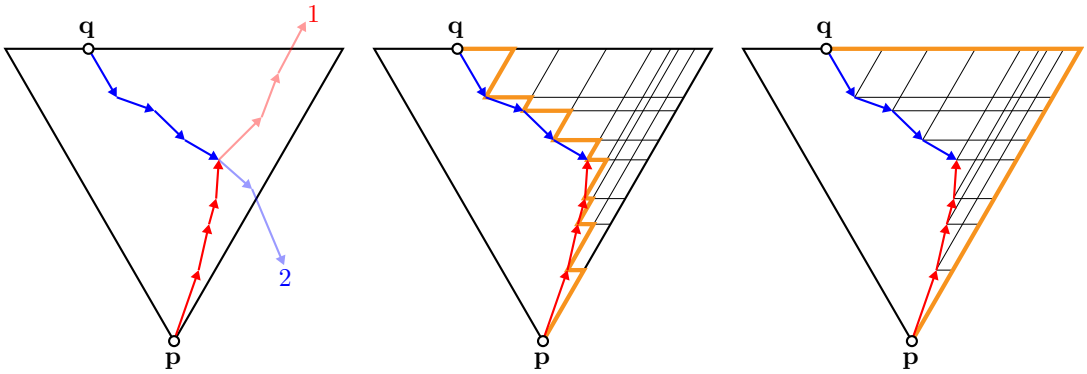

FIGURE 14. The TD-Delaunay triangulation is a geometric 2-spanner: the two paths $P_1(\mathbf{p})$ and $P_2(\mathbf{q})$ intersect (left), the Euclidean length of the path from $\mathbf{p}$ to $\mathbf{q}$ in $\mathrm{Del}_{\mathrm{TD}}(\mathbf{P})$ is bounded by the Euclidean length of the orange thick path (middle), and the latter projects to the boundary of the triangle $\bigtriangledown$ (right).

The TD-Delaunay triangulation has a surprizingly good stretch factor for a planar graph. But both the Euclidean Delaunay triangulation and the TD-Delaunay triangulation have an important drawback: their vertex degrees are unbounded. This is a real problem in practice where spanners are used for example for designing wireless networks, in which the degree is bounded by physical limitations of the devices. Bluetooth scatternets, for example, can be modeled as geometric spanners where master nodes must have at most 7 slave nodes.

In [BGHP10], Bonichon, Gavoille, Hanusse, and Perkovic consider a subgraph of the TD-Delaunay triangulation $\mathrm{Del}_{\mathrm{TD}}(\mathbf{P})$ constructed as follows. Color and orient the edges of $\mathrm{Del}_{\mathrm{TD}}(\mathbf{P})$ as explained in Section 2.5. For any $i \in [3]$ and any point $\mathbf{p} \in \mathbf{P}$, denote by

- $\mathsf{parent}_i(\mathbf{p})$ the target of the unique outgoing edge of $\mathrm{Del}_{\mathrm{TD}}(\mathbf{P})$ colored by i.
- $\mathsf{children}_i(\mathbf{p})$ all points $\mathbf{q} \in \mathbf{P}$ such that $\mathbf{p} = \mathsf{parent}_i(\mathbf{q})$.
- $\mathsf{closest}_i(\mathbf{p})$ the point of $\mathsf{children}_i(\mathbf{p})$ closest to $\mathbf{p}$ for the triangular distance.
- $\mathsf{first}_i(\mathbf{p})$ and $\mathsf{last}_i(\mathbf{p})$ the first and last points of $\mathsf{children}_i(\mathbf{p})$ in clockwise order around $\mathbf{p}$.

Note that $\mathsf{closest}_i(\mathbf{p})$, $\mathsf{first}_i(\mathbf{p})$ and $\mathsf{last}_i(\mathbf{p})$ may be undefined (if $\mathsf{children}_i(\mathbf{p}) = \varnothing$) or may coincide. Consider the subgraph H of the TD-Delaunay triangulation of $\mathbf{P}$ obtained by erasing at each vertex $\mathbf{p}$ all incoming arcs except the arcs $\mathsf{first}_i(\mathbf{p})$, $\mathsf{last}_i(\mathbf{p})$ and $\mathsf{closest}_i(\mathbf{p})$ for $i \in [3]$ (if they exist). It turns out that this subgraph H is a good spanner of $\mathrm{Del}_{\mathrm{TD}}(\mathbf{P})$ and it clearly has bounded degree.

Proposition 46 (Bonichon, Gavoille, Hanusse, and Perkovic [BGHP10])**.** *The subgraph H is a 3-spanner of the* TD*-Delaunay triangulation $\mathrm{Del}_{\mathrm{TD}}(\mathbf{P})$ and it has degree at most* 12*.*

Proof. The degree of any vertex $\mathbf{p}$ is at most 12 since we erased all but at most 9 incoming arcs, and it has at most 3 outgoing arcs (some may have been deleted).

To prove that H is a 3-spanner of $\mathrm{Del}_{\mathrm{TD}}(\mathbf{P})$, consider an arc from $\mathbf{p}$ to $\mathbf{q}$ in $\mathrm{Del}_{\mathrm{TD}}(\mathbf{P})$. By symmetry, we can assume that $\mathbf{q} = \mathsf{parent}_1(\mathbf{p})$. Since we kept $\mathsf{first}_i(\mathbf{r})$ and $\mathsf{last}_i(\mathbf{r})$ for all $\mathbf{r} \in \mathbf{P}$ and $i \in [3]$, the children $\mathsf{children}_1(\mathbf{q})$ form a path P in H. We consider the path from $\mathbf{p}$ to $\mathbf{q}$ in H using P to reach $\mathsf{closest}_1(\mathbf{q})$. Using similar arguments as in the proof of Theorem 45, we obtain that the ratio of the Euclidean length of the path from $\mathbf{p}$ to $\mathbf{q}$ in H by the Euclidean distance between $\mathbf{p}$ and $\mathbf{q}$ is at most 3. This is illustrated on Figure 15. It shows that H is a 3-spanner of $\mathrm{Del}_{\mathrm{TD}}(\mathbf{P})$. □

Corollary 47 (Bonichon, Gavoille, Hanusse, and Perkovic [BGHP10])**.** *The subgraph H of the* TD*-Delaunay triangulation $\mathbf{P}$ is a planar geometric 6-spanner with maximum degree* 12*.*

Improving on this naive construction, Bonichon, Gavoille, Hanusse, and Perkovic obtain in fact a planar geometric 6-spanner with maximum degree 6. The proof of this result can be found in [BGHP10].

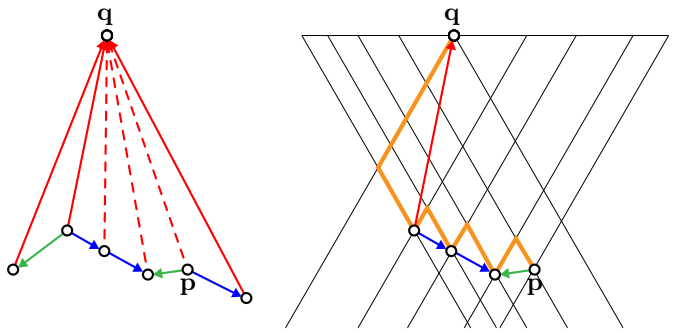

FIGURE 15. The subgraph H is a 3-spanner of the TD-Delaunay triangulation $\mathrm{Del}_{\mathrm{TD}}(\mathbf{P})$: the Euclidean length of the path from $\mathbf{p}$ to $\mathbf{q}$ through $\mathsf{closest}_1(\mathbf{q})$ in the subgraph H (left) is bounded by the Euclidean length to the orange thick path (right), which is at most 3 times the Euclidean distance between $\mathbf{p}$ and $\mathbf{q}$.

2.7. **Triangle contact representation of planar maps.** A *triangle contact system* is a set of triangles in the plane whose interiors are disjoint, but which can have vertex – edge contacts (however, vertex – vertex and edge – edge contacts are forbidden) [dFdMR94]. We suppose that the system is *maximal*, *i.e.* that any bounded connected component of the complement of the union of the triangles is adjacent to precisely 3 triangle edges. We associate to a triangle contact system $\mathcal{T}$ its *contact graph* $\mathcal{T}^\#$ whose nodes correspond to the triangles of $\mathcal{T}$ and whose edges connect pairs of triangles in contact. If a vertex of triangle $\triangle$ touches an edge of triangle $\triangle'$, then we orient the edge from $\triangle$ to $\triangle'$ in the contact graph $\mathcal{T}^\#$. With this orientation, the contact graph has outdegree precisely 3 at each internal node, and we can naturally get a Schnyder wood on $\mathcal{T}^\#$. See Figure 16.

Reciprocally, suppose that M is a triangulated map endowed with a canonical ordering $v_1, \dots, v_n$, *i.e.* such that

- v_1v_2 is an edge of the external face of M,
- the subgraph M_k of M induced by $v_1, \dots, v_k$ is a triangulation of a disk,
- v_{k+1} is on the external face of G_k and its neighbors in G_k form an interval on the boundary of G_k of length at least 2.

Let $\{T_1, T_2, T_3\}$ be the Schnyder wood constructed from this canonical order as in Section 2.4. Here, the roots of T_1, T_2 and T_3 are v_n, v_1 and v_2 respectively. We denote by $\pi_i(k)$ the index of the parent of v_k in the tree T_i.

We then construct a set of triangles $\mathcal{T} = \{\triangle_1, \dots, \triangle_k\}$, such that the basis of $\triangle_k$ is parallel to the horizontal axis and lies at ordinate k for all $k \in [n]$, and the apex of $\triangle_k$ is at ordinate $\pi_1(k)$ for all $2 < k < n$. We proceed as follows:

- We start with two triangles $\triangle_1$ et $\triangle_2$ at ordinate 1 and 2 respectively, of height at least n, and in contact.
- Suppose that the triangles $\triangle_1, \dots, \triangle_{k-1}$ are already constructed. Denote by g_k the abscissa of the point of ordinate k on the right edge of the triangle $\triangle_{\pi_3(k)}$, by d_k the abscissa of the point of ordinate k on the left edge of the triangle $\triangle_{\pi_2(k)}$, and define $m_k = \alpha g_k + (1-\alpha)\, d_k$ (where $\alpha \in [0,1]$ is a parameter to be chosen later). We then define $\triangle_k$ to be the triangle with vertices (g_k, k), $(m_k, \pi_1(k))$, and (d_k, k).
- Finally, we close with a triangle $\triangle_n$ at ordinate n in contact with both $\triangle_1$ and $\triangle_2$.

The resulting triangles form a triangle contact system $\mathcal{T}$ whose contact graph $\mathcal{T}^\#$ is the map M [dFdMR94]. An example is illustrated in Figure 16.

Exercice 48. What choice of parameter α yields isosceles/rectangle triangles?

Exercice 49. Show that any triangulated map can be realized as the contact graph of $\perp$ shapes, or of $\curlywedge$ shapes. See Figure 17.

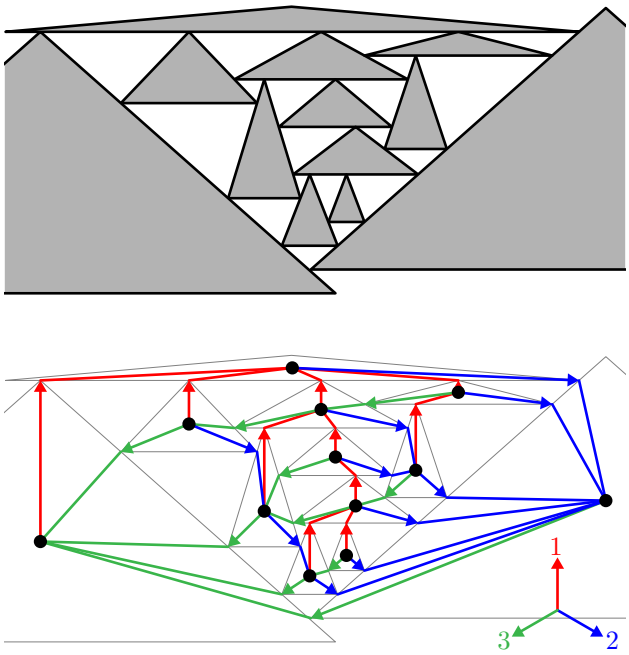

FIGURE 16. A triangle contact system $\mathcal{T}$ (top) and its contact graph $\mathcal{T}^\#$ (bottom).

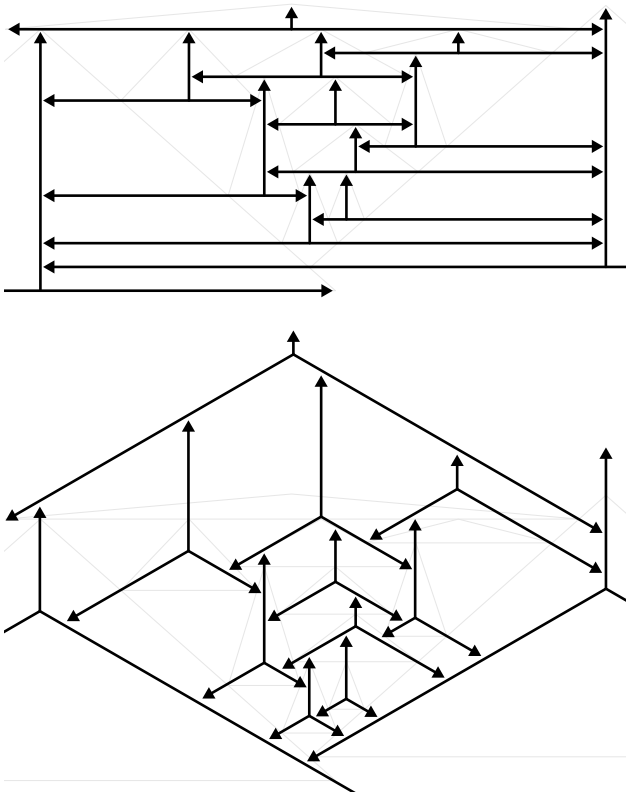

FIGURE 17. Contact graphs of $\perp$ shapes (top) and of $\curlywedge$ shapes (bottom).

3. Basic notions on polytopes

This section covers basic and classical knowledge from the theory of polytopes, needed later in these lecture notes for polytopal structures on triangulations and geometric graphs. Sections 3.3 and 3.4 are not needed later but present classical results in polytope theory. The reader is invited to consult [Zie95] for a more detailed reference on polytopes.

3.1. $\mathcal{V}$-polytopes versus $\mathcal{H}$-polytopes.

Polytopes are the high-dimensional generalizations of polygons in $\mathbb{R}^2$ and polyhedral solids in $\mathbb{R}^3$ (such as *e.g.* the classical Platonic solids). They can be defined in two (equivalent) ways.

Definition 50. A *$\mathcal{V}$-polytope* is the convex hull of finitely many points in $\mathbb{R}^d$. A *$\mathcal{H}$-polyhedron* is the intersection of finitely many half-spaces in $\mathbb{R}^d$, and a *$\mathcal{H}$-polytope* is a bounded $\mathcal{H}$-polyhedron.

Theorem 51. *A subset of $\mathbb{R}^d$ is a $\mathcal{V}$-polytope if and only if it is a $\mathcal{H}$-polytope.*

Definition 52. We call *convex polytope* (or just *polytope*) a subset of $\mathbb{R}^d$ which is a $\mathcal{V}$-polytope, or equivalently a $\mathcal{H}$-polytope. The *dimension* of a polytope P is the dimension of the affine hull of P.

Proof of Theorem 51. Different proofs are possible. A classical algorithmic proof follows from the *Fourier-Motzkin elimination procedure*, which proceeds by projections on coordinate hyperplanes (see *e.g.* [Zie95, Lect. 1]). Here, we follow the proof presented in [Mat02, Section 5.2], attributed to Edmonds.

We first prove that a $\mathcal{H}$-polytope is a $\mathcal{V}$-polytope by induction on the dimension d. It is clear when $d = 1$ since 1-dimensional polytopes are just line segments, so we assume that $d \geq 2$. Consider a $\mathcal{H}$-polytope P, defined as the intersection of a finite collection $\mathcal{H}$ of half-spaces in $\mathbb{R}^d$. For $H \in \mathcal{H}$ the intersection $F_H := P \cap \partial H$ is again a $\mathcal{H}$-polytope, and therefore a $\mathcal{V}$-polytope by induction hypothesis. Let $\mathcal{V}_H$ be a finite point set such that $F_H = \text{conv}(\mathcal{V}_H)$. We claim that P is the convex hull of $\mathcal{V} := \bigcup_{H\in\mathcal{H}} V_h$. Let $x \in P$ and ℓ be a line passing through x. The intersection $P \cap \ell$ is a line segment $[y, z]$ and there exists $H, K \in \mathcal{H}$ such that $y \in F_H$ and $z \in F_K$ (otherwise, if y is not on the boundary of one half-space, we could continue a little further on ℓ). It follows that $y \in \text{conv}(\mathcal{V}_H)$ and $z \in \text{conv}(\mathcal{V}_K)$ and thus that $x \in \text{conv}\{y, z\} \subseteq \text{conv}(\mathcal{V}_H \cup \mathcal{V}_K) \subseteq \text{conv}(\mathcal{V})$.

Conversely, we use duality to prove that a $\mathcal{V}$-polytope is a $\mathcal{H}$-polytope. This follows from the fact that a $\mathcal{H}$-polytope is a $\mathcal{V}$-polytope and that the dual of a $\mathcal{V}$-polytope containing the origin is a $\mathcal{H}$-polytope and reciprocally. □

Although mathematically equivalent, the $\mathcal{V}$-description and the $\mathcal{H}$-description are not computationally equivalent. Namely it is not immediate to pass from one to the other description. In fact, the size of one description can even be exponentially large with respect to the size of the other description. Examples will be presented soon. In any case, it is always interesting to understand the differences and the advantages of both descriptions.

Theoretically, the equivalence between $\mathcal{V}$-polytopes and $\mathcal{H}$-polytopes is helpful to prove properties of polytopes, such as the following four statements:

(i) Any projection of a polytope is a polytope.
(ii) The Minkowski sum of two polytopes is a polytope.
(iii) The intersection of a polytope with a polyhedron is a polytope.
(iv) Any section of a polytope (by an affine subspace) is a polytope.

The first two are immediate using $\mathcal{V}$-descriptions, while the last two are immediate using $\mathcal{H}$-descriptions.

Example 53. Classical families of polytopes include (see Figure 18):

(1) A d-dimensional *simplex* is the convex hull of $d + 1$ affinely independent points in $\mathbb{R}^d$, or equivalently the intersection of $d + 1$ affinely independent half-spaces in $\mathbb{R}^d$. The standard d-dimensional simplex is

$$\triangle_d := \text{conv}\{\mathbf{e}_1, \dots, \mathbf{e}_{d+1}\} = \big\{\mathbf{x} \in \mathbb{R}^{d+1} \mid x_i \geq 0,\ \forall i \in [d+1] \text{ and } \sum\nolimits_{i\in[d+1]} x_i = 1\big\}.$$

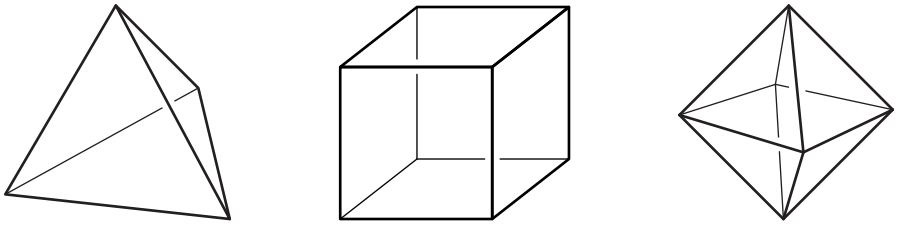

FIGURE 18. The 3-dimensional simplex (left), cube (middle), and octahedron (right).

(2) The standard d-dimensional *cube* is the polytope

$$\square_d := [-1,1]^d = \operatorname{conv}\{\pm 1\}^d = \left\{\mathbf{x} \in \mathbb{R}^d \;\middle|\; -1 \le x_i \le 1 \text{ for all } i \in [d]\right\}.$$

(3) The standard d-dimensional *cross-polytope* is the polytope

$$\diamond_d := \operatorname{conv}\{\pm \mathbf{e}_i \mid i \in [d]\} = \left\{\mathbf{x} \in \mathbb{R}^d \mid \sum\nolimits_{i\in[d]} \varepsilon_i x_i \le 1 \text{ for all } \varepsilon \in \{\pm 1\}^d\right\}.$$

Exercice 54. Show that any polytope is a projection of a sufficiently high dimensional simplex.

Interesting examples arise from combinatorial objects, as illustrated by the following exercices.

Exercice 55. The *matching polytope* $M(G)$ of a graph $G = (V, E)$ is defined as the convex hull of the characteristic vectors $\chi_M \in \mathbb{R}^E$ of all matchings M on G.

(1) Show that the matching polytope is contained in the polytope $N(G)$ defined by

$$x_e \ge 0 \quad \text{for all } e \in E, \qquad \text{and} \qquad \sum_{e \ni v} x_e \le 1 \quad \text{for all } v \in V.$$

(2) If G is bipartite, show that the polytopes $M(G)$ and $N(G)$ coincide. (Hint: Consider a point $\mathbf{x} \in N(G)$. If $\mathbf{x}$ has integer coordinates, show that it is the characteristic vector of a matching on G. Otherwise, show that one can slightly perturb the coordinates of $\mathbf{x}$ that are not integer, and conclude that $\mathbf{x}$ is not a vertex of $N(G)$).

Exercice 56. Given a supply function $\mu : M \to \mathbb{R}_{\ge 0}$ on a source set M and a demand function $\nu : N \to \mathbb{R}_{\ge 0}$ on a sink set N, the *transportation polytope* $P(\mu, \nu)$ is the polytope of $\mathbb{R}^{M\times N}$ defined by:

$$\forall m \in M,\ \forall n \in N, \quad x_{m,n} \ge 0, \quad \sum\nolimits_{n' \in N} x_{m,n'} = \mu(m), \quad \text{and} \quad \sum\nolimits_{m' \in M} x_{m',n} = \nu(n).$$

Call *support* of a point $\mathbf{x} \in P(\mu, \nu)$ the subgraph of $K_{M,N}$ consisting of the edges (m, n) for which $x_{m,n} > 0$. Show the following properties:

(1) $P(\mu, \nu)$ is non-empty if and only if $\sum_{m\in M} \mu(m) = \sum_{n\in N} \nu(n)$.
(2) Provided it is non-empty, $P(\mu, \nu)$ has dimension $(|M| - 1)(|N| - 1)$.
(3) A point of $P(\mu, \nu)$ is a vertex of $P(\mu, \nu)$ if and only if its support is a forest (*i.e.* contains no cycle). Moreover, a vertex of $P(\mu, \nu)$ is determined by its support.
(4) The supports of two adjacent vertices of $P(\mu, \nu)$ differ in precisely two edges.

The *Birkhoff polytope* of size m is a particular example of transportation polytope, whose supply and demand functions are both constant to m. Its vertices are precisely the permutation matrices.

Exercice 57. Let $G = (V, E)$ be a directed graph with incidence matrix $M_G \in \mathbb{R}^{V\times E}$. For $\beta \in \mathbb{R}^V$, the *orientation polytope* $P(G, \beta)$ is the polytope defined by

$$P(G, \beta) := \left\{\mathbf{x} \in \mathbb{R}^E \;\middle|\; -\mathbf{1} \le \mathbf{x} \le \mathbf{1} \text{ and } M_G \cdot \mathbf{x} = \beta\right\}.$$

Show that

(1) the vertices of $P(G, \beta)$ are β-orientations on G, *i.e.* orientations on G such that the difference of the indegree and outdegree of any vertex v of G is equal to β_v,
(2) the edges of $P(G, \beta)$ are given by reorientations of oriented cycles in β-orientations on G.

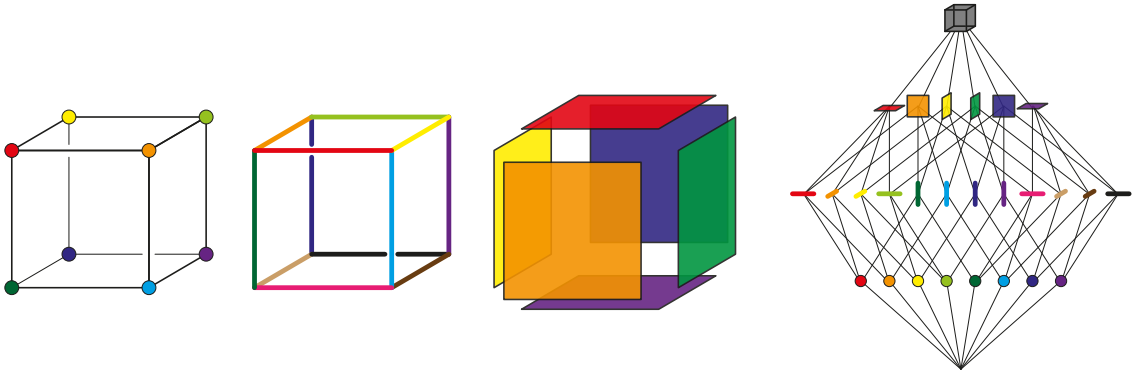

FIGURE 19. The face lattice of the 3-dimensional cube.

Later in these lecture notes, we describe families of polytopes related to combinatorial objects, in particular geometric graphs: the *secondary polytope* in Section 4.6, the *permutahedron* in Section 5.3, the *associahedron* in Section 5.4, the *polytope of pseudotriangulations* in Section 6.1, and the *brick polytope* in Section 6.6.

3.2. **Faces.** Given a polytope, we are interested in the combinatorics of its faces.

Definition 58. A *face* of a convex polytope P is defined to be

- either the polytope P itself,
- or the intersection of P with a supporting hyperplane of P,
- or the empty set.

The 0-, 1-, $(d-2)$-, and $(d-1)$-dimensional faces of a d-dimensional polytope P are called *vertices*, *edges*, *ridges*, and *facets* of P respectively.

The following intuitive facts are proved for example in [Zie95, Lect. 2].

Proposition 59. *(1) Every polytope is the convex hull of its vertices. Conversely, any point set W contains the vertices of the convex hull of W.*
(2) A face F of a polytope P is a polytope. The vertices of F are the vertices of P that lie in F. More generally, the faces of F are exactly the faces of P that lie in F.
(3) The inclusion poset $\mathcal{F}(P)$ of faces of a polytope P has the following properties:
- *$\mathcal{F}(P)$ is a graded lattice of rank $\dim(P)+1$, with rank function $\mathrm{rk}(F) = \dim(F)+1$;*
- *$\mathcal{F}(P)$ is both atomic (i.e. every face is the join of its vertices) and coatomic (i.e. every face is the meet of the facets containing it);*
- *every interval of $\mathcal{F}(P)$ is the face lattice of a polytope;*
- *it has the diamond property: every interval of rank 2 has 4 elements.*

Definition 60. Two polytopes P and Q are *combinatorially equivalent* if their face lattices $\mathcal{F}(P)$ and $\mathcal{F}(Q)$ are isomorphic.

Exercice 61. Describe the faces of the d-dimensional simplex, cube, and cross-polytope. What are their face lattices? See Figure 19.

The *polar* of a polytope $P = \mathrm{conv}(V) = \{\mathbf{x} \in \mathbb{R}^d \mid A\mathbf{x} \leq \mathbb{1}\}$ containing the origin is defined as the polytope $P^\diamond := \mathrm{conv}(A) = \{\mathbf{x} \in \mathbb{R}^d \mid V\mathbf{x} \leq \mathbb{1}\}$. Its face lattice is the opposite of the face lattice of P. For example, the d-dimensional cube and cross-polytope are polar to each other.

A d-dimensional polytope is

- *simplicial* if all its facets contain d vertices, and
- *simple* if all its vertices are contained in d facets.

For example, the simplex is both simple and simplicial, the cube is simple, and the cross-polytope is simplicial. The polar of a simple polytope is simplicial, and reciprocally.

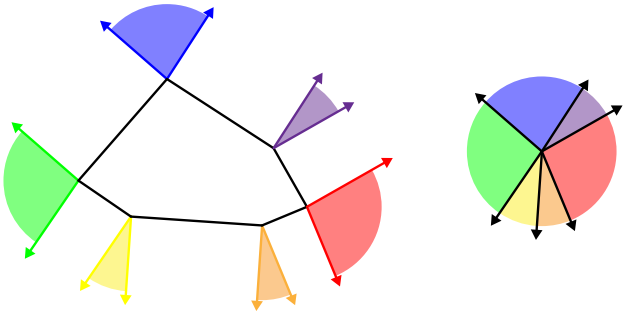

FIGURE 20. The normal fan of a polygon.

Exercice 62. Show that a polytope that is both simple and simplicial is either a simplex or a polygon.

Exercice 63. Describe the faces of the Cartesian product $P \times Q := \{(p,q) \mid p \in P, q \in Q\}$ of two polytopes P, Q in terms of the faces of P and Q.

The *boundary complex* ∂P of a polytope P is the polytopal complex formed by all its proper faces. In particular, if P is simplicial, then its boundary complex ∂P is *simplicial complex*, *i.e.* a collection of subsets of V closed by subsets: $A \subset B \in \partial P \implies A \in \partial P$.

The *normal cone* of a face F of a polytope P of $\mathbb{R}^d$ is the set

$$C^\diamond(F) := \big\{\gamma \in \mathbb{R}^d \mid \langle \gamma | \mathbf{x} \rangle = \max_{\mathbf{p} \in P} \langle \gamma | \mathbf{p} \rangle \text{ for all } \mathbf{x} \in F\big\}.$$

Note that the normal cone of a k-dimensional face has dimension $d-k$, and that maximal normal cones are the domains of linearity of the function $\gamma \to \max_{\mathbf{p} \in P} \langle \gamma | \mathbf{p} \rangle$. The *normal fan* of P is the collection of the normal cones of all faces of P. See Figure 20.

Exercice 64. What are the normal fan of the d-dimensional simplex, cube and cross-polytope.

3.3. **f-vector, h-vector, and Dehn-Sommerville relations.** The *f-vector* of the polytope P is the sequence $f(P) := \big(f_0(P), \dots, f_d(P)\big)$, where $f_i(P)$ denotes the number of i-dimensional faces of P. The *f-polynomial* of P is

$$f(P,x) := \sum_{i=0}^{d} f_i(P) x^i.$$

Exercice 65. What are the f-vectors of the d-dimensional simplex, cube, and cross-polytope?

Exercice 66. Show that $f(P^\diamond, x) = x^d ?1/x + x^{d?1} f(P, 1/x)$, where $P^\diamond$ denotes the polar of P.

Let P be a simple polytope in $\mathbb{R}^d$. Consider a generic linear functional $\phi : \mathbb{R}^d \to \mathbb{R}$, meaning that ϕ takes distinct values on distinct vertices of P. Orient the 1-skeleton of P in the ϕ-increasing direction. Finally, let $h_j(P)$ denote the number of vertices of P with indegree j in this directed graph. The *h-vector* of P is the sequence $h(P) := \big(h_0(P), \dots, h_d(P)\big)$ and the *h-polynomial* of P is

$$h(P,x) := \sum_{j=0}^{d} h_j(P) x^j$$

A priori, the h-vector and h-polynomial seem to depend not only on P but also on the chosen linear functional ϕ. The next lemma shows however that the linear functional ϕ is not relevant.

Lemma 67. *The f- and h-vectors of a simple polytope P satisfy the relations*

$$\forall\, 0 \le i \le d, \quad f_i(P) = \sum_{j=0}^{d} \binom{j}{i} h_j(P) \qquad \text{and} \qquad \forall\, 0 \le j \le d, \quad h_j(P) = \sum_{i=0}^{d} (-1)^{i+j} \binom{i}{j} f_i(P)$$

which translates on the f- and h-polynomials to the relation $f(P,x) = h(P, x+1)$. In particular, there is no dependence in the linear functional ϕ.

Proof. The equivalence between these three relations is the subject of the next exercice. We only prove the expression of the f-vector in terms of the h-vector. For this, we double count the number of pairs (v, F), where F is an i-face of P and v is the ϕ-maximal vertex of F. Once F is fixed, there is a unique such vertex v. Conversely, once v is fixed, there are $\binom{j}{i}$ choices for F if v has indegree i in the directed 1-skeleton of P. The result immediately follows. □

Exercice 68. Let $(f_i)_{0\leq i\leq d}$ and $(h_j)_{0\leq j\leq d}$ be integer sequences and let $f(x) := \sum_{i=0}^{d} f_i x^i$ and $h(x) := \sum_{j=0}^{d} h_j x^j$ denote the corresponding counting polynomials. Show that

$$f(x) = h(x+1) \quad \Longleftrightarrow \quad \forall i, \quad f_i = \sum_{j=0}^{d} \binom{j}{i} h_j \quad \Longleftrightarrow \quad \forall j, \quad h_j = \sum_{i=0}^{d} (-1)^{i+j} \binom{i}{j} f_i.$$

Exercice 69. What are the h-vectors of the d-dimensional simplex and cube?

Theorem 70 (Dehn-Sommerville relations)**.** *For a simple polytope P, the h-vector is symmetric: $h_j(P) = h_{d-j}(P)$ for all $0 \leq j \leq d$. This translates in terms of f-vectors to*

$$\sum_{i=j}^{d} (-1)^{i+j} \binom{i}{j} f_i(P) = \sum_{i=d-j}^{d} (-1)^{d+i-j} \binom{i}{d-j} f_i(P) \qquad \text{for all } 0 \leq j \leq d.$$

Proof. Consider the linear functionals ϕ and $-\phi$. The sum of the indegree in the graph oriented by ϕ and the indegree in the graph oriented by $-\phi$ is constant to d. This shows the relation on the h-entries. The relation on the f entries then follow from Lemma 67. □

Exercice 71. Write down the Dehn-Sommerville relations for a simplicial polytope.

Corollary 72 (Euler's relation)**.** *For a simple or simplicial polytope P,*

$$\sum_{i=0}^{d} (-1)^i f_i(P) = 1.$$

3.4. **Extreme polytopes.** In this section, we discuss the maximal and minimal face numbers for a polytope with n vertices.

3.4.1. *Many faces: cyclic polytopes.*

Definition 73. A d-dimensional *cyclic polytope* is the convex hull of finitely many points on the d-dimensional *moment curve*, parametrized by $\mu_d : t \mapsto (t, t^2, \dots, t^d)$.

Proposition 74. *(i) Cyclic polytopes are simplicial.*
(ii) For $j \leq \lfloor d/2 \rfloor$, all j-subsets of vertices define a $(j-1)$-face of a d-dimensional cyclic polytope.

Proof. To prove (i), we prove that any $d+1$ points on the moment curve are affinely dependent. Assume by contradiction that $\mu(t_1), \dots, \mu(t_{d+1})$ lie on a common hyperplane of equation $\sum_{i\in[d]} \alpha_i x_i = -\alpha_0$. Since $\mu(t_k) = (t_k, \dots, t_k^d)$, it implies that the polynomial $\sum_{i=0}^{d} \alpha_i t^i$ has at least $d+1$ roots $t_1, \dots, t_{d+1}$ although it has degree d, a contradiction.

To prove (ii), let $\mu(t_1), \dots, \mu(t_j)$ be j vertices of a cyclic polytope, and consider the hyperplane of equation $\sum_{i\in[d]} \alpha_i x_i = -\alpha_0$, where the coefficients α_i are the coefficients of the polynomial $\prod_{i\in[j]} (t - t_i)^2 = \sum_{i=0}^{d} \alpha_i t^i$. The points $\mu(t_1), \dots, \mu(t_j)$ clearly lie on this hyperplane, while all other points of the moment curve lie on the positive side of this hyperplane. It follows that $\mu(t_1), \dots, \mu(t_j)$ defines a face, and thus a $(j-1)$-face by simpliciality. □

A polytope where all $(\leq k)$-subset of vertices define a face is called *k-neighborly*. The cyclic polytope is therefore $\lfloor d/2 \rfloor$-neighborly.

Exercice 75. If $k > \lfloor d/2 \rfloor$, the d-dimensional simplex is the only k-neighborly d-dimensional polytope.

Corollary 76. *The h-vector of the polar of a d-dimensional cyclic polytope with n vertices is given by*

$$h_j = \binom{n-d+j-1}{j} \text{ for } j \le \lfloor d/2 \rfloor \qquad \text{and} \qquad h_j = \binom{n-j-1}{d-j} \text{ for } j > \lfloor d/2 \rfloor.$$

Proof. Since the cyclic polytope is neighborly, it has $\binom{n}{i}$ faces of dimension $i \le \lfloor d/2 \rfloor$. Therefore, its polar has $\binom{n}{d-i}$ faces of dimension $i > \lfloor d/2 \rfloor$. We therefore obtain for $j > \lfloor d/2 \rfloor$ that

$$(\star) \qquad \sum_{i=j}^{d} (-1)^{i+j} \binom{i}{j} \binom{n}{d-i} = \binom{n-j-1}{d-j}.$$

Finally, the values for $j \le \lfloor d/2 \rfloor$ are derived from the symmetry of the h-vector. □

Exercice 77. Consider Equality ($\star$).

(1) Show that it holds when $j = 0$ and $j = d$.
(2) Show that if it holds for (j, d) and $(j+1, d)$ then it holds for $(j+1, d+1)$. (Hint: use the relation $\binom{x+1}{y+1} = \binom{x}{y+1} + \binom{x}{y}$).
(3) Conclude that it is always valid.

Exercice 78. Consider the cyclic polytope $C_d(n) = \operatorname{conv}\{\mu_d(t_i) \mid i \in [n]\}$ for $t_1 < t_2 < \cdots < t_n$. Identify a d-subset $F \subset [n]$ with the point set $\{\mu_d(t_i) \mid i \in F\}$. Call *block* of $F \in [n]$ the intervals of F, and say that a block is *internal* if it does not contain 1 or n.

(1) Show that a point $\mu(r)$ is located on one or the other side of the affine hyperplane passing through F according to the sign of the VanDerMonde determinant

$$\det \begin{bmatrix} 1 & \dots & 1 & 1 \\ t_1 & \dots & t_d & r \\ \vdots & \ddots & \vdots & \vdots \\ t_1^d & \dots & t_d^d & r^d \end{bmatrix}.$$

(2) Remind and prove the product formula for this determinant.
(3) Deduce that a d-subset F of $[n]$ defines a facet of $C_d(n)$ if and only if all internal blocks have even size (*Gale's evenness criterion*).
(4) Deduce the following facts on cyclic polytopes:
   (a) $C_d(n)$ is neighborly.
   (b) All cyclic polytope are combinatorially equivalent.
   (c) The number of facets of $C_d(n)$ is

$$f_{d-1}(C_d(n)) = \binom{n - \lceil \frac{d}{2} \rceil}{\lfloor \frac{d}{2} \rfloor} + \binom{n-1-\lceil \frac{d-1}{2} \rceil}{\lfloor \frac{d-1}{2} \rfloor}.$$

(Hint: Prove first that the number of ways to choose a $2k$-subset of $[n]$ such that all blocks are even is $\binom{n-k}{k}$. To obtain the formula, distinguish the cases when the first block is even or odd).

Theorem 79 (Upper Bound Theorem, McMullen [McM70])**.** *The h-vector of any simple polytope P with n facets is bounded by:*

$$h_j(P) \le \binom{n-d+j-1}{j} \text{ for } j \le \lfloor d/2 \rfloor \qquad \text{and} \qquad h_j(P) \le \binom{n-j-1}{d-j} \text{ for } j > \lfloor d/2 \rfloor.$$

Therefore, the number of i-dimensional faces of P is bounded by

$$f_i(P) \le \sum_{j=i}^{\lfloor d/2 \rfloor} \binom{j}{i} \binom{n-d+j-1}{j} + \sum_{j > \lfloor d/2 \rfloor} \binom{j}{i} \binom{n-j-1}{d-j}.$$

Exercice 80. Write down the Upper Bound Theorem for simplicial polytopes.

Proof. The proof is based on the following two claims:

(1) $h_i(F) \leq h_i(P)$ for any facet F of P. To see this inequality, consider a linear functional ϕ obtained by a small perturbation of the linear functional defining the facet F and containing P in its positive side. Since all edges leaving face F are ϕ-increasing, the indegrees of any vertex of F are identical in the graph of F and in the graph of P both directed by ϕ.

(2) $\sum_F h_i(F) = (d-i)\,h_i(P) + (i+1)\,h_{i+1}(P)$, where F ranges over all facets of P. Consider a generic linear functional ϕ and orient the graphs of P and it facets accordingly. We check that the contribution of each vertex is identical on both sides. For this, we consider a vertex v of a facet F of P, and we denote by e the edge incident to v and not in F. We write $\text{indeg}(v, P)$ for the indegree of v in the graph of P and $\text{indeg}(v, F)$ for the indegree of v in the graph of F. There are three cases according to $\text{indeg}(v, P)$:
   (i) if $\text{indeg}(v, P) = i$, then $\text{indeg}(v, F) = i$ if e is outgoing F, and $\text{indeg}(v, F) = i - 1$ otherwise;
   (ii) if $\text{indeg}(v, P) = i + 1$, then $\text{indeg}(v, F) = i$ if e is incoming F, and $\text{indeg}(v, F) = i + 1$ otherwise;
   (iii) otherwise, $\text{indeg}(v, F) \neq i$.
   The formula immediately follows.

Using these two claims, we obtain

$$(d-i)\,h_i(P) + (i+1)\,h_{i+1}(P) \leq n\,h_i(P),$$

and therefore

$$h_{i+1}(P) \leq \frac{n+d-i}{i+1}\,h_i(P).$$

The Upper Bound Theorem follows by induction. □

3.4.2. *Few faces: stacked polytopes.* Let P be a d-dimensional polytope, and F be a facet of P. The operation of *stacking onto* F consists of constructing the polytope $P' = P \cup (F \star p)$, where p is a point beyond the facet F but beneath all other facets of P, and $F \star p$ denotes the pyramid $\text{conv}(F \cup \{p\})$.

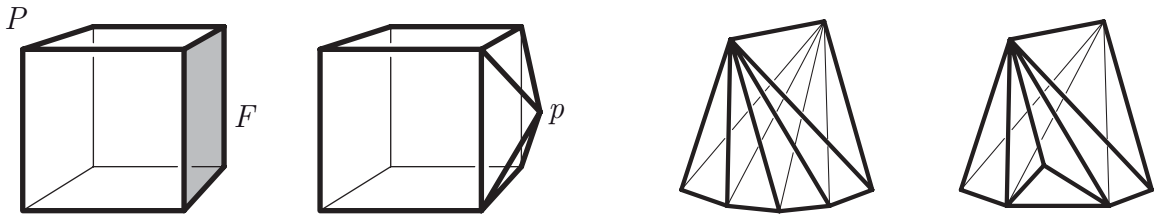

FIGURE 21. Stacking onto a facet of a polytope (left) and two combinatorially distinct stacked polytopes (right).

Observe that during this operation, we destroy the facet F, and create one new i-face for all $(i-1)$-face of F. In other words, the f-vector of the resulting polytope P' is given by:

$$\begin{aligned} f_0(P') &= f_0(P) + 1, \\ f_i(P') &= f_i(P) + f_{i-1}(F), \quad \text{for } 0 \leq i \leq d-2, \\ f_{d-1}(P') &= f_{d-1}(P) + f_{d-2}(F) - 1. \end{aligned}$$

Definition 81. A *stacked polytope* on $d+n$ vertices arises from a d-simplex by stacking $(n-1)$ times onto a facet $(n \geq 1)$.

In other words, we obtain a (convex) tree of n d-dimensional simplices, and thus, a stacked polytope is simplicial. The f-vector of a stacked polytope on $d+n$ vertices is given by:

$$\begin{aligned} f_0 &= d+n, \\ f_i &= \binom{d}{i+1} + n\binom{d}{i}, \quad \text{for } 0 \leq i \leq d-2, \\ f_{d-1} &= 2 + n(d-1). \end{aligned}$$

Exercice 82. A *rooted* stacked polytope is a stacked polytope where we have chosen a facet of which we have colored the vertices with d colors.

(1) Show that the choice of a facet an a d-coloring of its vertices induces a $(d+1)$-coloring of the graph of the stacked polytope. Deduce a bijection between the rooted stacked d-dimensional polytopes with $d+n$ vertices and the plane d-ary trees with n internal nodes. The latter are counted by the *Fuss-Catalan number* (see also Section 5.1):

$$\frac{1}{(d-1)n+1}\binom{dn}{n}.$$

(2) Conclude that the number X of combinatorially distinct d-dimensional stacked polytopes on $d+n$ vertices is bounded by

$$\frac{1}{d!\,\big(2+n(d-1)\big)\,\big((d-1)n+1\big)}\binom{dn}{n} \le X \le \frac{1}{(d-1)n+1}\binom{dn}{n}.$$

How good are these bounds?

Theorem 83 (Lower Bound Theorem, Barnette [Bar73])**.** *The f-vector of a simplicial d-dimensional polytope P with n vertices is componentwise larger or equal to the f-vector of a stacked d-dimensional polytope with n vertices. Furthermore, equality holds for some f-vector entries iff $d=3$, or $d\ge 4$ and P is stacked.*

3.5. **Graphs of polytopes.** The *graph* of a polytope P is the graph with same vertices and edges as P. It is often called *1-skeleton* of P. More generally, the *k-skeleton* of P is the collection of $(\le k)$-dimensional faces of P. A natural question is to determine necessary and sufficient conditions for a graph to be polytopal. It is easy in dimension ≤ 3, but becomes difficult in higher dimension.

3.5.1. *Dimension* 3.

Theorem 84 (Steinitz [Ste22])**.** *A graph is the 1-skeleton of a 3-dimensional polytope if and only if it is planar and 3-connected.*

Proof. The graph of a 3-dimensional polytope is planar (project it to a sphere surrounding it) and 3-connected (special case of Balinski's theorem below). For the reverse statement, different proofs are possible. [Zie95, Lect. 4] presents a proof base on ΔY operations (replacing a triangular face by a star with three edges), which preserve realizability. □

Theorem 85 (Whitney [Whi32])**.** *Let G be the graph of a 3-dimensional polytope P. The graphs of the 2-dimensional faces of P are precisely the induced cycles in G that do not separate G.*

In contrast to the easy 2- and 3-dimensional situations, d-dimensional polytopality becomes much more involved as soon as $d\ge 4$. For example, neighborly 4-dimensional polytopes illustrate the difference between the behavior of 3- and 4-dimensional polytopes:

(i) Starting from a neighborly 4-dimensional tope, and stacking vertices on undesired edges, Perles observed that every graph is an induced subgraph of the graph of a 4-dimensional polytope (while only planar graphs are induced subgraphs of graphs of 3-dimensional polytopes).
(ii) The existence of combinatorially different neighborly polytopes proves that the 2-dimensional faces of a 4-dimensional polytope cannot be derived from its graph (compare with Whitney's Theorem).

As a consequence of his work on realization spaces of 4-dimensional polytopes, Richter-Gebert underlined several deeper negative results: among others, 4-dimensional polytopality is NP-hard and cannot be characterized by a finite set of "forbidden minors" (see [RG96, Chap. 9]).

Exercice 86. Show that every graph is an induced subgraph of the graph of a 4-dimensional polytope. (Hint: start from a cyclic polytope and stack vertices on undesired edges).

3.5.2. *Necessary conditions for polytopality.* Although no reasonable characterization of polytopal graphs is possible [RG96], we gather in the following statement some interesting necessary conditions.

Proposition 87. *A d-dimensional polytopal graph G satisfies the following properties:*

(1) Balinski's Theorem*: G is d-connected* [Bal61].
(2) Principal Subdivision Property *(d-PSP): Every vertex of G is the principal vertex of a principal subdivision of K_{d+1}. Here, a* subdivision *of K_{d+1} is obtained by replacing edges by paths, and a* principal subdivision *of K_{d+1} is a subdivision in which all edges incident to a distinguished* principal vertex *are not subdivided* [Bar67].
(3) Separation Property*: The maximal number of components into which G may be separated by removing $n > d$ vertices equals $f_{d-1}\big(C_d(n)\big)$, the maximum number of facets of a d-dimensional polytope with n vertices* [Kle64].

Exercice 88. Show that the complete bipartite graph $K_{m,n}$ is not polytopal for any $n, m \geq 3$. (Hint: if a polytope P realizes $K_{m,n}$, the graph of any 3-dimensional face of P should contain a $K_{3,3}$ subgraph, which is non-planar).

Exercice 89. Which of the following graphs are polytopal? In which dimension?

(i) the complete graph K_8 where we delete the edges of a perfect matching,
(ii) the complete graph K_7 where we delete a 7-cycle,
(iii) the complete graph K_6 where we delete a 6-cycle,
(iv) the Cartesian product of two complete graphs $K_n \times K_m$,
(v) the graphs of Figure 22.

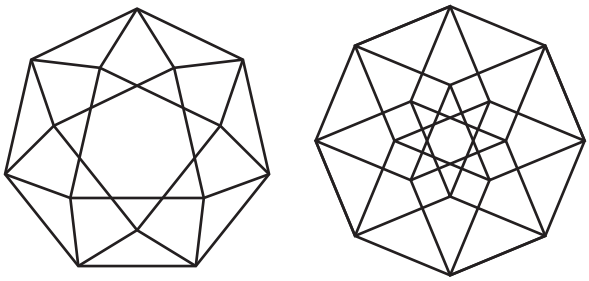

FIGURE 22. Are these graphs polytopal?

3.5.3. *Simple polytopes.* Simple polytopes (where every vertex contained in dimensional-many facets) have somehow much nicer properties than general polytopes. In particular, the following statement affirms that a simple polytope is determined by its graph:

Theorem 90 (Blind and Mani-Levitska [BML87], Kalai [Kal88])**.** *Two simple polytopes with isomorphic graphs are combinatorially equivalent.*

Proof. We follow the proof of Kalai [Kal88]. The idea is to recognize the graphs of the faces of a simple polytope P in terms of certain acyclic orientations of the graph of P. We say that an acyclic orientation of the graph of P is *good* if the graph of each face of P has a unique sink. The result follows from two observations:

(1) Good acyclic orientations of P can be recognized from the graph of P. For any acyclic orientation O of the graph of P, denote by $h_j(O)$ the number of vertices of P with indegree j for O, and define $F(O) := h_0(O) + 2\,h_1(O) + \cdots + 2^d\,h_d(O)$. Since each face of P has at least one sink for O and each indegree j vertex of P is the sink of 2^j faces of P (because P is simple!), $F(O)$ is greater or equal to the number of non-empty faces of P, with equality if and only if O is a good orientation. Good acyclic orientations are therefore those which minimize $F(O)$.

(2) A regular induced subgraph of the graph of P is the graph of a face of P if and only if its vertices are initial with respect to some good acyclic orientation of P. The "only if" direction is immediate: slightly perturb a linear functional defining a face F to obtain a good acyclic orientation for which the vertices of F form an initial subset. Conversely, for the "if" direction, consider a k-regular subgraph H of the graph of P induced by an initial subset of vertices with respect to a good orientation O. Let v be a sink of H directed by O, and let F be the k-dimensional face containing the k edges of H incident to v. Since O is a good orientation, v is the unique sink of the graph of F directed by O. Therefore, all vertices of F are vertices of H. This implies that H coincides with the graph of F since both are k-regular and one is a subgraph of the other. □

Remark 91. Although the proof of Theorem 90 is not constructive, it was later turned to a polynomial algorithm in [Fri09].

Exercice 92. Prove that all induced cycles of length 3, 4 and 5 in the graph of a simple d-dimensional polytope P are graphs of 2-dimensional faces of P. Is it still true for cycles of length 6? (Hint: 3-dimensional cube).

3.5.4. *Diameters of polytopes.* The *diameter* of a graph G is the minimal number $\delta(G)$ such that any two vertices of G can be connected by a path with at most $\delta(G)$ edges. The diameter of a polytope P is the diameter of its 1-skeleton. Denote by $\Delta(d,n)$ the maximal diameter of a d-dimensional polytope with at most n facets.

Diameters of polytopes are closely related to linear programming and its resolution via the classical simplex algorithm. Indeed, the value of $\Delta(d,n)$ is a lower bound for the number of iterations needed by the simplex algorithm with any pivot rule. A longstanding open question is to determine whether $\Delta(d,n)$ is polynomial in both d and n. This question is called "Polynomial Hirsch Conjecture". The name comes from a much stronger conjecture, recently disproved by Santos [San12]:

Theorem 93 (Santos [San12])**.** *The Hirsch conjecture is wrong: there exists d-dimensional polytopes with n facets whose diameter is strictly more than $n-d$.*

Santos' proof goes beyond the focus of these lecture notes. Let us just mention that his first counterexample was a 43-dimensional polytope with 86 facets and diameter at least 44! The same method was then improved to reach 20-dimensional counterexamples to the Hirsch conjecture.

For now, the current best bound on $\Delta(d,n)$ is polynomial in n but exponential in d:

Theorem 94 (Kalai and Kleitman [KK92])**.** *The maximal diameter of a d-dimensional polytope with n facets is bounded by*

$$\Delta(d,n) \leq n^{\log_2(d)+1}.$$

In fact, there is even a linear upper bound in n for fixed dimension (although the dependence in d is not as good):

Theorem 95 (Barnette [Bar74], Larman [Lar70])**.** *The maximal diameter of a d-dimensional polytope with n facets is bounded by*

$$\Delta(d,n) \leq \frac{2^{d-2}}{3} n.$$

3.6. **The incidence cone of a directed graph.** Let $(\mathbf{e}_1,\dots,\mathbf{e}_n)$ be the canonical basis of $\mathbb{R}^n$ and $\mathbb{1} := \sum \mathbf{e}_i$.

Definition 96. The *incidence configuration* of the directed multigraph G is the vector configuration $I(G) := \{\mathbf{e}_j - \mathbf{e}_i \mid (i,j) \in G\} \subset \mathbb{R}^n$. The *incidence cone* of G is the cone $C(G) \subset \mathbb{R}^n$ generated by $I(G)$, *i.e.* its positive span.

In other words, the incidence configuration of a directed multigraph consists of the column vectors of its incidence matrix. Observe that the incidence cone is contained in the linear subspace of equation $\langle \mathbb{1} | x \rangle = 0$.

Lemma 97. *Consider a subgraph H of G. Then the vectors of $I(H)$:*

(i) are independent if and only if H has no (not necessarily oriented) cycle, that is, if H is a forest;

(ii) span the hyperplane $\langle \mathbb{1} | x \rangle = 0$ if and only if H is connected and spanning;

(iii) form a basis of the hyperplane $\langle \mathbb{1} | x \rangle = 0$ if and only if H is a spanning tree;

(iv) form a circuit if and only if H is a (not necessarily oriented) cycle; the positive and negative parts of the circuit correspond to the subsets of edges oriented in one or the other direction along this cycle; in particular, $I(H)$ is a positive circuit if and only if H is an oriented cycle;

(v) form a cocircuit if and only if H is a minimal (not necessarily oriented) cut; the positive and negative parts of the cocircuit correspond to the edges in one or the other direction in this cut; in particular, $I(H)$ is a positive cocircuit if and only if H is an oriented cut.

Lemma 98. *Consider a subgraph H of G. The incidence configuration $I(H)$ is the set of vectors of $I(G)$ contained in a k-face of $C(G)$ if and only if H has $n-k$ connected components and the quotient graph G/H is acyclic. In particular:*

(i) The cone $C(G)$ has dimension $n-1$ (since we assumed that the undirected graph underlying G is connected).

(ii) The cone $C(G)$ is pointed if and only if G is an acyclic directed graph.

(iii) If G is acyclic, it induces a partial order on its set of nodes. The rays of $C(G)$ correspond to the edges of the Hasse diagram of G. The cone is simple if and only if the Hasse diagram of G is a tree.

(iv) The facets of $C(G)$ correspond to the complements of the minimal directed cuts in G. Given a minimal directed cut in G, the characteristic vector of its sink is a normal vector of the corresponding facet.

4. Triangulations, flips, and the secondary polytope

This section is devoted to triangulations of planar point sets: minimal and maximal numbers of triangulations of an n-point set, regular triangulations and secondary polytope. Although presented here in the plane, the construction and properties of the secondary polytope extend in higher dimension. A very clear and interesting presentation can be found in [DRS10, Chap. 5].

4.1. **Triangulations.** Let $\mathbf{P}$ be a point set (in general position) in the plane. A *triangulation* of $\mathbf{P}$ is a set T of triangles with corners in $\mathbf{P}$ such that

(i) the union of the triangles of T covers the convex hull of $\mathbf{P}$,
(ii) any two triangles of $\mathbf{P}$ intersect in a proper face of both (possibly empty).

We often consider that a triangulation is a set of edges rather than triangles. A triangulation T is *full* if no point of $\mathbf{P}$ is in the interior of a triangle of T. Equivalently, a full triangulation of $\mathbf{P}$ can be seen as a maximal crossing free geometric graph on $\mathbf{P}$.

Exercice 99. Show that any full triangulation of a point set with i interior points and b boundary points has $i+b$ vertices, $3i+2b-3$ edges, and $2i+b-2$ triangles. (Hint: apply Euler's formula).

Exercice 100. Let T be a triangulation of a point set, with i_k interior vertices and b_k boundary vertices of degree k for each k. Show that

$$\sum_{k\geq 3}(6-k)i_k + \sum_{k\geq 2}(4-k)b_k = 6.$$

(Hint: apply Euler's formula and double counting). Observe that it implies that

$$6 + \sum_{k\geq 7} i_k + \sum_{k\geq 5} b_k \leq 3i_3 + 2i_4 + i_5 + 2b_2 + b_3.$$

4.2. **The number of triangulations.** We now give examples of point sets for which we can compute the number of (full) triangulations.

Exercice 101 (Catalan number)**.** Show that the number of triangulations of a convex n-gon is the $(n-2)$-Catalan number $C_{n-2} := \frac{1}{n-1}\binom{2n-4}{n-2}$. (Hint: see Section 5.1).

Exercice 102 (Double chain)**.** Show that the number of full triangulations of the double chain $X_{m,n}$ with $m+n$ vertices, represented in Figure 23 (left), is $C_{m-2}C_{n-2}\binom{m+n-2}{n-1}$. (Hint: Observe that any triangulation of X_n contains all edges of the two chains, and thus is formed by three independent triangulations). Deduce that the total number of triangulations of $X_{m,n}$ is

$$\sum_{\substack{0\leq i\leq m-2\\ 0\leq j\leq n-2}} \binom{m-2}{i}\binom{n-2}{j} C_i C_j \binom{i+j+2}{i+1}.$$

Exercice 103 (Double circle)**.** Using the inclusion-exclusion formula, show that the number of full triangulations of the double circle O_n with $2n$ vertices, represented in Figure 23 (right), is $\sum_{i\in[n]}(-1)^i\binom{n}{i}C_{n+i-2}$. (Hint: a triangulation of O_n can be seen a triangulation of a convex $2n$-gon containing none of the even ears). What about all triangulations?

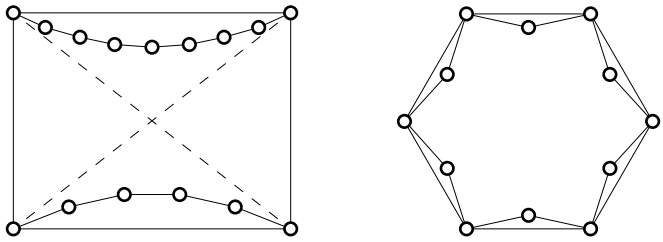

Figure 23. The double chain $X_{9,6}$ (left) and the double circle O_6 (right) configurations. Marked edges are forced in all full triangulations.

In general, we cannot give explicit formulas for the number of (full) triangulations of an arbitrary point set. However, we can give upper and lower bounds on the number of triangulations of a set of n points.

Proposition 104. *Any set of n points in general position in the plane, with i interior and b boundary points, has at least $C_{b-2}2^{i-b+2} = \Omega(2^n n^{-3/2})$ and at most $59^i\,7^b/\binom{i+b+6}{6} \leq 59^n$ full triangulations.*

Proof. We closely follow the presentation of [DRS10, p. 112 & 115] and refer the reader to the references and improvements discussed therein.

For the lower bound, denote by $m(i,b)$ the minimum number of triangulations of a point set with i interior points and b boundary points. We prove by induction that $m(i,3) \geq 2^{i-1}$. The result can be checked by case analysis or order type enumeration for up to 7 interior points, so we can assume that $i = 8$. For each interior point $\mathbf{p}$, we join $\mathbf{p}$ to the three boundary points and triangulate the three resulting triangles. If these three triangles contain i_1, i_2, and i_3 interior points respectively, induction hypothesis ensures that there are at least $2^{i_1-1}2^{i_2-1}2^{i_3-1} = 2^{i-4}$ such triangulations. We thus obtain that $m(i,3) \geq i2^{i-4} \geq 2^{i-1}$ since $i \geq 8$. Finally, if $b \geq 4$, we first choose a triangulation of the boundary points and then fill each triangle with a triangulation of the interior points. We get $m(i,b) \geq C_{b-2}2^{i-b+2}$.

For the upper bound, denote by $M(i,b)$ the maximum number of triangulations of a point set with $i+b$ points at most i are interior. For a point $\mathbf{p}$ in a point set $\mathbf{P}$, we say that a triangulation T of $\mathbf{P}$ is obtained by *inserting* $\mathbf{p}$ in a triangulation T' of $\mathbf{P} \setminus \mathbf{p}$, and that T' is obtained by *deleting* $\mathbf{p}$ in T, if all triangles of T not incident to $\mathbf{p}$ appear in T'. Observe that the number h_k of triangulations of $\mathbf{P}$ obtained by inserting $\mathbf{p}$ in a given triangulation T' and in which $\mathbf{p}$ has degree k is bounded by

- $h_3 = 1$, $h_4 \leq 3$, $h_5 \leq 9$ and $h_6 \leq 28$ if $\mathbf{p}$ is an interior point (since we need to remove $k-3$ edges of T' and connect the vertices of the resulting region to $\mathbf{p}$),
- $h_2 \leq 1$, $h_3 \leq 1$ and $h_4 \leq 2$ if $\mathbf{p}$ is a boundary point (since we need to remove $k-x$ edges of T' when x vertices of $\operatorname{conv}(\mathbf{P} \setminus \mathbf{p})$ are visible from $\mathbf{p}$).

Using this observation, we now show by induction that $M(i,b) \leq 59^i\,7^b/\binom{i+b+6}{6}$. The result is clear for $b = 3$ and $i = 0$ as $M(0,3) = 1 \leq 49/12 = 59^0\,7^3/\binom{0+3+6}{6}$. Now let $\mathbf{P}$ be a configuration of $i+b$ points, at most i of them being interior, and denote by $T(\mathbf{P})$ the number of triangulations of $\mathbf{P}$, and by $I_k(\mathbf{P})$ (resp. $B_k(\mathbf{P})$) the sum over all triangulations of $\mathbf{P}$ of the number of interior (resp. boundary) vertices of degree k. Deleting a point $\mathbf{p}$ of $\mathbf{P}$ yields a configuration of $i+b-1$ points with at most $i-1$ interior points if $\mathbf{p}$ is an interior point of $\mathbf{P}$, and of $i+b-1$ points with at most i interior points if $\mathbf{p}$ is a boundary point of $\mathbf{P}$. Moreover, the number of triangulations of $\mathbf{P}$ in which $\mathbf{p}$ has degree k is at most the number of ways of inserting $\mathbf{p}$ with degree k in triangulations of $\mathbf{P} \setminus \mathbf{p}$. Therefore, using the observations above,

$$I_3(\mathbf{P}) \leq i\,M(i-1,b), \quad I_4(\mathbf{P}) \leq 3i\,M(i-1,b), \quad I_5(\mathbf{P}) \leq 9i\,M(i-1,b), \quad I_6(\mathbf{P}) \leq 28i\,M(i-1,b),$$
$$B_2(\mathbf{P}) \leq b\,M(i,b-1), \quad B_3(\mathbf{P}) \leq b\,M(i,b-1), \quad B_4(\mathbf{P}) \leq 2b\,M(i,b-1).$$

Moreover, summing over all triangulations of $\mathbf{P}$ the last inequality of Exercice 100, we have

$$\begin{aligned} 6\,T(\mathbf{P}) + \sum_{k\geq 7} I_k(\mathbf{P}) + \sum_{k\geq 5} B_k(\mathbf{P}) &\leq 3\,I_3(\mathbf{P}) + 2\,I_4(\mathbf{P}) + I_5(\mathbf{P}) + 3\,B_2(\mathbf{P}) + B_3(\mathbf{P}) \\ &\leq 18i\,M(i-1,b) + 3b\,M(i,b-1). \end{aligned}$$

Adding all these inequalities together, we get

$$(6+i+b)\,T(\mathbf{P}) = 6\,T(\mathbf{P}) + \sum_{k\geq 3} I_k(\mathbf{P}) + \sum_{k\geq 2} B_k(\mathbf{P}) \leq 59i\,M(i-1,b) + 7b\,M(i,b-1).$$

The result follows by induction hypothesis:

$$(6+i+b)\,M(i,b) \le 59i\,M(i-1,b) + 7b\,M(i,b-1) \le 59i\,\frac{59^{i-1}\,7^b}{\binom{i+b+5}{6}} + 7b\,\frac{59^i\,7^{b-1}}{\binom{i+b+5}{6}}$$
$$= (i+b)\,\frac{59^i\,7^b}{\binom{i+b+5}{6}} = (6+i+b)\,\frac{59^i\,7^b}{\binom{i+b+6}{6}}. \qquad \square$$

4.3. **Flips.** A *flip* is an operation on triangulations of $\mathbf{P}$ defined as follows (see Figure 24):

diagonal flip: if two triangles **pqr** and **prs** form a convex quadrilateral **pqrs**, replace the diagonal **pr** by the other diagonal **qs** of **pqrs**.

insertion/deletion flip: If a point **p** is contained in the interior of a triangle **uvw**, then insert the edges **pu**, **pv**, and **pw** or *vice versa*.

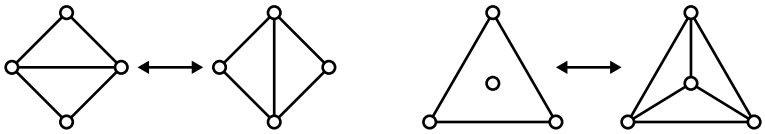

FIGURE 24. A diagonal flip (left) and an insertion/deletion flip (right).

The *flip graph* is the graph whose vertices are the triangulations of $\mathbf{P}$ and whose edges are flips between them. An example is illustrated on Figure 25.

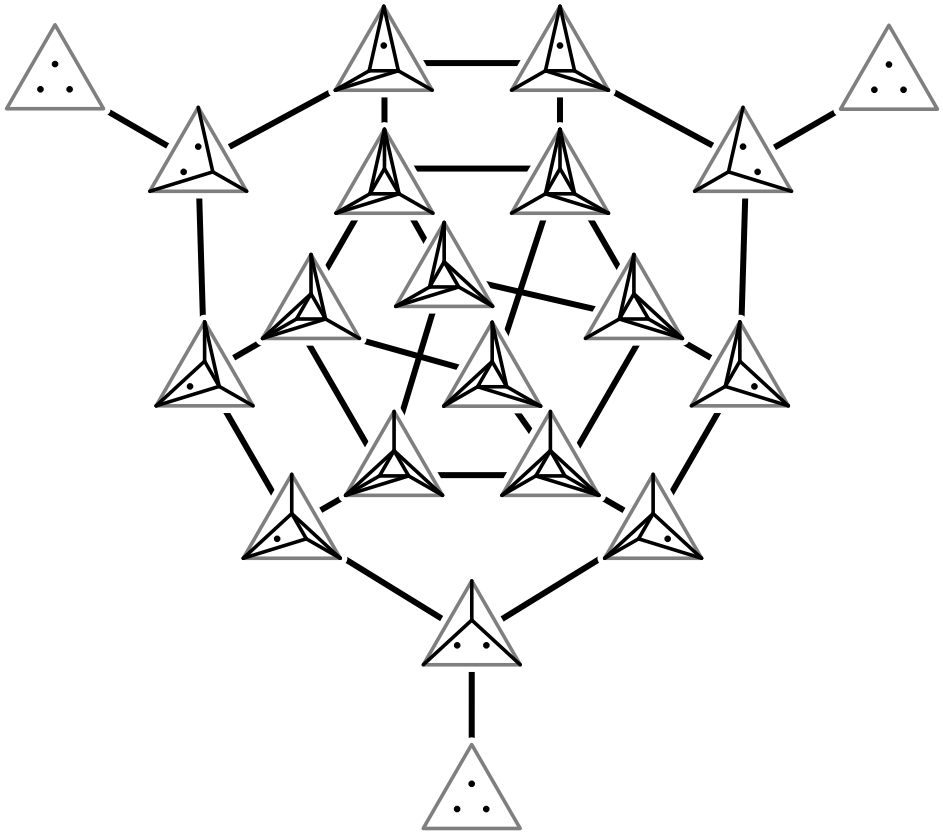

FIGURE 25. The flip graph on triangulations of a point configuration. The three copies of the trivial triangulation should coincide.

Proposition 105. *The flip graph is connected.*

Proof. This property will follow from Proposition 109 as any triangulation can be flipped to the Delaunay triangulation, even when using only diagonal flips. □

Exercice 106. The *placing triangulation* of $\mathbf{P} = \{\mathbf{p}_1, \dots, \mathbf{p}_n\}$ is constructed iteratively by placing the points $\mathbf{p}_1, \dots, \mathbf{p}_n$ one by one. The point $\mathbf{p}_i$ remains isolated if it lies in the convex hull of $\{\mathbf{p}_1, \dots, \mathbf{p}_{i-1}\}$. Otherwise, $\mathbf{p}_i$ gets connected to the points of $\mathrm{conv}\{\mathbf{p}_1, \dots, \mathbf{p}_{i-1}\}$ visible from it.

Show that any triangulation of a planar point set $\mathbf{P}$ can be flipped to the placing triangulation, and deduce Proposition 105.

Remark 107. Proposition 105 is no longer true in higher dimension. In fact, Santos proved that it already fails in dimension 5 [San00].

4.4. **Delaunay triangulation.** Let $\mathbf{P}$ be a point set in the plane. The *Voronoi region* $\mathrm{Vor}(\mathbf{p}, \mathbf{P})$ of a point $\mathbf{p} \in \mathbf{P}$ is the region of the plane closer to $\mathbf{p}$ than to any other point of $\mathbf{P}$, that is,

$$\mathrm{Vor}(\mathbf{p}, \mathbf{P}) := \left\{ \mathbf{x} \in \mathbb{R}^2 \;\middle|\; \|\mathbf{x} - \mathbf{p}\| \leq \|\mathbf{x} - \mathbf{q}\| \text{ for all } \mathbf{q} \in \mathbf{P} \right\}.$$

The Voronoi regions are polygonal regions, they are pairwise internally disjoint and they cover the complete plane. The *Voronoi diagram* $\mathrm{Vor}(\mathbf{P})$ of $\mathbf{P}$ is the polygonal diagram formed by the Voronoi regions $\mathrm{Vor}(\mathbf{p}, \mathbf{P})$ for all $\mathbf{p} \in \mathbf{P}$. See Figure 26 (left).

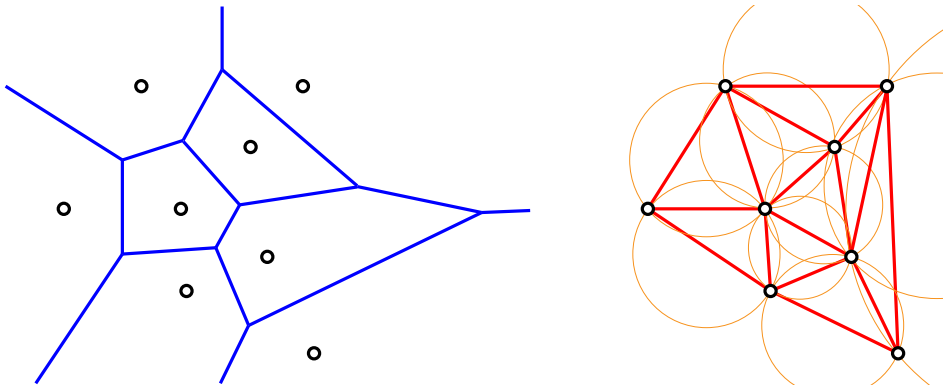

FIGURE 26. The Voronoi diagram (left) and the Delaunay triangulation (right) of a planar point set.

The *Delaunay triangulation* $\mathrm{Del}(\mathbf{P})$ of $\mathbf{P}$ is the dual geometric triangulation to the Voronoi diagram $\mathrm{Vor}(\mathbf{P})$: its vertex set is the point set $\mathbf{P}$ and its edges connect two points $\mathbf{p}$ and $\mathbf{q}$ if the Voronoi regions $\mathrm{Vor}(\mathbf{p}, \mathbf{P})$ and $\mathrm{Vor}(\mathbf{q}, \mathbf{P})$ intersect. Note that it is a triangulation given that no circle contains four or more point of the set $\mathbf{P}$. The following statement characterizes the edges and the triangles in the Delaunay triangulation. An *empty circle* is a circle whose interior disk contains no point of $\mathbf{P}$. See Figure 26 (right).

Proposition 108. *Let* $\mathbf{p}, \mathbf{q}, \mathbf{r}$ *be points of* $\mathbf{P}$.

(i) $\mathbf{pq}$ *is a Delaunay edge iff there exists an empty circle passing through* $\mathbf{p}$ *and* $\mathbf{q}$.
(ii) $\mathbf{pqr}$ *is a Delaunay triangle iff the circumcircle of* $\mathbf{p}, \mathbf{q}, \mathbf{r}$ *is an empty circle.*

Proof. Exercice. (Hint: Consider the circle centered at a point of the intersection of the Voronoi regions and passing through the Voronoi sites). □

In any triangulation, if $\mathbf{pqr}$ and $\mathbf{pqs}$ are two triangles such that $\mathbf{s}$ is contained in the circumcircle of $\mathbf{pqr}$, then the flip of edge $\mathbf{pq}$ to edge $\mathbf{rs}$ is always possible and is called a *Lawson flip*.

Proposition 109. *From any initial triangulation* T *of a planar point set* $\mathbf{P}$*, repeatedly performing Lawson flips leads to the Delaunay triangulation* $\mathrm{Del}(\mathbf{P})$.

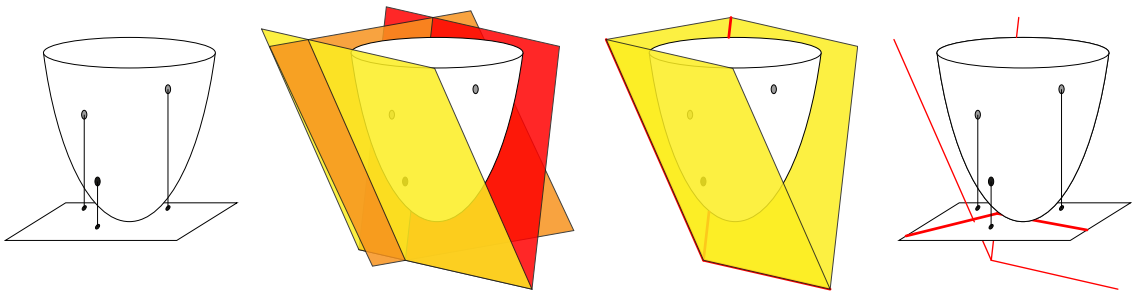

FIGURE 27. The Voronoi diagram by projection of the upper enveloppe of the tangent planes to the paraboloid.

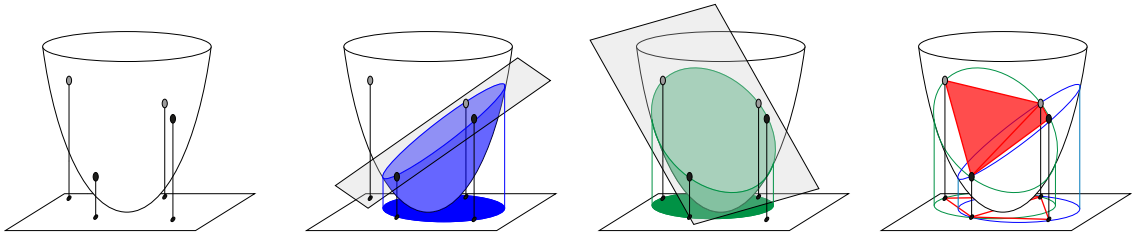

FIGURE 28. The Delaunay triangulation by projection of the lower convex hull of the points on the paraboloid.

This result will follow from the following interpretation of the Delaunay triangulation and of the corresponding flips. See the illustrations in Figure 27 and Figure 28.

Proposition 110. *Let $\mathcal{P}$ denote the paraboloïd of equation $z = x^2 + y^2$. For $\mathbf{p} = (x, y) \in \mathbb{R}^2$, we denote by $\hat{\mathbf{p}} = (x, y, x^2 + y^2)$ its lifted point to the paraboloïd $\mathcal{P}$.*

(i) The Voronoi diagram $\mathrm{Vor}(\mathbf{P})$ *is the vertical projection of the upper convex hull of the planes tangent to the paraboloïd $\mathcal{P}$ to the lifted points $\hat{\mathbf{p}}$ for $\mathbf{p} \in \mathbf{P}$.*

(ii) The Delaunay triangulation $\mathrm{Del}(\mathbf{P})$ *is the vertical projection of the lower convex hull of the lifted points $\hat{\mathbf{p}}$ for $\mathbf{p} \in \mathbf{P}$.*

Proof. The plane $H(\mathbf{p})$ tangent to the paraboloïd at the lifted point $\hat{\mathbf{p}}$ is defined by the equation $z = 2\langle \mathbf{p} | \mathbf{x} \rangle - \|\mathbf{p}\|^2$. Therefore, for two points $\mathbf{p}, \mathbf{q} \in \mathbf{P}$, the hyperplane $H(\mathbf{p})$ is above the hyperplane $H(\mathbf{q})$ iff $\|\mathbf{p} - \mathbf{x}\| \leq \|\mathbf{q} - \mathbf{x}\|$. This proves (i).

To prove (ii), we show that the portion of the paraboloïd below the plane defined by the lifted points $\hat{\mathbf{p}}, \hat{\mathbf{q}}, \hat{\mathbf{r}}$ projects to the disk circumscribed to $\mathbf{p}, \mathbf{q}, \mathbf{r}$. Indeed, for a point (x, y, z) in this portion, we have $z = x^2 + y^2$ and $z \leq \lambda x + \mu y$ for some $\lambda, \mu \in \mathbb{R}$. This leads to the equation $(x - \lambda/2)^2 + (y - \mu/2)^2 \leq \lambda^2/4 + \mu^2/4$ of a disk. Finally, the circle defining this disk clearly contains $\mathbf{p}, \mathbf{q}, \mathbf{r}$. □

Exercice 111. Using Proposition 110, prove Proposition 109. What is the maximal possible number of Lawson flips required to reach the Delaunay triangulation?

Exercice 112 (A non-Delaunay triangulation)**.** Prove that the triangulated map illustrated on Figure 29 (left) cannot be realized as a Delaunay triangulation (Hint: The sum of the angles marked a, b, or c in a Delaunay realization cannot exceed 3π, so that one of the angles marked d would exceed π).

Exercice 113 (Stacked Delaunay triangulations)**.** We say that a triangulation T is *stacked* if

- either T is reduced to a triangle,
- or T is obtained from a stacked triangulation refining a triangle **pqr** into three triangles **pqt**, **qrt**, and **prt** (one can imagine that we stacked a flat tetrahedron **pqrt** on the triangle **pqr**).

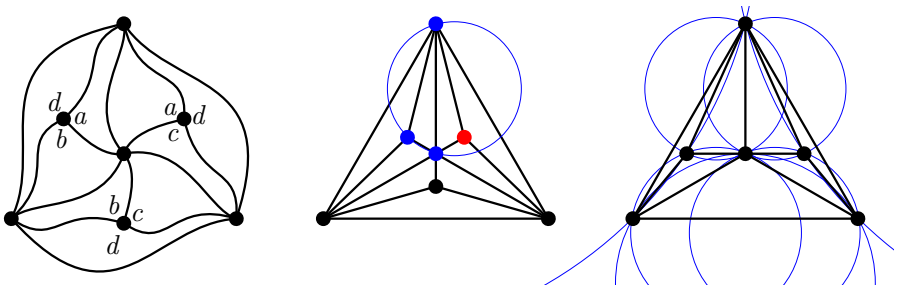

FIGURE 29. A triangulated map M (left), a geometric realization of M (middle) that is not Delaunay Delaunay (the red point violates the circumcircle to the blue points), an a Delaunay realization of M minus a vertex (right).

The *construction tree* of T is the tree whose nodes correspond to triangles of T and where the children of triangle **pqr** are the three triangles **pqt**, **qrt**, **prt** refining it. See Figure 30 (we just forgot colors from Figure 13).

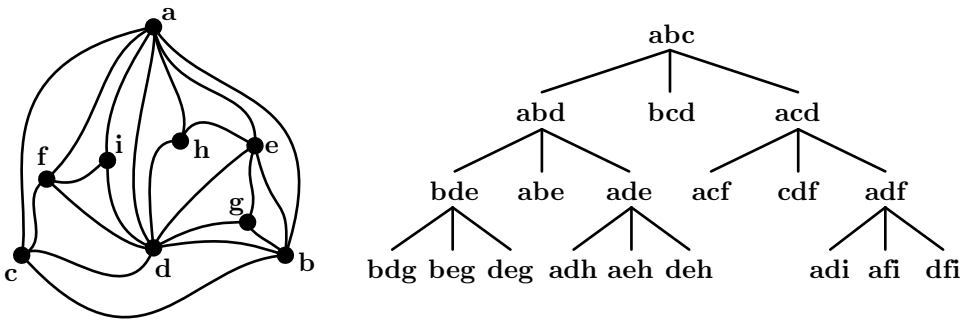

FIGURE 30. A stacked triangulation (left) and its construction tree (right).

(1) Consider a Delaunay triangulation T with an internal vertex **t** of degree 3, and denote by **p**, **q** and **r** the three vertices adjacent to **t** and by R the triangles of T distinct from **pqt**, **qrt**, and **prt**. Since **t** lies in the exterior of all circumcircles to the triangles of R, there exists a small disk D centered at **t** and disjoint from the circumcircles to the triangles of R. Choose a point **u** in $D \cap$ **pqt** and **v** in **prt** both on the tangent to the circumcircle of **qrt** at **t**. Show that the triangulation obtained by refining **pqt** with **u** and/or **prt** with **v** is still a Delaunay triangulation.
(2) Deduce that a stacked triangulation is realizable as a Delaunay triangulation if and only if its construction tree has no ternary node after deletion of its leaves (Note: in contrast, Exercice 43 describes a TD-Delaunay realization for any stacked triangulation).
(3) Generalize these results to arbitrary dimension.
(4) Using stereographic projection, derive a characterization of the stacked polytopes (see Section 3.4.2) which are inscribable in a sphere (*i.e.* realizable by a polytope with all vertices on the sphere).

4.5. **Regular triangulations and subdivisions.** Let $\mathbf{P}$ be a planar point set and $\omega : \mathbf{P} \to \mathbb{R}$ a height function. We denote by $S(\mathbf{P}, \omega)$ the polyhedral subdivision of $\mathbf{P}$ obtained as the projection of the lower convex hull of the lifted point set $\{(\mathbf{p}, \omega(\mathbf{p})) \mid \mathbf{p} \in \mathbf{P}\}$. A triangulation (or a polyhedral subdivision) T is *regular* if there exists a height function $\omega : \mathbf{P} \to \mathbb{R}$ such that $T = S(\mathbf{P}, \omega)$.

When a point lies in the interior of a polygonal region of $S(\mathbf{P}, \omega)$, it can be lifted on or above the lower envelope of the lifted points. We distinguish these subdivisions by drawing the point or not in the projection. See Figure 32.

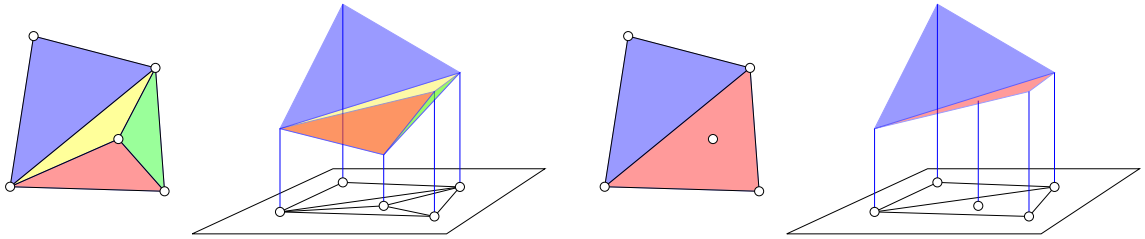

FIGURE 31. Two regular triangulations with some valid height functions.

Example 114. Consider the point configuration $\mathbf{P} = \{(0,0),(3,0),(0,3),(3,3),(1,1)\}$. It has nine regular polyhedral subdivisions, four of which are triangulations

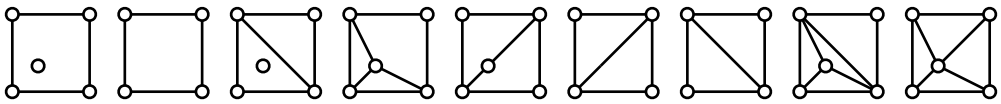

FIGURE 32. Regular subdivisions of the point set $\{(0,0),(3,0),(0,3),(3,3),(1,1)\}$. We only mark the central point when it lies on the lower hull of the lifted points.

Exercice 115. Find a height function for each of these regular subdivisions. How can you be sure that we did not forget any regular subdivision? (Hint: see the next section).

Examples of regular triangulations of $\mathbf{P}$ are the placing and the pulling triangulations:

(1) The placing triangulation (see Exercice 106) is the regular triangulation obtained from a lifted function $\omega : \mathbf{P} \to \mathbb{R}$ such that $\omega(\mathbf{p}_{i+1}) \gg \omega(\mathbf{p}_i) > 0$.
(2) The *pulling triangulation* is the regular triangulation obtained from a lifted function ω such that $\omega(\mathbf{p}_{i+1}) \ll \omega(\mathbf{p}_i) < 0$.

However, not all triangulations are regular. The classical example (called "mother of all example" in [DRS10]) is represented on Figure 33. The refinement poset on regular subdivisions of this point configuration is represented in Figure 34.

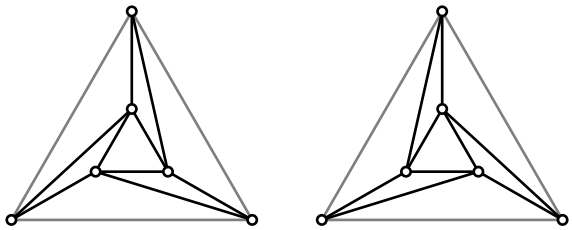

FIGURE 33. Two non-regular triangulations.

Exercice 116. Show that the triangulations of Figure 33 are not regular. (Hint: suppose their exists a height function whose lower envelope projects to one of these triangulations. Up to an affine function, assume that the height of the three interior vertices is 0, and give inequalities on the height of the remaining three vertices to find a cyclic contradiction).

Exercice 117. Show that all triangulations of a point set in convex position are regular.

4.6. **Secondary polytope.** We now study the secondary polytope and secondary fan of a planar point set. These objects were introduced by Gelfand, Kapranov, and Zelevinsky [GKZ94]. The results presented here for planar point sets extend to higher dimension. See [DRS10].

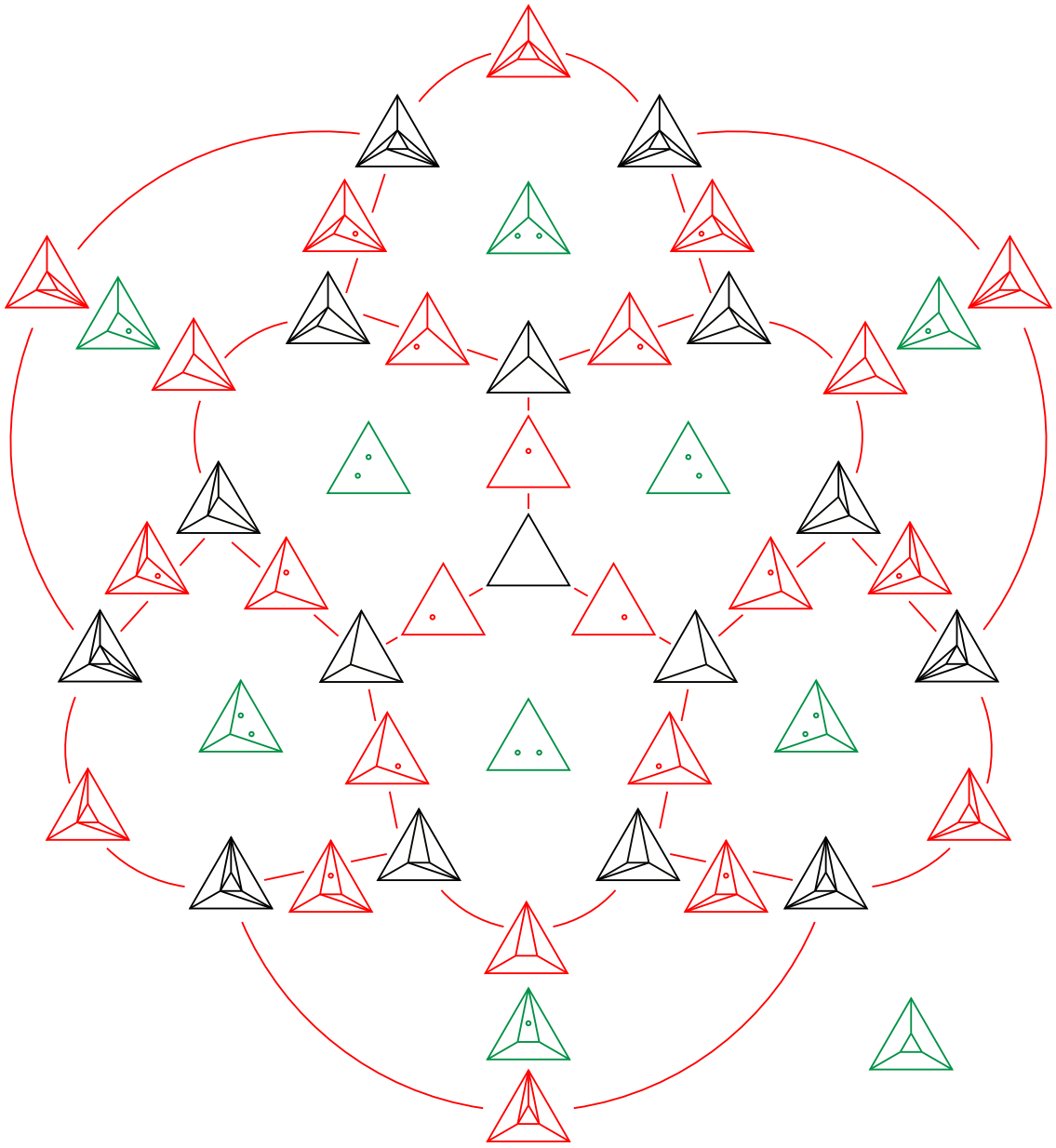

FIGURE 34. The refinement poset on regular subdivisions of the mother of all configuration.

Definition 118. The *volume vector* of a triangulation T of a point set $\mathbf{P}$ is the vector of $\mathbb{R}^{\mathbf{P}}$ defined by

$$\Phi(T) := \left(\sum_{\mathbf{p} \in \triangle \in T} \mathrm{vol}(\triangle) \right)_{\mathbf{p} \in \mathbf{P}}$$

In other words, the coordinate corresponding to point $\mathbf{p} \in \mathbf{P}$ is the area of the star of $\mathbf{p}$ in T. The *secondary polytope* $\Sigma\mathsf{Poly}(\mathbf{P})$ of $\mathbf{P}$ is the convex hull of the volume vectors of all triangulations of $\mathbf{P}$,

$$\Sigma\mathsf{Poly}(\mathbf{P}) := \mathrm{conv}\left\{ \Phi(T) \mid T \text{ triangulation of } \mathbf{P} \right\}.$$

For example, the secondary polytope of the mother of all example is represented in Figure 35.

Definition 119. The *secondary cone* of a subdivision S of a point set $\mathbf{P}$ is the polyhedral cone

$$C(S) := \left\{ \omega \in \mathbb{R}^{\mathbf{P}} \;\middle|\; S \text{ refines } S(\mathbf{P}, \omega) \right\}$$

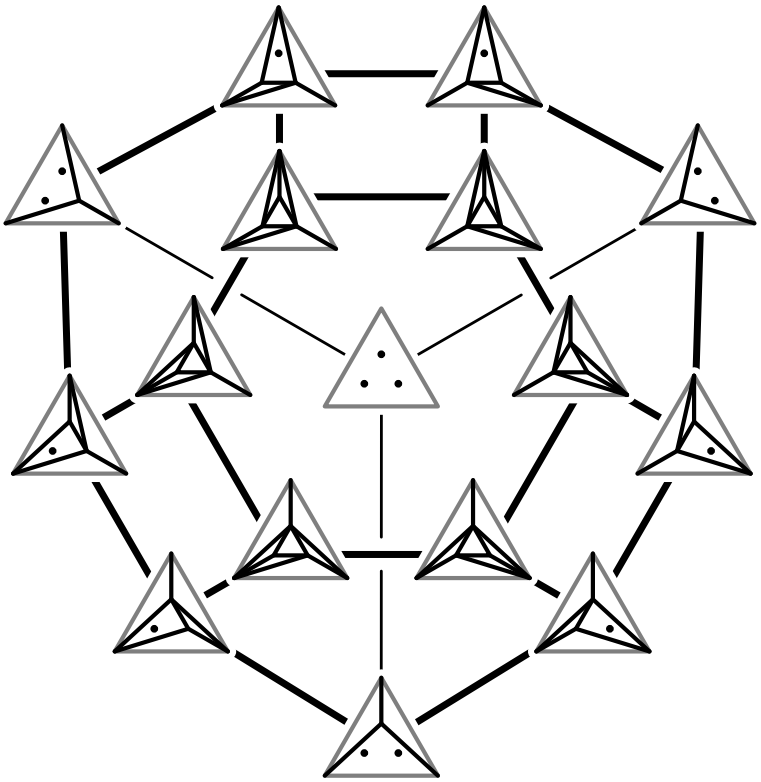

FIGURE 35. The secondary polytope of the mother of all example.

corresponding to all height functions whose lower convex hull projects to S. The *secondary fan* $\Sigma\mathsf{Fan}(\mathbf{P})$ of $\mathbf{P}$ is collection of the secondary cones of all subdivisions of $\mathbf{P}$,

$$\Sigma\mathsf{Fan}(\mathbf{P}) := \{C(S) \mid S \text{ subdivision of } \mathbf{P}\}.$$

It is a complete polyhedral fan.

Example 120. Consider the point configuration $\mathbf{P} = \{(0,0),(3,0),(0,3),(3,3),(1,1)\}$ of Example 114. The volume vectors of the four triangulations are given by:

$$(9,9/2,9/2,9,0) \qquad (9/2,9,9,9/2,0) \qquad (3,15/2,15/2,9/2,9/2) \qquad (3,9/2,9/2,6,9).$$

The projection of the secondary polytope $\Sigma\mathsf{Poly}(\mathbf{P})$ on the plane generated by the last two coordinate vectors is represented in Figure 36 (left). We look at what height functions produce the nine regular subdivisions of Figure 32. Without loss of generality (affine invariance), we restrict our attention to the height functions $\omega : \mathbf{P} \to \mathbb{R}$ with $\omega_1 = \omega_2 = \omega_3 = 0$. The nine regular subdivisions of Figure 32 then correspond to the following inequalities:

(i) $\omega_4 = \omega_5 = 0$,
(ii) $\omega_4 = 0$, $\omega_5 > 0$,
(iii) $\omega_4 > 0$, $\omega_5 = 0$,
(iv) $\omega_4 + 3\omega_5 = 0$, $\omega_5 < 0$,
(v) $\omega_4 < 0$, $\omega_4 - 3\omega_5 = 0$,
(vi) $\omega_4 < 0$, $\omega_4 - 3\omega_5 < 0$,
(vii) $\omega_4 > 0$, $\omega_5 > 0$,
(viii) $\omega_4 + 3\omega_5 > 0$, $\omega_5 < 0$,
(ix) $\omega_4 + 3\omega_5 < 0$, $\omega_4 - 3\omega_5 > 0$.

The corresponding secondary fan $\Sigma\mathsf{Fan}(\mathbf{P})$ is represented in Figure 36 (middle). Finally, the refinement poset of regular subdivisions of $\mathbf{P}$ is represented in Figure 36 (right).

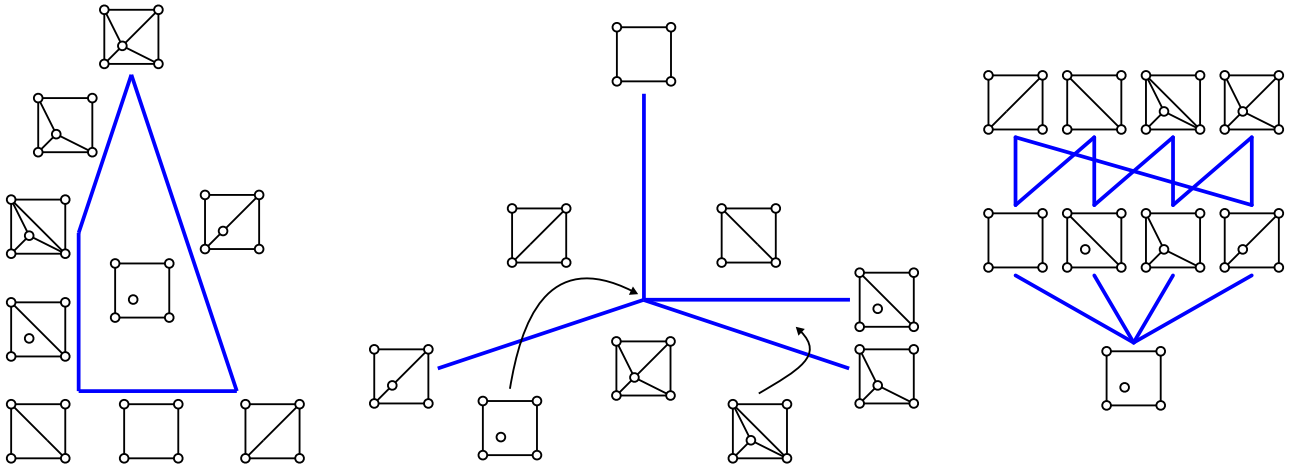

FIGURE 36. The secondary polytope (left), the secondary fan (middle), and the poset of regular subdivisions (right) of the set $\{(0,0),(3,0),(0,3),(3,3),(1,1)\}$.

Theorem 121 (Gelfand, Kapranov, and Zelevinsky [GKZ94])**.** *Let* $\mathbf{P}$ *be a planar point set in general position.*

(i) The dimension of the secondary polytope $\Sigma\mathsf{Poly}(\mathbf{P})$ *is* $|\mathbf{P}|-3$.
(ii) The secondary fan $\Sigma\mathsf{Fan}(\mathbf{P})$ *is the inner normal fan of the secondary polytope* $\Sigma\mathsf{Poly}(\mathbf{P})$.
(iii) The face lattice of the secondary polytope $\Sigma\mathsf{Poly}(\mathbf{P})$ *is isomorphic to the refinement poset of regular subdivisions of* $\mathbf{P}$.

Proof. We start with (i). The lower bound on $\dim(\Sigma\mathsf{Poly}(\mathbf{P}))$ is obtained by induction on $|\mathbf{P}|$. It is clear when $|\mathbf{P}|=3$ since the secondary polytope is reduced to a single point. For $|\mathbf{P}|\geq 4$, consider an arbitrary point $\mathbf{p}\in\mathbf{P}$. If $\mathbf{p}$ lies in the convex hull of $\mathbf{P}\smallsetminus\mathbf{p}$, a triangulation T of $\mathbf{P}$ is a triangulation of $\mathbf{P}\smallsetminus\mathbf{p}$ iff $\Phi(T)_{\mathbf{p}}=0$. Therefore,

$$\Sigma\mathsf{Poly}(\mathbf{P}\smallsetminus\mathbf{p})=\Sigma\mathsf{Poly}(\mathbf{P})\cap\left\{\mathbf{x}\in\mathbb{R}^{\mathbf{P}}\;\middle|\;x_{\mathbf{p}}=0\right\}.$$

Similarly, if $\mathbf{p}$ is on the convex hull of $\mathbf{P}$, we obtain that

$$\Sigma\mathsf{Poly}(\mathbf{P}\smallsetminus\mathbf{p})=\Sigma\mathsf{Poly}(\mathbf{P})\cap\left\{\mathbf{x}\in\mathbb{R}^{\mathbf{P}}\;\middle|\;x_{\mathbf{p}}=\mathrm{vol}(\mathrm{conv}(\mathbf{P}))-\mathrm{vol}(\mathrm{conv}(\mathbf{P}\smallsetminus\mathbf{p}))\right\}.$$

It immediately follows by induction that $\dim(\Sigma\mathsf{Poly}(\mathbf{P}))\geq|\mathbf{P}|-3$. To prove the reverse inequality, we exhibit three independent linear relations satisfied by the volume vectors of the triangulations of $\mathbf{P}$. First, since a triangulation T of $\mathbf{P}$ decomposes the convex hull of $\mathbf{P}$ into triangles, we obtain:

$$\mathrm{vol}(\mathrm{conv}(\mathbf{P}))=\sum_{\triangle\in T}\mathrm{vol}(\triangle)=\sum_{\triangle\in T}\sum_{\mathbf{p}\in\triangle}\frac{\mathrm{vol}(\triangle)}{3}=\frac{1}{3}\sum_{\mathbf{p}\in\mathbf{P}}\sum_{\mathbf{p}\in\triangle\in T}\mathrm{vol}(\triangle)=\frac{1}{3}\sum_{\mathbf{p}\in\mathbf{P}}\Phi(T)_{\mathbf{p}}.$$

The other two linear relations are obtained from the center of mass $\mathrm{cm}(\mathrm{conv}(\mathbf{P}))$ of the convex hull of $\mathbf{P}$:

$$\mathrm{vol}(\mathrm{conv}(\mathbf{P}))\cdot\mathrm{cm}(\mathrm{conv}(\mathbf{P}))=\sum_{\triangle\in T}\mathrm{vol}(\triangle)\cdot\mathrm{cm}(\triangle)=\sum_{\triangle\in T}\mathrm{vol}(\triangle)\cdot\left(\frac{1}{3}\sum_{\mathbf{p}\in\triangle}\mathbf{p}\right)=\frac{1}{3}\sum_{\mathbf{p}\in\mathbf{P}}\Phi(T)_{\mathbf{p}}\cdot\mathbf{p},$$

since the center of mass of a triangle $\mathbf{pqr}$ coincides with its vertex barycenter $(\mathbf{p}+\mathbf{q}+\mathbf{r})/3$. Note that this equality between two points in the plane gives two independent relations.

We now prove (ii). Consider a lifting function $\omega:\mathbf{P}\to\mathbb{R}$ and a triangulation T of $\mathbf{P}$. Let $f_{T,\omega}:\mathbb{R}^2\to\mathbb{R}$ denote the piecewise linear map such that $f_{T,\omega}(\mathbf{p})=\omega(\mathbf{p})$ for $\mathbf{p}\in\mathbf{P}$, and which is affine on each triangle of T. Then the volume below the surface defined by $f_{T,\omega}$ is

$$\int_{\mathrm{conv}(\mathbf{P})}f_{T,\omega}(\mathbf{x})\,d\mathbf{x}=\sum_{\triangle\in T}\int_{\triangle}f_{T,\omega}(\mathbf{x})\,d\mathbf{x}=\sum_{\triangle\in T}\frac{\mathrm{vol}(\triangle)}{3}\sum_{\mathbf{p}\in\triangle}\omega(\mathbf{p})=\frac{1}{3}\sum_{\mathbf{p}\in\mathbf{P}}\omega(\mathbf{p})\cdot\sum_{\mathbf{p}\in\triangle\in T}\mathrm{vol}(\triangle)=\frac{\langle\Phi(T)|\omega\rangle}{3}.$$

It follows that for any lifting function $\omega : \mathbf{P} \to \mathbb{R}$ and any triangulation T of $\mathbf{P}$ distinct from the regular triangulation $S(\mathbf{P}, \omega)$ induced by ω, we have

$$\langle \Phi(S(\mathbf{P}, \omega))|\omega\rangle < \langle \Phi(T)|\omega\rangle.$$

Said differently, for any regular triangulation T of $\mathbf{P}$, the normal cone of $\Phi(T)$ in $\Sigma\mathsf{Poly}(\mathbf{P})$ is the secondary cone $C(T)$ of T. This achieves the proof of Point (ii).

Finally, Point (iii) is immediate from (ii) and the definition of the secondary fan. □

Exercice 122. Compute the volume vectors of all triangulations of the mother of all configuration. What happens to the volume vectors of the two non-regular triangulations? What happens if we slightly rotate the three outer vertices clockwise? (Hint: show that one of the two triangulations of Figure 33 becomes regular while the other remains non-regular). Deduce that some triangulations are non-regular even under small perturbations of their vertex sets.

5. Permutahedra and associahedra

This section focusses on the associahedron. The boundary complex of its polar is isomorphic to the simplicial complex of crossing-free internal diagonals of a convex polygon. In particular, its vertices correspond to triangulations of the polygon, and its edges correspond to flips between triangulations. Such a polytope can be constructed as the secondary polytope of a convex polygon. We present in this section an alternative construction of the associahedron [Lod04], with a more combinatorial flavor. It connects the associahedron to the braid arrangement and to the permutahedron.

5.1. **Catalan families.** This section is devoted to triangulations of a convex polygon, which are combinatorially equivalent to other relevant Catalan families. The following proposition provides some classical examples. A list of Catalan families can be found in [Sta12, Exercice 6.19].

Proposition 123. *The following Catalan families are in bijective correspondence:*

(i) triangulations of a convex $(n+3)$-gon,
(ii) binary trees with $n+1$ internal nodes,
(iii) rooted plane trees with $n+2$ nodes,
(iv) Dyck paths of length $2n+2$ (i.e. paths with up steps $\nearrow$ and down steps $\searrow$ starting at $(0,0)$ finishing at $(n+1,n+1)$ and which never go below the horizontal axis),
(v) valid bracketings of a non-associative product on $n+2$ elements.

Proof. The bijections between the first four families are illustrated on Figure 37. Finally, a binary tree gives a bracketing of its leafs. For example, the binary tree of Figure 37 corresponds to the bracketing $((x_1((x_2x_3)x_4)(x_5x_6))$.

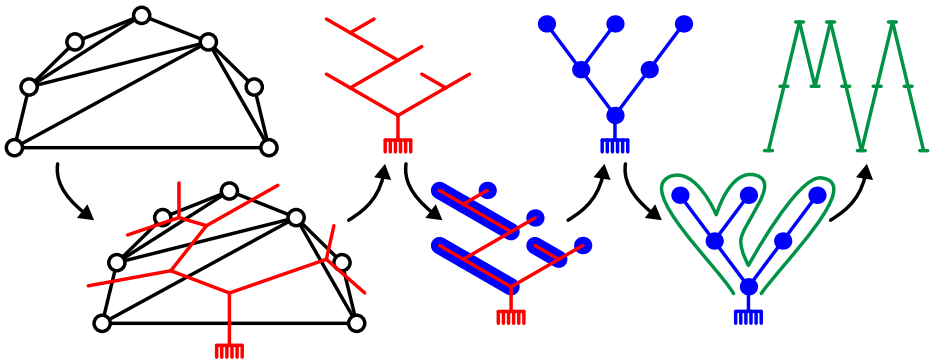

Figure 37. Bijections between Catalan families. □

Remark 124. It is not difficult (exercice) to work out what does a flip between two triangulations translates through these bijections to the different Catalan families. In particular, it is called a rotation on binary trees. This is illustrated on Figure 38.

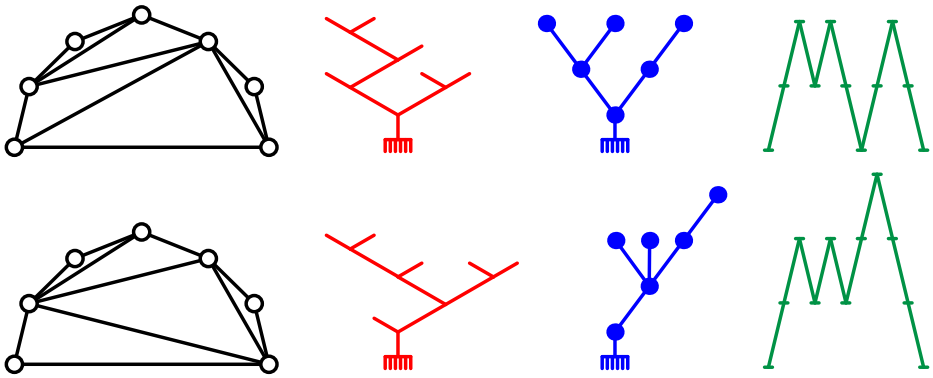

Figure 38. Flips on the different Catalan families.

Proposition 125. *The number of triangulations of the $(n+3)$-gon is the $(n+1)$st Catalan number*

$$C_{n+1} = \frac{1}{n+2}\binom{2n+2}{n+1}.$$

Proof. There are several different possible proofs of this result. Here, we use a recursion formula on the number T_n of triangulations of the $(n+3)$-gon. This formula translates the fact that one can transform a triangulation of the $(n+3)$-gon into a triangulation of the $(n+2)$-gon by flattening the triangle containing the boundary edge $[0, n+2]$. This transformation is not one-to-one: the number of triangulations of the $(n+3)$-gon that could give rise to a given triangulation T of the $(n+2)$-gon is the degree of vertex 0 in T. Since the average degree of vertex 0 in a triangulation of the $(n+2)$-gon is $2(2n+1)/(n+2)$, we get the induction formula

$$T_n = \frac{2(2n+1)}{n+2} T_{n-1}.$$

From this, we deduce that

$$T_n = \frac{2^{n+1}(2n+1)(2n-1)\dots 3\cdot 1}{(n+2)(n+1)\dots 2\cdot 1} = \frac{(2n+2)!}{(n+2)!(n+1)!} = \frac{1}{n+2}\binom{2n+2}{n+1} = C_{n+1}. \qquad \square$$

Exercice 126. (1) Prove that the number T_n of triangulations of the $(n+3)$-gon satisfies

$$T_n = \sum_{j\in[n+1]} T_{j-2}\cdot T_{n-j}.$$

(Hint: Decompose any triangulation of the $(n+3)$-gon as the triangle $0, j, n+2$ containing the boundary edge $[0, n+2]$ together with a triangulation of the $(j+1)$-gon and a triangulation of the $(n+3-j)$-gon).

(2) Derive from this equation that the generating function

$$T(x) := \sum_{n\in\mathbb{N}} T_{n-1}\, x^n$$

satisfies the functional equation

$$T(x) = 1 + xT(x)^2.$$

(3) Deduce that

$$T(x) = \frac{1+\sqrt{1-4x}}{2x}.$$

(4) Using that

$$(1+y)^{1/2} = \sum_{n\in\mathbb{N}} \binom{1/2}{n} y^n, \qquad \text{where } \binom{1/2}{n} = \frac{1/2(1/2-1)(1/2-2)\dots(1/2-n+1)}{n!},$$

deduce the formula for the Catalan number.

Exercice 127. Show directly that the inductive formula in the proof of Proposition 125 holds for the other families of Proposition 123.

Proposition 128. *The number of non-crossing sets of k diagonals of the $(n+3)$-gon is*

$$\frac{1}{n+3+k}\binom{n+3+k}{k+1}\binom{n}{k}.$$

Exercice 129. Check that Proposition 128 indeed gives the expected number of diagonals, flips, and triangulations.

5.2. **The associahedron as a simplicial complex.** The *simplicial associahedron* is the simplicial complex of crossing-free subsets of diagonals of the $(n+3)$-gon. We have

- vertices $\longleftrightarrow$ diagonals of the $(n+3)$-gon,
- ridges $\longleftrightarrow$ flips between triangulations,
- facets $\longleftrightarrow$ triangulations of the $(n+3)$-gon.

This simplicial complex was defined by Stasheff in [Sta63].

Exercice 130. What is the number of vertices, ridges, facets of the simplicial associahedron? What is the number of k-dimensional faces. (Hint: check Proposition 128).

The 2-dimensional simplicial associahedron and its dual are represented in Figure 39. The simplicial associahedron can be realized as the boundary complex of the secondary polytope of a convex polygon, see *e.g.* Figure 40 (left). We present below other relevant constructions of the associahedron, with a more combinatorial flavor.

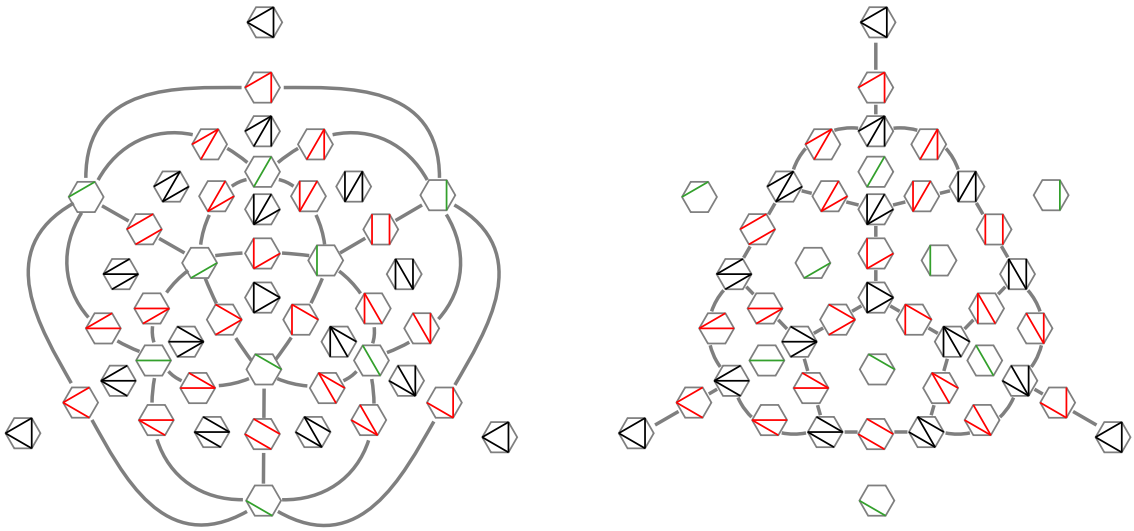

FIGURE 39. The 2-dimensional simplicial associahedron (left) and its dual (right).

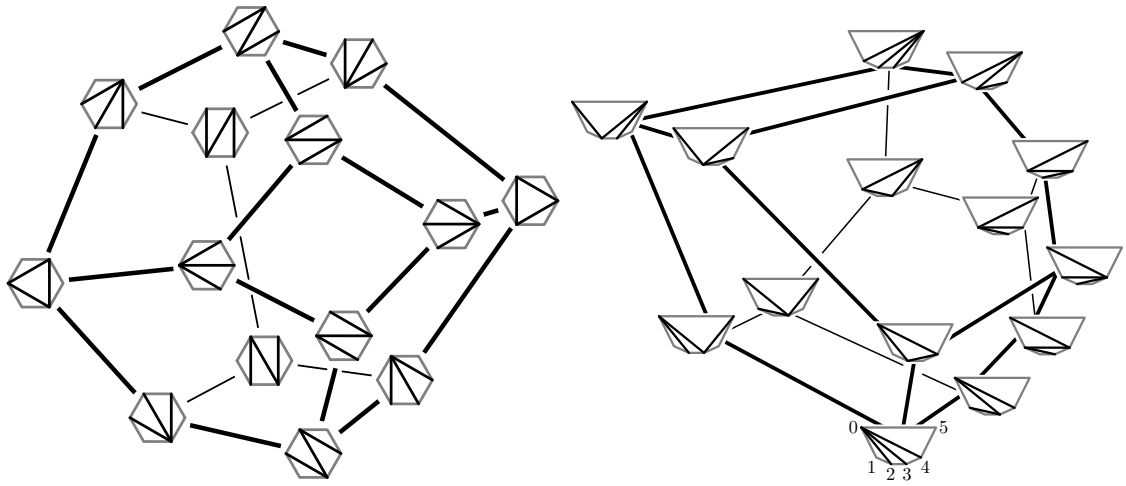

FIGURE 40. Two realizations of the 3-dimensional associahedron: as the secondary polytope of a regular hexagon (left) and using Loday's coordinates (right).

The facet-ridge graph of the associahedron is the flip graph on triangulations of a polygon. The diameter of this graph has been extensively studied. The following exercices prepare the recent result of Pournin [Pou14] which is too technical to be proven in these notes.

Exercice 131. Show that the diameter of the n-dimensional associahedron is at most $2n-4$ for $n \geq 10$. (Hint: Denote by T_i the triangulation of the $(n+3)$-gon where all diagonal are incident to vertex i. Show that any triangulation T can be flipped to T_i using at most $|T \smallsetminus T_i|$ flips. Using that the average degree of a vertex in the union of two triangulations is $4-12/(n+3)$, conclude to obtain the bound $2n-4$).

Exercice 132. Show that the diameter of the n dimensional associahedron is at least $3n/2$. (Hint: show that any two triangulations of a $2m$-gon containing respectively all even and all odd ears, are at distance at least $3m$).

Theorem 133 (Pournin [Pou14])**.** *The diameter of the n-dimensional associahedron is precisely $2n-4$ for $n > 9$.*

5.3. **The permutahedron and the braid arrangement.** The following polytope is a classical polytope with applications to algebraic combinatorics and Coxeter groups [Hum90]. We denote by $(\mathbf{e}_1, \dots, \mathbf{e}_{n+1})$ the canonical basis of $\mathbb{R}^{n+1}$.

Definition 134. The *permutahedron* $\mathsf{Perm}(n)$ is the convex polytope obtained equivalently as

(i) either the convex hull of the vectors $\sum_{i\in[n+1]} \sigma_i \mathbf{e}_i \in \mathbb{R}^{n+1}$ for all permutations $\sigma \in \mathfrak{S}_{n+1}$,

(ii) or the intersection of the hyperplane $\mathbb{H} := \mathbf{H}^{=}([n+1])$ with the half-spaces $\mathbf{H}^{\geq}(R)$ for $\varnothing \neq R \subset [n+1]$, where

$$\mathbf{H}^{=}(R) := \left\{ \mathbf{x} \in \mathbb{R}^{n+1} \;\middle|\; \sum_{r\in R} x_r = \binom{|R|+1}{2} \right\} \quad \text{and} \quad \mathbf{H}^{\geq}(R) := \left\{ \mathbf{x} \in \mathbb{R}^{n+1} \;\middle|\; \sum_{r\in R} x_r \geq \binom{|R|+1}{2} \right\},$$

(iii) or the Minkowski sum of all segments $[\mathbf{e}_r, \mathbf{e}_s]$ for $r \neq s \in [n+1]$.

The normal fan of the permutahedron is the fan defined by the *braid arrangement* in $\mathbb{H}$, *i.e.* the arrangement of the hyperplanes $\{\mathbf{x} \in \mathbb{H} \mid x_r = x_s\}$ for $r \neq s \in [n+1]$. Its k-dimensional cones correspond to the surjections from $[n+1]$ to $[k+1]$, or equivalently to the ordered partitions of $[n+1]$ into $k+1$ parts.

Exercice 135. (1) Show that the set of surjections from $[n+1]$ to $[k+1]$ is in bijection with the set of ordered partitions of $[n+1]$ into $k+1$ parts. (Hint: partition $[n+1]$ according to the images under a surjection).

(2) Show that the number of surjections from a finite set A to a finite set B, with $|A| \geq |B|$ is given by

$$\sum_{p=0}^{|B|} (-1)^p \binom{|B|}{p} (|B|-p)^{|A|}.$$

(Hint: Apply the inclusion-exclusion formula to the sets $X_b := \{f : A \to B \mid b \notin f(A)\}$ for $b \in B$ to compute the number of applications from A to B that are not surjections, and conclude).

(3) Deduce the number of k-dimensional faces of the permutahedron.

The 3-dimensional permutahedron and braid arrangement are represented in Figures 41 and 42 respectively.

5.4. **Loday's associahedron.** Let $\mathbf{P}$ denote a convex $(n+3)$-gon whose vertices are labeled from left to right by $0, \dots, n+2$ and such that $[0, n+2]$ is the top boundary edge.

For a triangulation T of $\mathbf{P}$, we denote by T^* the corresponding binary tree, whose nodes are labeled in infix search labeling. Equivalently (exercice), the node dual to triangle ijk with $i < j < k$ is labeled by j^*. The *Loday vector* of the triangulation T is the vector $\mathrm{Lod}(T)$ whose jth coordinate is the product of the number of leaves in the left subtree by the number of leaves in the right subtree of node j^* in the dual tree T^*.

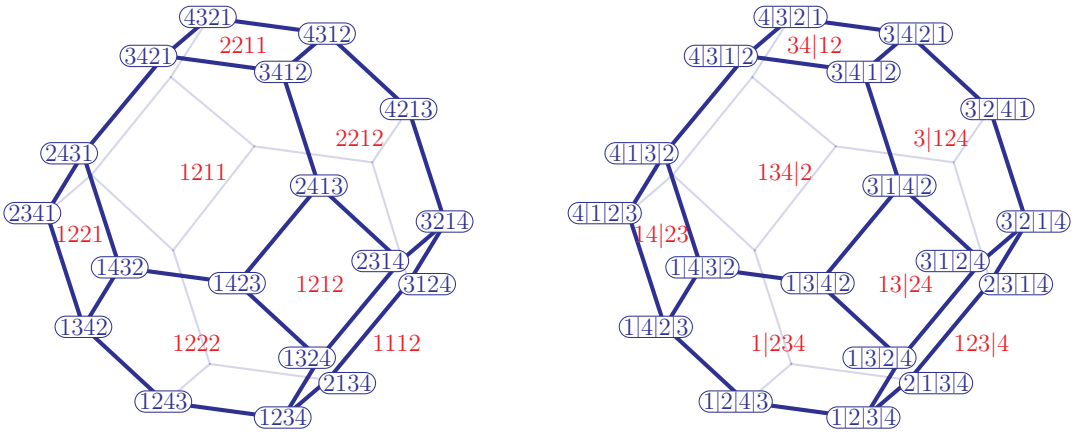

FIGURE 41. The 3-dimensional permutahedron $\mathsf{Perm}(3)$, with faces labeled by surjections (left) or ordered partitions (right).

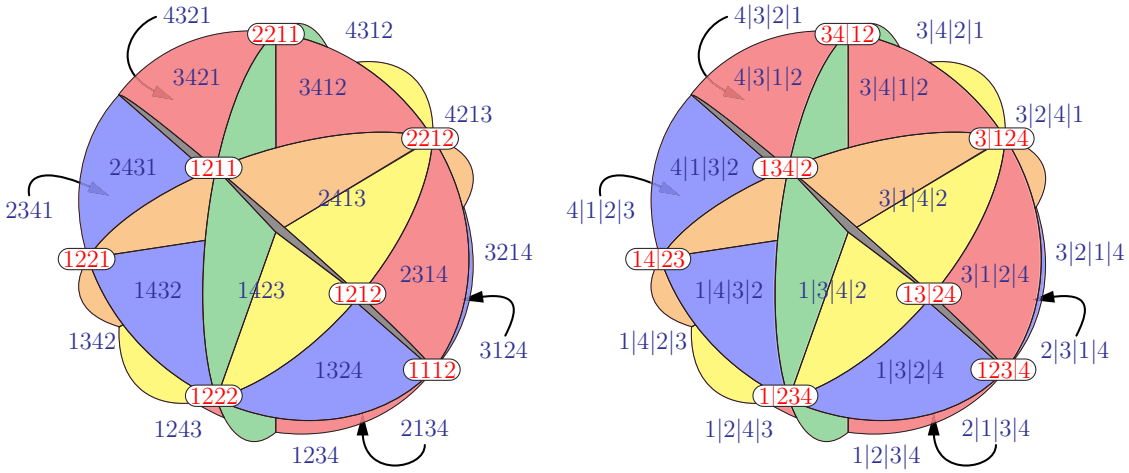

FIGURE 42. The 3-dimensional braid fan, with cones labeled by surjections (left) or ordered partitions (right).

For a diagonal δ of $\mathbf{P}$, we denote by $\mathsf{B}(\delta)$ the labels of the points of $\mathbf{P}$ below δ. We denote by $\mathbf{H}^{\geq}(\delta)$ the half-space $\mathbf{H}^{\geq}(\mathsf{B}(\delta))$ and by $\mathbf{H}^{=}(\delta)$ the hyperplane $\mathbf{H}^{=}(\mathsf{B}(\delta))$.

Finally, for a subset $R \subset [n+1]$, we denote by $\triangle_R := \operatorname{conv}\{\mathbf{e}_r \mid r \in R\}$ the face of the standard n-dimensional simplex $\triangle_{[n+1]}$.

Proposition 136 (Loday [Lod04])**.** *Let δ be either an internal diagonal or the upper boundary edge $[0, n+2]$ of $\mathbf{P}$, and let T be a triangulation of $\mathbf{P}$.*

(i) The point $\operatorname{Lod}(T)$ is contained in the half-space $\mathbf{H}^{\geq}(\delta)$.

(ii) The point $\operatorname{Lod}(T)$ lies on the hyperplane $\mathbf{H}^{=}(\delta)$ if and only if δ belongs to T.

Proof. For any $j \in [n+1]$, the coordinate $\operatorname{Lod}(T)_j$ is the product of the number of leaves in the left subtree by the number of leaves in the right subtree of node j^* in the dual tree T^*. We can also interpret it as the number of paths between two leaves of T^* whose maximum is reached at j^*.

Assume first that δ belongs to T. Consider a path π between two leaves of T^*. Then the maximum of π is below δ if and only if the two endpoints of π are below δ. Therefore,

$$\sum_{j \in \mathsf{B}(\delta)} \operatorname{Lod}(T)_j = \binom{|\mathsf{B}(\delta)|+1}{2}$$

since it counts precisely all paths between two leaves of T^* below δ.

Assume now that δ does not belong to T. We prove by induction on $|\mathsf{B}(\delta)|$ that $\mathrm{Lod}(T)$ lies in the half-space $\mathbf{H}^{\geq}(\delta)$ but not on the hyperplane $\mathbf{H}^{=}(\delta)$. Let uvw be any triangle of T which crosses δ and such that $v \in \mathsf{B}(\delta)$. Let δ_1 and δ_2 denote the two diagonals connecting the endpoints of δ to v. By induction hypothesis, we obtain

$$\begin{aligned}\sum_{j\in\mathsf{B}(\delta)} \mathrm{Lod}(T)_j &= \sum_{j\in\mathsf{B}(\delta_1)} \mathrm{Lod}(T)_j + \mathrm{Lod}(T)_v + \sum_{j\in\mathsf{B}(\delta_2)} \mathrm{Lod}(T)_j \\ &> \binom{|\mathsf{B}(\delta_1)|+1}{2} + \big(\mathsf{B}(\delta_1)+1\big)\big(\mathsf{B}(\delta_2)+1\big) + \binom{|\mathsf{B}(\delta_2)|+1}{2} \\ &= \binom{|\mathsf{B}(\delta)|+1}{2},\end{aligned}$$

since $|\mathsf{B}(\delta)| = |\mathsf{B}(\delta_1)| + |\mathsf{B}(\delta_2)| + 1$. □

Theorem 137 (Loday [Lod04])**.** *The following equivalent descriptions define an n-dimensional associahedron $\mathsf{Asso}(n)$:*

(i) the convex hull of the points $\mathrm{Lod}(T)$ for all triangulations T of $\mathbf{P}$,
(ii) the intersection of the hyperplane $\mathbb{H}$ with the half-spaces $\mathbf{H}^{\geq}(\delta)$ for all diagonals δ of $\mathbf{P}$,
(iii) the Minkowski sum of the faces $\triangle_I$ of the standard simplex, for I interval of $[n+1]$.

Proof. Consider the convex hull $\mathrm{conv}\{\mathrm{Lod}(T)\}$ of the points $\mathrm{Lod}(T)$, for all triangulations T of $\mathbf{P}$. For any internal diagonal δ of $\mathbf{P}$, the hyperplane $H^{=}(\delta)$ supports *a priori* a face of $\mathrm{conv}\{\mathrm{Lod}(T)\}$. For a triangulation T of $\mathbf{P}$ containing the diagonal δ, consider the triangulations $T_1, \dots, T_{n-1}$ of $\mathbf{P}$ obtained by flipping each internal diagonal $\delta_1, \dots, \delta_{n-1}$ of T distinct from δ. By Proposition 136, the point $\mathrm{Lod}(T_i)$ is contained in all $H^{=}(\delta_j)$ for $j \neq i$ but not in $H^{=}(\delta_i)$. Therefore, the points $\mathrm{Lod}(T), \mathrm{Lod}(T_1), \dots, \mathrm{Lod}(T_{n-1})$ are affine independent, and they are all contained in the hyperplane $H^{=}(\delta)$. The face supported by $H^{=}(\delta)$ is thus a facet of $\mathrm{conv}\{\mathrm{Lod}(T)\}$. It follows that each point $\mathrm{Lod}(T)$ is in fact a vertex of $\mathrm{conv}\{\mathrm{Lod}(T)\}$, as the intersection of at least n facets. The lattice of crossing-free sets of internal diagonals of $\mathbf{P}$ thus injects in the face lattice of $\mathrm{conv}\{\mathrm{Lod}(T)\}$, since the vertex-facet incidences are respected. Since both are face lattices of n-dimensional polytopes, they must be isomorphic. As a consequence, $\mathrm{conv}\{\mathrm{Lod}(T)\}$ is indeed an associahedron and its facet supporting hyperplanes are precisely the hyperplanes $H^{=}(\delta)$, for all internal diagonals δ of $\mathbf{P}$. This proves Parts (i) and (ii) of the statement.

For Part (iii), recall that the minimum of a linear functional $f : \mathbb{R}^{n+1} \to \mathbb{R}$ on a Minkowski sum is the sum of the minimums of f on each summand. For any $I, J \subseteq [n+1]$, The minimum of the functional $f_J(\mathbf{x}) = \sum_{j\in J} x_j$ on the face $\triangle_I$ of the standard simplex is 1 if $I \subseteq J$ and 0 otherwise. It follows that for an interval J, the minimum of f_J on the Minkowski sum $\sum_I \triangle_I$, for I non-empty interval of $[n+1]$, is the number of non-empty subintervals of J, thus $\binom{|J|+1}{2}$. We conclude that the Minkowski sum $\sum_I \triangle_I$ for I non-empty interval of $[n+1]$ coincides with the intersection of the hyperplane $\mathbb{H}$ with the half-spaces $\mathbf{H}^{\geq}(\delta)$ for all diagonals δ of $\mathbf{P}$. □

For example, Loday's 2-dimensional associahedron is represented in Figure 43 (right) and Loday's 3-dimensional associahedron is represented in Figure 40 (right).

5.5. **Normal fan.** The normal fan of Loday's associahedron $\mathsf{Asso}(n)$ is closely related to the braid arrangement discussed in Section 5.3. We need the following lemma, whose proof is immediate from the definition of the Loday vector.

Lemma 138. *Let T and $\widetilde{T}$ be two triangulations of $\mathbf{P}$ related by a flip, let $\delta \in T$ and $\tilde{\delta} \in \widetilde{T}$ be the two diagonals of $\mathbf{P}$ such that $T \smallsetminus \delta = \widetilde{T} \smallsetminus \tilde{\delta}$, and let $i < j \in [n+1]$ label the two intermediate vertices of the quadrilateral with diagonals δ and $\tilde{\delta}$. If δ^* is directed from i^* to j^*, then $\tilde{\delta}^*$ is directed from j^* to i^*, and the difference $\mathrm{Lod}(\widetilde{T}) - \mathrm{Lod}(T)$ is a positive multiple of $\mathbf{e}_i - \mathbf{e}_j$.*

Proof. A flip in the triangulation T is a rotation in its dual binary tree T^*. Any node k^* of T^* not incident to the rotated edge is preserved: it keeps the same children, and thus the coordinate $\mathrm{Lod}(T)_k$ is preserved. Since the sum of all coordinates is preserved, it follows that the vector $\mathrm{Lod}(\widetilde{T}) - \mathrm{Lod}(T)$ is a multiple of $\mathbf{e}_i - \mathbf{e}_j$. Finally, it is easy to check that $\mathrm{Lod}(\widetilde{T})_i - \mathrm{Lod}(T)_i > 0$

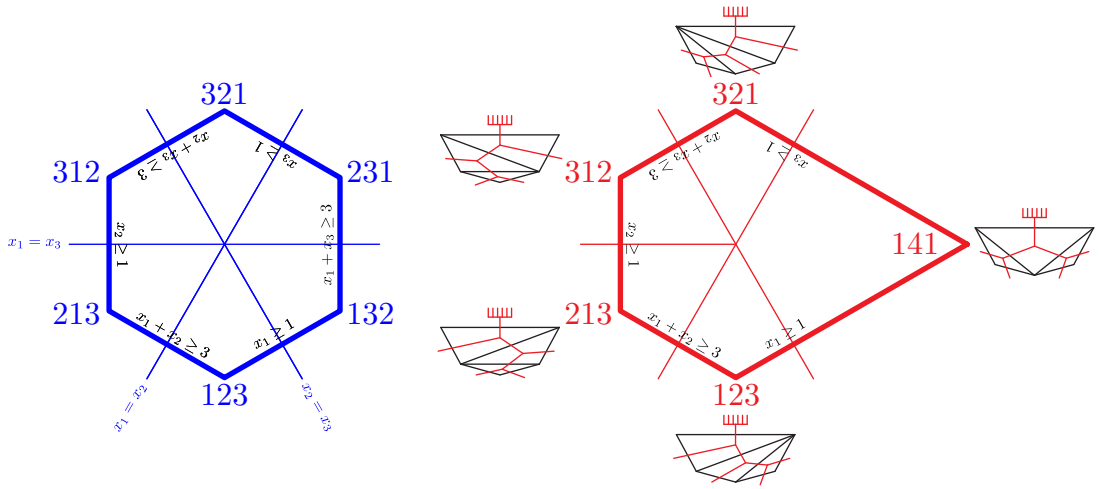

FIGURE 43. The 2-dimensional permutahedron Perm(2) (left) and Loday's associahedron Asso(2) (right).

since it is the product of the number of leaves in the left child of i by the number of leaves in the right child of j. □

Proposition 139. *For any triangulation T of $\mathbf{P}$, the cone $C(T)$ of the vertex $\mathrm{Lod}(T)$ of the associahedron $\mathsf{Asso}(n)$ is the incidence cone of the dual tree T^* while the normal cone $C^\diamond(T)$ of $\mathrm{Lod}(T)$ is the braid cone of the dual tree T^*, that is,*

$$C(T) = \mathrm{cone}\{\mathbf{e}_i - \mathbf{e}_j \mid i^*j^* \in T^*\} \qquad \text{and} \qquad C^\diamond(T) = \bigcap_{i^*j^* \in T^*} \{\mathbf{u} \in H \mid u_i \leq u_j\},$$

where $i^*j^* \in T^*$ means that i^*j^* is an oriented arc of T^*.

Proof. Lemma 138 ensures that $C(T) = \mathrm{cone}\{\mathbf{e}_i - \mathbf{e}_j \mid i^*j^* \in T^*\}$. It then follows by polarity that $C^\diamond(T) = \bigcap_{i^*j^* \in T^*} \{\mathbf{u} \in H \mid u_i \leq u_j\}$. □

Given a triangulation T of $\mathbf{P}$, its dual binary tree T^*, oriented towards its root, is an acyclic graph labeled by $[n+1]$ and its transitive closure defines a partial order $\prec_T$ on $[n+1]$. Remember that a *linear extension* of $\prec_T$ is a linear order $\prec_L$ such that $i \prec_T j$ implies $i \prec_L j$. Equivalently, it can be seen as a permutation σ of $[n+1]$ such that $i \prec_T j$ implies $\sigma(i) < \sigma(j)$.

Proposition 140. *For any triangulation T of $\mathbf{P}$, the normal cone $C^\diamond(T)$ in $\mathsf{Asso}(n)$ is the union of the normal cones $C^\diamond(\sigma)$ in $\mathsf{Perm}(n)$ of all linear extensions σ of the transitive closure of T^*.*

This proposition defines a surjection κ from the permutations of $[n+1]$ to the triangulations of $\mathbf{P}$, which sends a permutation σ of $[n+1]$ to the unique triangulation T of $\mathbf{P}$ such that $C^\diamond(T)$ contains $C^\diamond(\sigma)$. By Proposition 140, the fiber $\kappa^{-1}(T)$ of a triangulation T of $\mathbf{P}$ is the set of linear extensions of the dual tree T^*. The surjection κ can be expressed combinatorially either on triangulations or on binary trees as follows:

(1) Fix a permutation σ of $[n+1]$. For $i \in \{0, \dots, n+1\}$, define $\pi_i(\sigma)$ to be the x-monotone path in $\mathbf{P}$ joining the vertices 0 and $n+2$ and passing through the vertices of $[n+1] \setminus \sigma^{-1}([i])$, with the convention that $[0] = \varnothing$. The sequence of paths $\pi_0(\sigma), \pi_1(\sigma), \dots, \pi_{n+1}(\sigma)$ sweeps the polygon $\mathbf{P}$, starting from the lower hull of $\mathbf{P}$ and ending with the single edge $[0, n+2]$. The triangulation $\kappa(\sigma)$ associated to the permutation σ is the union of the paths $\pi_0(\sigma), \pi_1(\sigma), \dots, \pi_{n+1}(\sigma)$.
(2) The dual binary tree of $\kappa(\sigma)$ can also be obtained by successive insertion in binary search tree of the values of the permutation σ, read from right to left.

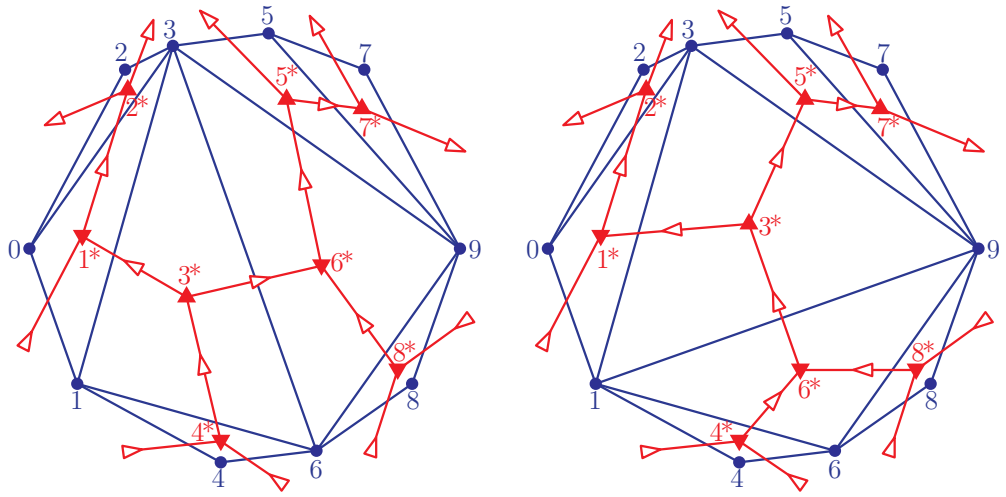

FIGURE 44. Two triangulations T^{ex} and $\widetilde{T}^{\mathrm{ex}}$ of the polygon $\mathbf{P}^{\mathrm{ex}}$ and their spines.

Exercice 141. For a triangulation T of $\mathbf{P}$ and a permutation σ of $[n+1]$, prove that the following assertions are equivalent:

(i) The dual tree T^* is a directed path (with blossoms) labeled by σ.
(ii) The transitive closure $\prec_T$ of the dual tree T^* is the linear order defined by σ.
(iii) The fiber of T with respect to the map κ is the singleton $\kappa^{-1}(T) = \{\sigma\}$.
(iv) The vertex $\mathrm{Lod}(T)$ of $\mathsf{Asso}(n)$ coincides with the vertex $(\sigma(1), \dots, \sigma(n+1))$ of $\mathsf{Perm}(n)$.
(v) The cone $C(T)$ of $\mathsf{Asso}(n)$ coincides with the cone $C(\sigma)$ of $\mathsf{Perm}(n)$.
(vi) The normal cone $C^\diamond(T)$ of $\mathsf{Asso}(n)$ coincides with the normal cone $C^\diamond(\sigma)$ of $\mathsf{Perm}(n)$.

5.6. **Further realizations of the associahedron.** In [HL07], Hohlweg and Lange extend Loday's construction of the associahedron to obtain many relevant realizations of the associahedron, which all fulfill the properties discussed in the last two sections.

Consider a convex $(n+3)$-gon $\mathbf{P}$ with no two points on the same vertical line. We label the vertices of $\mathbf{P}$ from 0 to $n+2$ by increasing x-coordinate. We call *up* and *down points* the vertices of the upper and lower hull of $\mathbf{P}$ respectively, and we call *up labels* $U \subseteq [n+1]$ and *down labels* $D \subseteq [n+1]$ their respective label sets. See Example 142 and Figure 44.

Let δ be a diagonal of $\mathbf{P}$ (internal or not). We denote by $\mathsf{A}(\delta)$ the set of labels $j \in [n+1]$ of the points above the line supporting δ where we include the endpoints of δ if they are down, and exclude them if they are up. Similarly, we denote by $\mathsf{B}(\delta)$ the set of labels $j \in [n+1]$ of the points below the line supporting δ where we include the endpoints of δ if they are up, and exclude them if they are down.

Let T be a triangulation of $\mathbf{P}$. The *spine* of T is its oriented and labeled dual tree T^*, with

- an internal node j^* for each triangle ijk of T where $i < j < k$,
- an arc δ^* for each internal diagonal δ of T, oriented from the triangle below δ to the triangle above δ, and
- an outgoing (resp. incoming) blossom δ^* for each top (resp. bottom) boundary edge δ of $\mathbf{P}$.

The *up nodes* and *down nodes* are the internal nodes of T^* labeled by up and down labels respectively. Observe that an up node has indegree one and outdegree two, while a down node has indegree two and outdegree one. See Example 142 and Figure 44.

Example 142. To illustrate these definitions, consider the decagon $\mathbf{P}^{\mathrm{ex}}$ with $U^{\mathrm{ex}} = \{2, 3, 5, 7\}$ and $D^{\mathrm{ex}} = \{1, 4, 6, 8\}$ represented in Figure 44. We have *e.g.* $\mathsf{A}(\mathbf{27}) = \{3, 5\}$ and $\mathsf{B}(\mathbf{28}) = \{1, 2, 4, 6\}$. Two triangulations T^{ex} (left) and $\widetilde{T}^{\mathrm{ex}}$ (right) of $\mathbf{P}^{\mathrm{ex}}$ and their spines are represented.The vertices of the polygon are represented with dots •, while the up and down nodes of the spines are respectively represented with up and down triangles ▲ and ▼.

As in Loday's construction, we can use these spines to construct a relevant realization $\mathsf{Asso}(\mathbf{P})$ of the associahedron. We describe the vertices of $\mathsf{Asso}(\mathbf{P})$, which correspond to triangulations of $\mathbf{P}$. Consider a triangulation T of $\mathbf{P}$ with spine T^*. Let Π be the set of all *undirected maximal paths* in T^*, that is, undirected paths connecting two blossoms of T^*. Note that a path $\pi \in \Pi$ is not directed although each edge of π is oriented (as an arc of the spine T^*). For any $j \in [n+1]$, we denote by $\mathsf{R}(j)$ the set of paths of Π whose edge orientation is reversed at node j^*. In other words, if j is a down (resp. up) label, then $\mathsf{R}(j)$ is the set of paths of Π which use the two incoming (resp. outgoing) arcs of j^*. It follows that $|\mathsf{R}(j)|$ is the product of the number of blossoms in the two incoming (resp. outgoing) subtrees of j^* in T^*. Associate to the triangulation T of $\mathbf{P}$ the point $\mathrm{HL}(T) \in \mathbb{R}^{n+1}$ with coordinates

$$x_j(T) := \begin{cases} |\mathsf{R}(j)| & \text{if } j \in D, \\ n+2-|\mathsf{R}(j)| & \text{if } j \in U. \end{cases}$$

The following statement, as well as results similar to the properties of Loday's associahedron described in the previous section, are proved in [HL07]. See also [LP13] for a presentation using spines.

Theorem 143 (Hohlweg and Lange [HL07])**.** *The following equivalent descriptions define an associahedron* $\mathsf{Asso}(\mathbf{P})$*:*

(i) the convex hull of the points $\mathrm{HL}(T)$ *for all triangulations* T *of* $\mathbf{P}$*,*

(ii) the intersection of the hyperplane $\mathbb{H}$ *with the half-spaces* $\mathbf{H}^{\geq}(\delta)$ *for all diagonals* δ *of* $\mathbf{P}$*.*

For example, Figure 40 illustrates two 3-dimensional associahedra of Hohlweg and Lange.

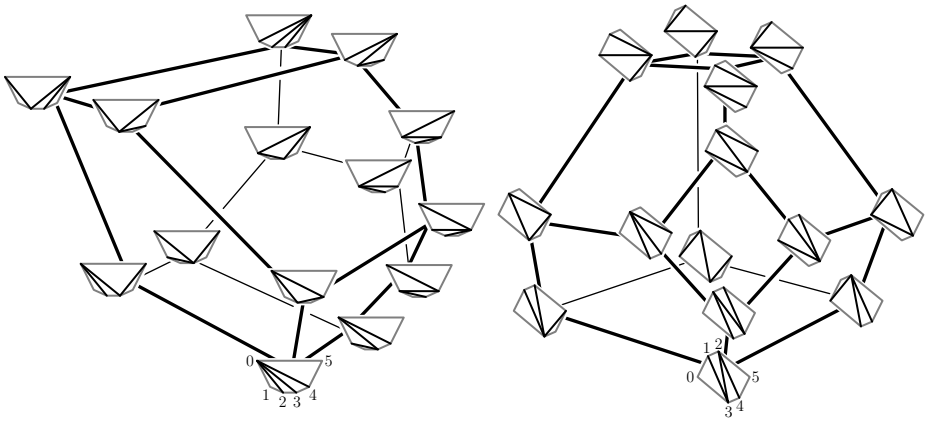

FIGURE 45. Two Hohlweg-Lange's associahedra. The left one is Loday's associahedron.

6. Further flip graphs and brick polytopes

The last section of these lecture notes explores a more specific topic. We first interpret two relevant graphs of flips on geometric graphs (on pseudotriangulations and on multitriangulations) as flip graphs on pseudoline arrangements with contact points supported by a given sorting network. We then construct the brick polytope of a sorting network $\mathcal{N}$. Under certain conditions on the network $\mathcal{N}$, this polytope realizes the flip graph on pseudoline arrangements supported by $\mathcal{N}$. This section is based on [PP12] and [PS12].

6.1. Pseudotriangulations.

In this section, $\mathbf{P}$ denotes a planar point set in general position with i interior points and b boundary points, and $n = i + b$. A set of edges with endpoints in $\mathbf{P}$ is *pointed* if all edges incident to a given point of $\mathbf{P}$ are contained in an open half-space (thus, they form a pointed cone). Equivalently, each point of $\mathbf{P}$ is incident to an angle greater than π.

Definition 144. A *pseudotriangle* is a simple polygon Δ with precisely three convex corners, connected by three concave chains. A line is said to be *tangent* to Δ if:

(i) either it passes through a corner of Δ and separates its two incident edges;
(ii) or it passes through a concave vertex of Δ and does not separate its two incident edges.

Figure 46 (left) shows three pseudotriangles with their pairwise common tangents.

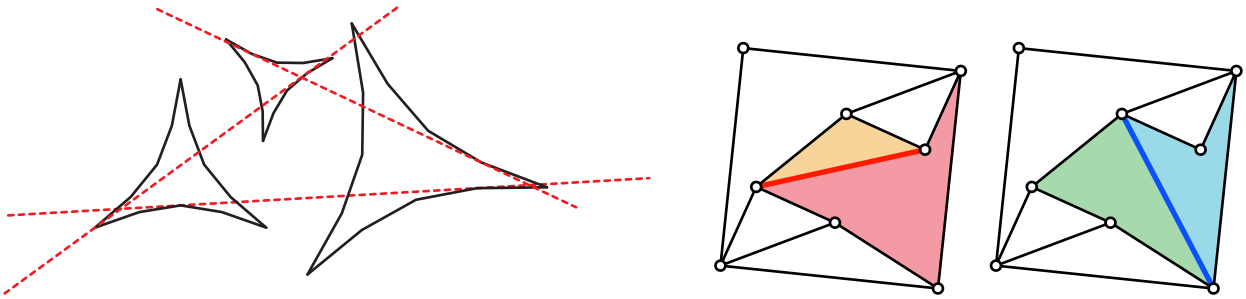

Figure 46. Three pseudotriangles and their common tangents (left), and two pseudotriangulations of a point set connected by a flip (right).

Definition 145. A *pseudotriangulation* of the point set $\mathbf{P}$ is a set T of edges between points of $\mathbf{P}$ which satisfies the following four equivalent properties:

(i) T decomposes the convex hull of $\mathbf{P}$ into $n-2$ non-overlapping pseudotriangles;
(ii) T decomposes the convex hull of $\mathbf{P}$ into non-overlapping pseudotriangles and has minimal cardinality for this property;
(iii) T is a crossing-free and pointed set of $2n-3$ edges;
(iv) T is a maximal crossing-free and pointed set of edges.

Examples of pseudotriangulations are illustrated on Figure 46 (right).

Proof. We need to prove that these four properties are indeed equivalent. Assume that T decomposes the convex hull of $\mathbf{P}$ into non-overlapping polygons. Let f denote the number of polygons of T and let p denote the number of pointed vertices of $\mathbf{P}$ in T. For $\mathbf{p} \in \mathbf{P}$, let $\deg(\mathbf{p})$ and $\operatorname{cor}(\mathbf{p})$ denote the degree and the number of convex corners incident to $\mathbf{p}$. Note that $\operatorname{cor}(\mathbf{p}) = \deg(\mathbf{p}) - 1$ if $\mathbf{p}$ is pointed in T, and $\operatorname{cor}(\mathbf{p}) = \deg(\mathbf{P})$ otherwise. We have

$$2e = \sum_{\mathbf{p}\in\mathbf{P}} \deg(\mathbf{p}) = \sum_{\mathbf{p}\in\mathbf{P}} \operatorname{cor}(\mathbf{p}) + p \geq 3f + p.$$

By application of Euler's formula, we therefore get that

$$e \leq 3n - 3 - p \qquad \text{and} \qquad f \leq 2n - 2 - p,$$

with equality if all bounded faces of T are pseudotriangles. These inequalities ensure that (i) $\Longrightarrow$ (ii) and (iii) $\Longrightarrow$ (iv).

We claim moreover that there exists a crossing-free pointed set of $2n-3$ edges that decomposes the convex hull of $\mathbf{P}$ into $n-2$ non-overlapping pseudotriangles. It can be constructed by induction on $|\mathbf{P}|$: delete temporarily a point $\mathbf{p}$ of the convex hull of $\mathbf{P}$, construct a suitable set of edges for $\mathbf{P} \setminus \mathbf{p}$, and add the point $\mathbf{P}$ together with the two tangents from $\mathbf{p}$ to the convex hull of $\mathbf{P} \setminus \mathbf{p}$. Together with the above inequalities, this ensures that (ii) $\Longrightarrow$ (i) and (iv) $\Longrightarrow$ (iii).

Finally, we obtain that (i) $\Longleftrightarrow$ (iii) by one more application of the previous inequalities. □

Proposition 146. *For any internal edge e in a pseudotriangulation T of $\mathbf{P}$, there is a unique pseudotriangulation T' of $\mathbf{P}$ distinct from T and containing $T \setminus e$. Moreover, the edge e' in $T' \setminus T$ can be equivalently characterized as follows:*

- *e' is the unique common tangent between the two pseudotriangles of T incident to e;*
- *the two pseudotriangles of T incident to e form a pseudoquadrangle; the edges e and e' are the only interior edges on the two geodesics between pairs of opposite angles of this pseudoquadrangle.*

The transformation from T to T' is called a flip. *See Figure 46 (right) for an illustration.*

Proof. By edge count, $T \setminus e$ decomposes the convex hull of $\mathbf{P}$ into $n-4$ pseudotriangles and a pseudoquadrangle, obtained by glueing the two pseudotriangles of T incident to e. There is only two ways to pseudotriangulate a pseudoquadrangle: include either of the two geodesics between opposite corners of the pseudoquadrangle. □

Exercice 147. Flip all the internal edges of the pseudotriangulation of Figure 46.

Exercice 148. Show that the flip graph on pseudotriangulations of a planar point set $\mathbf{P}$ with i interior points and b boundary points is $(2i+b-3)$-regular and connected.

It turns out that the flip graph on pseudotriangulations of $\mathbf{P}$ is polytopal. The proof, based on rigidity properties of pseudotriangulations and the polyhedron of expansive motions of a point set, is omitted in these notes.

Theorem 149 (Rote, Santos and Streinu [RSS03])**.** *For any planar point set $\mathbf{P}$ with i interior points and b boundary points, there exists an $(2i+b-3)$-dimensional polytope, called* pseudotriangulation polytope*, whose vertices correspond to pseudotriangulations of $\mathbf{P}$ and whose edges correspond to flips between them. More generally, the boundary complex of the polar of this polytope is isomorphic to the simplicial complex of crossing-free and pointed sets of internal edges of $\mathbf{P}$.*

Two examples of pseudotriangulation polytopes are represented in Figure 47. We refer to the survey article of Rote, Santos and Streinu [RSS08] for more details and references on pseudotriangulations and their applications.

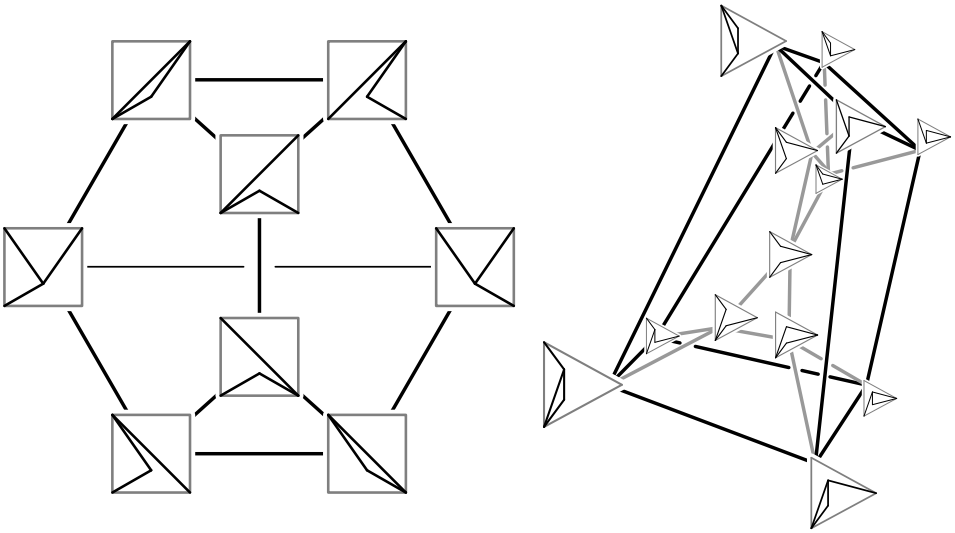

FIGURE 47. Two pseudotriangulation polytopes [RSS03]. The rightmost picture represents the Schlegel diagram of a 4-dimensional polytope (see [Zie95, Chap. 5]).

6.2. **Multitriangulations.** Let $\mathbf{P}$ denote the vertex set of a convex n-gon. We are interested in the following generalization of triangulations, introduced by Capoyleas and Pach [CP92] in the context of extremal theory for geometric graphs. See Figure 48.

Definition 150. For $\ell \in \mathbb{N}$, an *ℓ-crossing* is a set of ℓ mutually crossing edges of $\mathbf{P}$. A *k-triangulation* of the n-gon is a maximal $(k+1)$-crossing-free set of edges of $\mathbf{P}$.

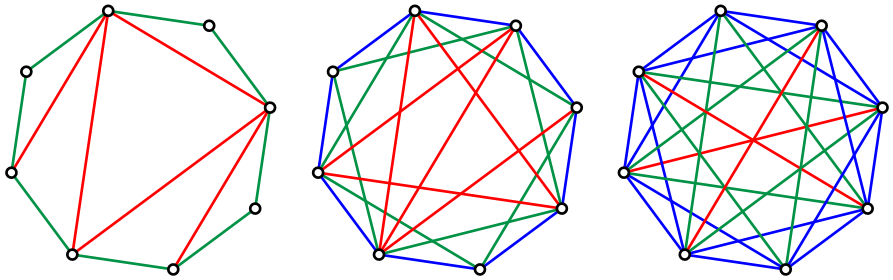

FIGURE 48. 1-, 2-, and 3-triangulations of the octogon. Relevant, boundary, and irrelevant edges are in red, green and blue respectively.

Observe that an edge can be involved in a $(k+1)$-crossing only if there remain at least k vertices on each side. Such an edge is called *k-relevant*. An edge with exactly (resp. strictly less than) $k-1$ vertices on one side is a *k-boundary* edge (resp. a *k-irrelevant* edge). By maximality, every k-triangulation consists of all the nk k-irrelevant plus k-boundary edges and some k-relevant edges of $\mathbf{P}$.

Exercice 151. What are the 1-triangulations of the n-gon $\mathbf{P}$? Describe the k-triangulations of the n-gon for $n \leq 2k+3$.

In [PS09], the triangles and their bisectors are generalized for k-triangulations as follows.

Definition 152. A *k-star* is a star polygon of type $\{2k+1/k\}$, that is, a set of edges of the form $\{s_j s_{j+k} \mid j \in \mathbb{Z}_{2k+1}\}$, where $s_0, s_1, \dots, s_{2k}$ are cyclically ordered around the unit circle. A *(strict) bisector* of a k-star is a (strict) bisector of one of its angles $s_{j-k}s_j s_{j+k}$.

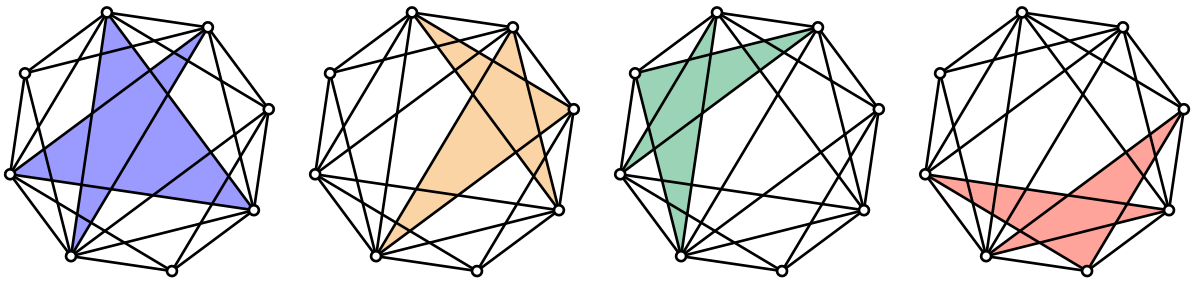

FIGURE 49. The four 2-stars of the 2-triangulation of Figure 48.

As for $k=1$, where triangles provide a powerful tool to study triangulations, k-stars are useful to understand k-triangulations. In the following theorem, we point out five properties of stars proved in [PS09]. Figures 49 and 50 illustrate these results on the 2-triangulation of Figure 48.

Theorem 153 (Pilaud and Santos [PS09])**.** *Let T be a k-triangulation of the n-gon. Then*

(i) T contains exactly $n-2k$ k-stars and $k(n-2k-1)$ k-relevant edges.
(ii) Each edge of T belongs to zero, one, or two k-stars, depending on whether it is k-irrelevant, k-boundary, or k-relevant.
(iii) Every pair of k-stars of T has a unique common strict bisector.

(iv) Flipping any k-relevant edge e of T into the common strict bisector f of the two k-stars containing e produces a new k-triangulation $T\triangle\{e,f\}$ of the n-gon. T and $T\triangle\{e,f\}$ are the only two k-triangulations of the n-gon containing $T\setminus\{e\}$.

(v) The flip graph on k-triangulations of the n-gon is connected and regular of degree $k(n-2k-1)$.

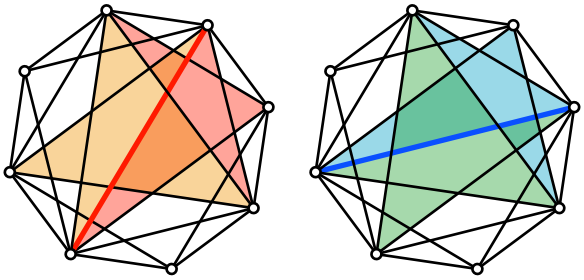

FIGURE 50. Two 2-triangulations of the octogon connected by a flip.

Exercice 154. Prove (i) assuming (ii) in Theorem 153. (Hint: double counting).

6.3. **Pseudoline arrangements in the Möbius strip.** Let $\mathcal{M} := \mathbb{R}^2/(x,y) \simeq (x+\pi,-y)$ denote the *Möbius strip* (without boundary). A *pseudoline* is the image λ under the canonical projection $\pi : \mathbb{R}^2 \to \mathcal{M}$ of the graph $\{(x,f(x)) \mid x \in \mathbb{R}\}$ of a continuous and *π-antiperiodic* function $f : \mathbb{R} \to \mathbb{R}$ (that is, which satisfies $f(x+\pi) = -f(x)$ for all $x \in \mathbb{R}$). When we consider two pseudolines, we always assume that they have a finite number of intersection points. Thus, these intersection points can only be either *crossing points* or *contact points*. Any two pseudolines always have an odd number of crossing points (in particular, at least one). A *pseudoline arrangement with contact points* is a finite set Λ of pseudolines such that any two of them have exactly one crossing point and possibly some contact points. See Figure 51.

We are only interested in *simple* arrangements, that is, where no three pseudolines meet in a common point. The *support* of Λ is the union of its pseudolines. Observe that Λ is completely determined by its support together with its set of contact points. The *first level* of Λ is the external hull of the support of Λ, *i.e.* the boundary of the external face of the complement of the support of Λ. We define inductively the *kth level* of Λ as the external hull of the support of Λ minus its first $k-1$ levels.

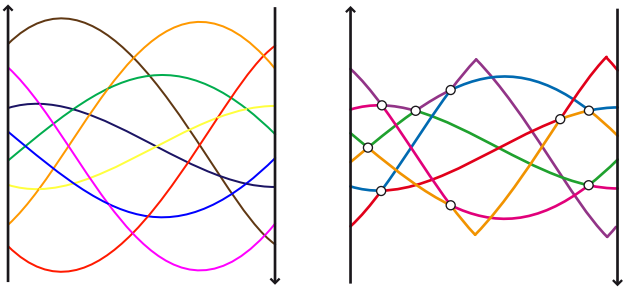

FIGURE 51. Two pseudoline arrangements in the Möbius strip, one without and one with contact points (white circles)

Remark 155. The usual definition of pseudoline arrangements does not allow contact points. Here, they play a crucial role since we are interested in all pseudoline arrangements which share a common support, and which only differ by their sets of contact points. To simplify the exposition, we omit to specify that we work with pseudoline arrangements *with contact points*. Pseudoline arrangements are also classically defined on the projective plane rather than the Möbius strip. The projective plane is obtained from the Möbius strip by adding a point at infinity.

There is a natural flip operation on pseudoline arrangements with contact points: exchange a contact between two pseudolines λ and μ with the unique crossing between λ and μ. The flip graph on pseudoline arrangements with the same support is connected and c-regular, where c denotes the number of contact points (or equivalently, the number of vertices of the support minus $\binom{n}{2}$).

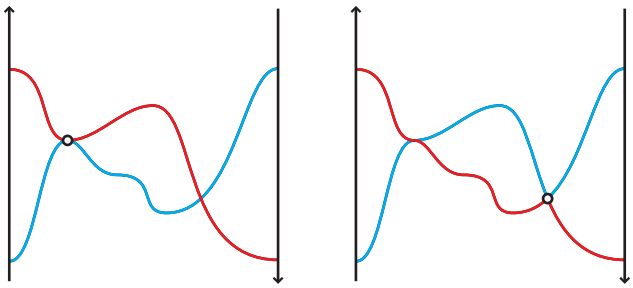

FIGURE 52. A flip in a pseudoline arrangement on the Möbius strip.

In fact, the flip graph on pseudotriangulations supported by $\mathcal{S}$ is the facet-ridge graph of the simplicial complex $\Delta(\mathcal{S})$ whose ground set is the set of vertices of the support $\mathcal{S}$ and whose facets are the sets of contact points of pseudoline arrangements supported by $\mathcal{S}$. This simplicial complex is pure of dimension c and it is known to be a sphere. An interesting open question is to determine whether this sphere is polytopal:

Question 156. Is the simplicial complex $\Delta(\mathcal{S})$ the boundary complex of a simplicial polytope? (This question is still open in general.)

6.4. **Duality.** In this section, we connect triangulations, pseudotriangulations, multitriangulations and flip graphs on pseudoline arrangements. This connection appeared in [PP12]. We start with the classical point-line duality in the plane.

Point-line duality — To a given oriented line in the Euclidean plane, we associate its angle $\theta \in \mathbb{R}/2\pi\mathbb{Z}$ with the horizontal axis and its algebraic distance $d \in \mathbb{R}$ to the origin (*i.e.* the value of $\langle(-v,u)|\cdot\rangle$ on the line, where (u,v) is its unitary direction vector). Since the same line oriented in the other direction gives an angle $\theta+\pi$ and a distance $-d$, this parametrization naturally associates a point of the Möbius strip $\mathcal{M} := \mathbb{R}^2/(\theta,d) \sim (\theta+\pi,-d)$ to each line of the Euclidean plane. In other words, the line space of the Euclidean plane is (isomorphic to) the Möbius strip.

Via this parametrization, the set of lines passing through a point $\mathbf{p}$ forms a pseudoline $\mathbf{p}^*$. The pseudolines $\mathbf{p}^*$ and $\mathbf{q}^*$ dual to two distinct points $\mathbf{p}$ and $\mathbf{q}$ have a unique crossing point, namely the line $(\mathbf{pq})$. Thus, for a finite point set $\mathbf{P}$ in the Euclidean plane, the set $\mathbf{P}^* := \{\mathbf{p}^* \mid \mathbf{p} \in \mathbf{P}\}$ is a pseudoline arrangement without contact points (see Figure 53). Note that we always assume general position in the remaining of the text to avoid triple point intersections.

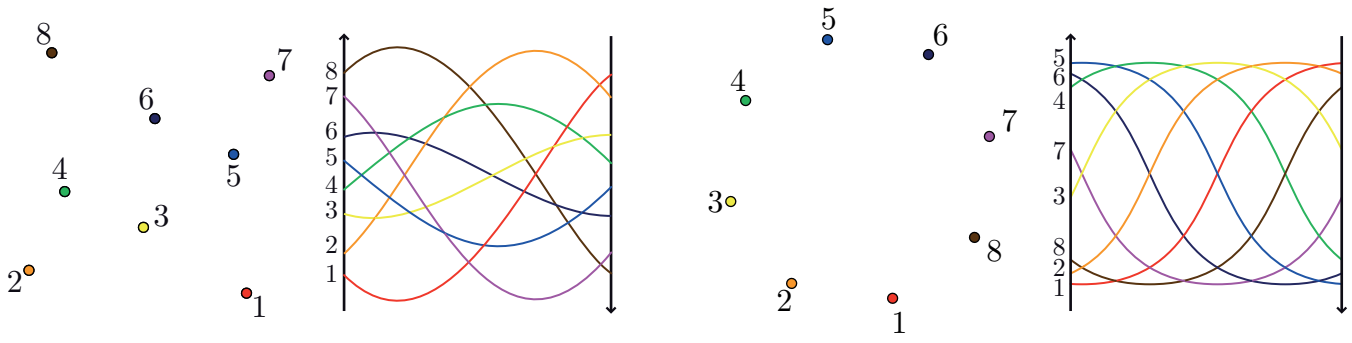

FIGURE 53. Two point sets and their dual pseudoline arrangements.

Exercice 157. Describe the successive orders of the pseudolines from bottom to top directly in the primal. These sequence of permutations is called the *allowable sequence* of the point set.

Exercice 158. Compare the k-edges of a point set $\mathbf{P}$ and the kth level in the dual pseudoline arrangement $\mathbf{P}^*$.

Triangulations — Let T be a triangulation of the convex polygon $\mathbf{P}$. Then:

(i) the set Δ^* of all bisectors to a triangle Δ of T is a pseudoline;
(ii) the dual pseudolines Δ_1^*, Δ_2^* of any two triangles Δ_1, Δ_2 of T have a unique crossing point (the unique common bisector to Δ_1 and Δ_2) and possibly a contact point (when Δ_1 and Δ_2 share a common edge);
(iii) the set $T^* := \{\Delta^* \mid \Delta \text{ triangle of } T\}$ is a pseudoline arrangement (with contact points);
(iv) T^* is supported by $\mathbf{P}^*$ minus its first level (see Figure 54 (right)).

The next statement asserts that there is in fact a duality between triangulations of the convex polygon $\mathbf{P}$ and pseudoline arrangements supported by the dual arrangement $\mathbf{P}^*$ minus its first level.

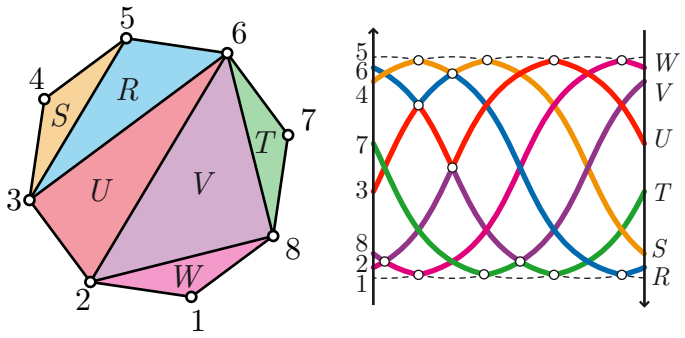

FIGURE 54. A triangulation T of a convex polygon $\mathbf{P}$ and the dual arrangement T^* of T, drawn on the dual arrangement $\mathbf{P}^*$ of P of Figure 53 (right). Each pseudoline of T^* corresponds to a triangle of T; each contact point in T^* corresponds to an edge in T; each crossing point in T^* corresponds to a common bisector in T.

Proposition 159. *Let $\mathbf{P}$ be the vertex set of a convex polygon, and $\mathbf{P}^{*1}$ denote the support of its dual pseudoline arrangement minus its first level. Then:*

(1) The dual arrangement $T^* := \{\Delta^* \mid \Delta$ triangle of $T\}$ of a triangulation T of $\mathbf{P}$ is supported by $\mathbf{P}^{*1}$.
(2) The primal set of edges $E := \{[\mathbf{p}, \mathbf{q}] \mid \mathbf{p}, \mathbf{q} \in \mathbf{P},\ \mathbf{p}^* \wedge \mathbf{q}^*$ contact point of $\Lambda\}$ of a pseudoline arrangement Λ supported by $\mathbf{P}^{*1}$ is a triangulation of $\mathbf{P}$.

The first point was discussed above. We give two independent proofs for the second point:

Proof 1. Observe first that

$$|E| = \binom{|\mathbf{P}^*|}{2} - \binom{|\Lambda|}{2} = \binom{|\mathbf{P}|}{2} - \binom{|\mathbf{P}| - 2}{2} = 2|\mathbf{P}| - 3.$$

Let $\mathbf{p}, \mathbf{q}, \mathbf{r}, \mathbf{s}$ be four points of $\mathbf{P}$ in cyclic order. Let $\mathbf{t}$ be the intersection of $[\mathbf{p}, \mathbf{r}]$ and $[\mathbf{q}, \mathbf{s}]$. We use the pseudoline $\mathbf{t}^*$ as a *witness* to prove that $[\mathbf{p}, \mathbf{r}]$ and $[\mathbf{q}, \mathbf{s}]$ cannot both be in E. For this, we count crossings of $\mathbf{t}^*$ with $\mathbf{P}^*$ and Λ respectively:

(i) Since the point $\mathbf{t}$ is not in $\mathbf{P}$, the set $\mathbf{P}^* \cup \{\mathbf{t}^*\} = (\mathbf{P} \cup \{\mathbf{t}\})^*$ is a (non-simple) pseudoline arrangement, and $\mathbf{t}^*$ crosses $\mathbf{P}^*$ exactly $|\mathbf{P}|$ times.
(ii) Since $\mathbf{t}^*$ is a pseudoline, it crosses each pseudoline of Λ at least once. Thus, it crosses Λ at least $|\Lambda| = |\mathbf{P}| - 2$ times.
(iii) For each of the points $\mathbf{p}^* \wedge \mathbf{r}^*$ and $\mathbf{q}^* \wedge \mathbf{s}^*$, replacing the crossing point by a contact point removes two crossings with $\mathbf{t}^*$.

Thus, $[\mathbf{p}, \mathbf{r}]$ and $[\mathbf{q}, \mathbf{s}]$ cannot both be in E, and E is crossing-free. □

Proof 2. A flip on a triangulation T of $\mathbf{P}$ translates in the dual to a flip on the dual pseudoline arrangement T^*. Thus, the flip graph on triangulations of $\mathbf{P}$ is a subgraph of the flip graph on pseudoline arrangements supported by $\mathbf{P}^{*1}$. Since both are connected and regular of degree $|\mathbf{P}|-3$, they coincide. In particular, any pseudoline arrangement supported by $\mathbf{P}^{*1}$ is the dual of a pseudotriangulation of $\mathbf{P}$. □

Pseudotriangulations — Let T be a pseudotriangulation of a point set $\mathbf{P}$ in general position. Then:

(i) the set Δ^* of all tangents to a pseudotriangle Δ of T is a pseudoline;
(ii) the dual pseudolines Δ_1^*, Δ_2^* of any two pseudotriangles Δ_1, Δ_2 of T have a unique crossing point (the unique common tangent to Δ_1 and Δ_2) and possibly a contact point (when Δ_1 and Δ_2 share a common edge);
(iii) the set $T^* := \{\Delta^* \mid \Delta \text{ pseudotriangle of } T\}$ is a pseudoline arrangement (with contact points);
(iv) T^* is supported by $\mathbf{P}^*$ minus its first level (see Figure 55 (right)).

The next statement asserts that there is in fact a duality between pseudotriangulations of a point set $\mathbf{P}$ and pseudoline arrangements supported by the dual arrangement $\mathbf{P}^*$ minus its first level.

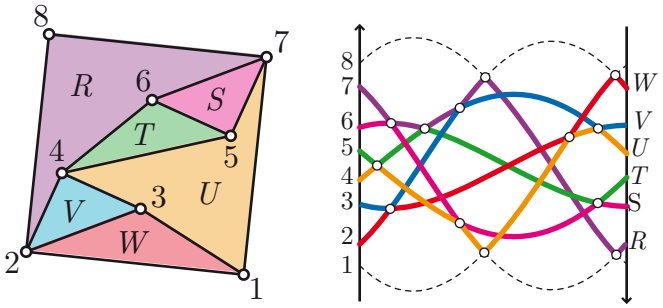

FIGURE 55. A pseudotriangulation T of the point set $\mathbf{P}$ of Figure 53 (left), and the dual arrangement T^* of T, drawn on the dual arrangement $\mathbf{P}^*$ of P of Figure 53 (right). Each pseudoline of T^* corresponds to a pseudotriangle of T; each contact point in T^* corresponds to an edge in T; each crossing point in T^* corresponds to a common tangent in T.

Proposition 160. *Let $\mathbf{P}$ be a finite point set in general position in the plane, and $\mathbf{P}^{*1}$ denote the support of its dual pseudoline arrangement minus its first level. Then:*

(1) The dual arrangement $T^* := \{\Delta^* \mid \Delta$ pseudotriangle of $T\}$ of a pseudotriangulation T of $\mathbf{P}$ is supported by $\mathbf{P}^{*1}$.
(2) The primal set of edges $E := \{[\mathbf{p}, \mathbf{q}] \mid \mathbf{p}, \mathbf{q} \in \mathbf{P},\ \mathbf{p}^* \wedge \mathbf{q}^*$ contact point of $\Lambda\}$ of a pseudoline arrangement Λ supported by $\mathbf{P}^{*1}$ is a pseudotriangulation of $\mathbf{P}$.

Exercice 161. Adapt the two proofs of Proposition 159 to the case of pseudotriangulations.

Multitriangulations — Let T be a k-triangulation of a convex polygon $\mathbf{P}$. Then:

(i) the set S^* of all bisectors to a k-star S of T is a pseudoline;
(ii) the dual pseudolines S_1^*, S_2^* of any two k-stars S_1, S_2 of T have a unique crossing point (the unique common bisector to S_1 and S_2) and possibly some contact points (when S_1 and S_2 share some common edges);
(iii) the set $T^* := \{S^* \mid S$ k-star of $T\}$ is a pseudoline arrangement (with contact points);
(iv) T^* is supported by $\mathbf{P}^*$ minus its first k levels (see Figure 56 (right)).

The next statement asserts that there is in fact a duality between multitriangulations of the convex polygon $\mathbf{P}$ and pseudoline arrangements supported by the dual arrangement $\mathbf{P}^*$ minus its first k levels.

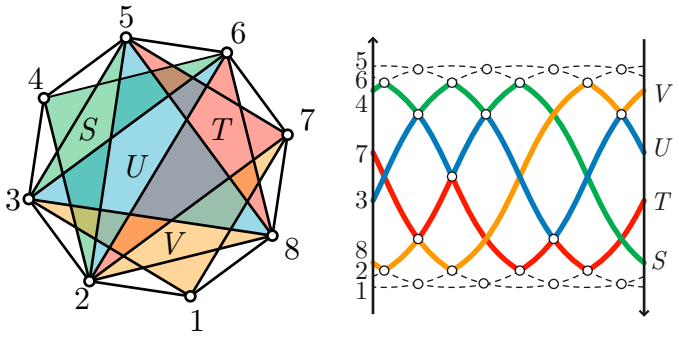

FIGURE 56. A 2-triangulation T of the octogon and the dual arrangement T^* of T, drawn on the dual arrangement $\mathbf{P}^*$ of P. Each pseudoline of T^* corresponds to a 2-star of T; each contact point in T^* corresponds to an edge in T; each crossing point in T^* corresponds to a common bisector in T.

Proposition 162. *Let $\mathbf{P}$ be the vertex set of a convex polygon, and $\mathbf{P}^{*k}$ denote the support of its dual pseudoline arrangement minus its first k levels. Then:*

(1) The dual arrangement $T^* := \{S^* \mid S \text{ } k\text{-star of } T\}$ of a k-triangulation T of $\mathbf{P}$ is supported by $\mathbf{P}^{*k}$.

(2) The primal set of edges $E := \{[\mathbf{p}, \mathbf{q}] \mid \mathbf{p}, \mathbf{q} \in \mathbf{P},\ \mathbf{p}^* \wedge \mathbf{q}^* \text{ contact point of } \Lambda\}$ of a pseudoline arrangement Λ supported by $\mathbf{P}^{*k}$ is a k-triangulation of $\mathbf{P}$.

Exercice 163. Adapt the two proofs of Proposition 159 to the case of multitriangulations.

6.5. **Pseudoline arrangements on (sorting) networks.** A *network* $\mathcal{N}$ is a set of n horizontal lines (called *levels*, and labeled from bottom to top), together with m vertical segments (called *commutators*, and labeled from left to right) joining two consecutive horizontal lines, such that no two commutators have a common endpoint — see *e.g.* Figure 57. The *bricks* of $\mathcal{N}$ are its $m-n+1$ bounded cells. We say that a network is *alternating* when the commutators adjacent to each intermediate level are alternatively located above and below it.

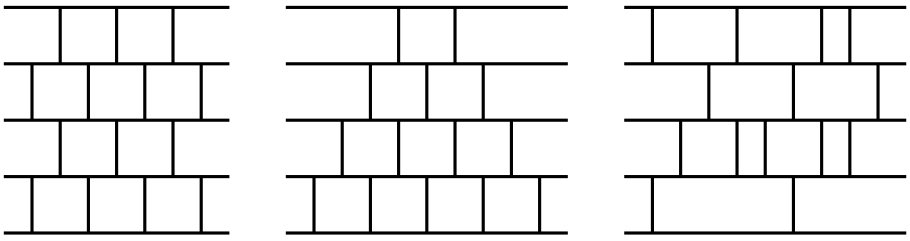

FIGURE 57. Three networks with 5 levels, 14 commutators and 10 bricks. The first two are alternating, while the last one is not.

A *pseudoline* is an abscissa monotone path on the network $\mathcal{N}$. A *contact* between two pseudolines is a commutator whose endpoints are contained one in each pseudoline, and a *crossing* between two pseudolines is a commutator traversed by both pseudolines. A *pseudoline arrangement* (with contacts) is a set of n pseudolines supported by $\mathcal{N}$ such that any two of them have precisely one crossing, some (perhaps zero) contacts, and no other intersection — see Figure 58. Observe that in a pseudoline arrangement, the pseudoline which starts at level ℓ necessarily ends at level $n+1-\ell$ and goes up at $n-\ell$ crossings and down at $\ell-1$ crossings. We denote by $\mathrm{Arr}(\mathcal{N})$ the set of pseudoline arrangements supported by $\mathcal{N}$. We say that a network is *sorting* when it supports at least one pseudoline arrangement.

The flip operation on pseudoline arrangements on $\mathcal{N}$ is defined as in the previous section. An example is illustrated on Figure 58.

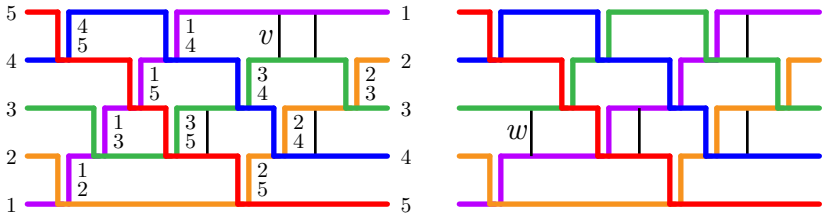

FIGURE 58. Two pseudoline arrangements, both supported by the rightmost network $\mathcal{N}$ of Figure 57, and related by a flip. The left one is the greedy pseudoline arrangement $\Gamma(\mathcal{N})$, whose flips are all decreasing. It is obtained by sorting the permutation $(5, 4, 3, 2, 1)$ according to the network $\mathcal{N}$.

6.6. **Brick polytopes.** We denote by $\Delta(\mathcal{N})$ the simplicial complex whose ground set is the set of commutators of $\mathcal{N}$ and whose facets are the sets of contacts of the pseudoline arrangements supported by $\mathcal{N}$. It is known that this simplicial complex is a sphere, and a natural open question is to determine whether it is the boundary complex of a polytope. This section answers this question for a special family of sorting networks. The construction presented here appeared in [PS12].

Definition 164. Let $\mathcal{N}$ be a sorting network with n levels. The *brick vector* of a pseudoline arrangement Λ supported by $\mathcal{N}$ is the vector $\omega(\Lambda) \in \mathbb{R}^n$ whose ith coordinate is the number of bricks of $\mathcal{N}$ located below the ith pseudoline of Λ (the one which starts at level i and finishes at level $n+1-i$). The *brick polytope* $\Omega(\mathcal{N}) \subset \mathbb{R}^n$ of the sorting network $\mathcal{N}$ is the convex hull of the brick vectors of all pseudoline arrangements supported by $\mathcal{N}$:

$$\Omega(\mathcal{N}) := \operatorname{conv}\{\omega(\Lambda) \mid \Lambda \in \operatorname{Arr}(\mathcal{N})\} \subset \mathbb{R}^n.$$

We start by observing that the brick polytope is not full dimensional. Define the *depth* of a brick of $\mathcal{N}$ to be the number of levels located above it, and let $D(\mathcal{N})$ be the sum of the depths of all the bricks of $\mathcal{N}$. Since any pseudoline arrangement supported by $\mathcal{N}$ covers each brick as many times as its depth, all brick vectors are contained in the following hyperplane:

Lemma 165. *The brick polytope $\Omega(\mathcal{N})$ is contained in the hyperplane of equation $\sum_{i=1}^n x_i = D(\mathcal{N})$.*

Exercice 166. Describe the action of the vertical and horizontal reflections of the network on the brick polytope.

Exercice 167. Describe the simplicial complex $\Delta(\mathcal{N})$ and the brick polytope $\Omega(\mathcal{N})$ for the network $\mathcal{N}$ with 2 levels and m commutators.

Definition 168. The *contact graph* of a pseudoline arrangement Λ is the directed multigraph $\Lambda^\#$ with a node for each pseudoline of Λ and an arc for each contact of Λ oriented from the pseudoline passing above the contact to the pseudoline passing below it.

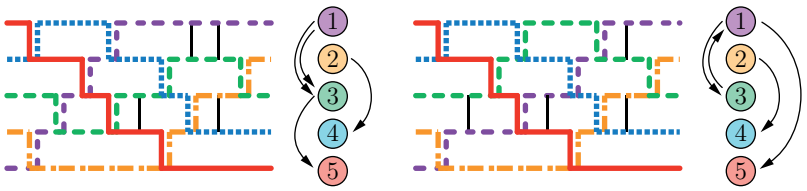

FIGURE 59. The contact graphs of the pseudoline arrangements of Figure 58. The connected components are preserved by the flip.

Lemma 169. *The contact graphs of all pseudoline arrangements supported by $\mathcal{N}$ have the same connected components.*

We call a sorting network *reducible* (resp. *irreducible*) when the contact graphs of the pseudoline arrangements it supports are disconnected (resp. connected). We call irreducible components of a sorting network $\mathcal{N}$ the networks obtained by restriction of $\mathcal{N}$ to the connected components of the contact graphs of the pseudoline arrangements supported by $\mathcal{N}$. We restrict to irreducible sorting networks due to the following statement.

Proposition 170. *Let $\mathcal{N}$ be a sorting network whose irreducible components are $\mathcal{N}_1, \dots, \mathcal{N}_p$. Then the simplicial complex $\Delta(\mathcal{N})$ is isomorphic to the join of the simplicial complexes $\Delta(\mathcal{N}_1), \dots, \Delta(\mathcal{N}_p)$ and the brick polytope $\Omega(\mathcal{N})$ is a translate of the product of the brick polytopes $\Omega(\mathcal{N}_1), \dots, \Omega(\mathcal{N}_p)$.*

Among irreducible sorting networks, the following networks have the fewest commutators:

Definition 171. An irreducible sorting network $\mathcal{N}$ is *minimal* if it satisfies the following equivalent conditions:

(i) $\mathcal{N}$ has n levels and $m = \binom{n}{2} + n - 1$ commutators.
(ii) The contact graph of a pseudoline arrangement supported by $\mathcal{N}$ is a tree.
(iii) The contact graphs of all pseudoline arrangements supported by $\mathcal{N}$ are trees.

For example, the networks of Figure 57 all have 5 levels and 14 commutators. The rightmost is reducible, but the other two are minimal. To be convinced, draw the greedy pseudoline arrangement on these networks, and check that its contact graph is connected.

We use the contact graph $\Lambda^\#$ to describe the cone of the brick polytope $\Omega(\mathcal{N})$ at the brick vector $\omega(\Lambda)$:

Theorem 172. *The cone of the brick polytope $\Omega(\mathcal{N})$ at the brick vector $\omega(\Lambda)$ is precisely the incidence cone $C(\Lambda^\#)$ of the contact graph $\Lambda^\#$ of Λ:*

$$\operatorname{cone}\{\omega(\Lambda') - \omega(\Lambda) \mid \Lambda' \in \operatorname{Arr}(\mathcal{N})\} = \operatorname{cone}\left\{\mathbf{e}_j - \mathbf{e}_i \;\middle|\; (i,j) \in \Lambda^\#\right\}.$$

Proof. Assume that Λ' is obtained from Λ by flipping a contact from its i^{th} pseudoline to its j^{th} pseudoline. Then the difference $\omega(\Lambda') - \omega(\Lambda)$ is a positive multiple of $\mathbf{e}_j - \mathbf{e}_i$. This immediately implies that the incidence cone $C(\Lambda^\#)$ is included in the cone of $\Omega(\mathcal{N})$ at $\omega(\Lambda)$.

Reciprocally, we have to prove that any facet F of the cone $C(\Lambda^\#)$ is also a facet of the brick polytope $\Omega(\mathcal{N})$. According to Lemma 98 (iv), there exists a minimal directed cut from a source set U to a sink set V (which partition the vertices of $\Lambda^\#$) such that $\mathbb{1}_V := \sum_{v \in V} \mathbf{e}_v$ is a normal vector of F. We denote by γ the commutators of $\mathcal{N}$ which correspond to the arcs of $\Lambda^\#$ between U and V. We claim that for any pseudoline arrangement Λ' supported by $\mathcal{N}$, the scalar product $\langle \mathbb{1}_V | \omega(\Lambda') \rangle$ equals $\langle \mathbb{1}_V | \omega(\Lambda) \rangle$ when γ is a subset of the contacts of Λ', and is strictly bigger than $\langle \mathbb{1}_V | \omega(\Lambda) \rangle$ otherwise.

Remember first that the set of all pseudoline arrangements supported by $\mathcal{N}$ and whose set of contacts contains γ is connected by flips. Since a flip between two such pseudoline arrangements necessarily involves either two pseudolines of U or two pseudolines of V, the corresponding incidence vector is orthogonal to $\mathbb{1}_V$. Thus, the scalar product $\langle \mathbb{1}_V | \omega(\Lambda') \rangle$ is constant on all pseudoline arrangements whose set of contacts contains γ.

Reciprocally, we consider a pseudoline arrangement Λ' supported by $\mathcal{N}$ which minimizes the scalar product $\langle \mathbb{1}_V | \omega(\Lambda') \rangle$. There is clearly no arc from U to V in $\Lambda'^\#$, otherwise flipping the corresponding contact in Λ' would decrease the value of $\langle \mathbb{1}_V | \omega(\Lambda') \rangle$. We next prove that we can join Λ to Λ' by flips involving two pseudolines of U or two pseudolines of V. As a first step, we show that we can transform Λ and Λ' into pseudoline arrangements $\hat{\Lambda}$ and $\hat{\Lambda}'$ in which the first pseudoline coincide, using only flips involving two pseudolines of U or two pseudolines of V. We can then conclude by induction on the number of levels of $\mathcal{N}$.

Assume first that the first pseudoline (the one which starts at level 1 and ends at level n) of Λ and Λ' is in U. We sweep this pseudoline from left to right in Λ. If there is a contact above and incident to it, the above pseudoline must be in U. Otherwise we would have an arc between V and U in $\Lambda^\#$. Consequently, we are allowed to flip this contact. By doing this again and again we obtain a pseudoline arrangement $\hat{\Lambda}$ whose first pseudoline starts at the bottom leftmost point and goes up whenever possible until getting to the topmost level. Since this procedures only relies

on the absence of arc from V to U in $\Lambda^\#$, we can proceed identically on Λ' to get a pseudoline arrangement $\hat{\Lambda}'$ with the same first pseudoline. Finally, if the first pseudoline of Λ and Λ' is in V, then we can argue similarly but sweeping the pseudoline from right to left. □

Corollary 173. *The brick polytope of an irreducible sorting network with n levels has dimension $n-1$. In general, the brick polytope of a sorting network with n levels and p irreducible components has dimension $n-p$.*

Proof. Direct application of Lemma 98 (i), Proposition 170, and Theorem 172. □

Corollary 174. *The brick vector $\omega(\Lambda)$ is a vertex of the brick polytope $\Omega(\mathcal{N})$ if and only if the contact graph $\Lambda^\#$ of Λ is acyclic.*

Proof. Direct application of Lemma 98 (ii) and Theorem 172. □

Theorem 175. *For any minimal irreducible sorting network $\mathcal{N}$, the simplicial complex $\Delta(\mathcal{N})$ is the boundary complex of the polar of the brick polytope $\Omega(\mathcal{N})$. In particular, the graph of $\Omega(\mathcal{N})$ is the flip graph $G(\mathcal{N})$.*

Proof. Since the contact graphs of the pseudoline arrangements supported by $\mathcal{N}$ are trees (see Definition 171), the brick polytope $\Omega(\mathcal{N})$ has one vertex for each pseudoline arrangement supported by $\mathcal{N}$. Moreover, the 1-skeleton of the brick polytope is the flip graph on these pseudoline arrangements. We conclude using for example Theorem 90. □

In the following two examples, we denote by $\mathcal{B}_\ell$ the bubble sorting network with ℓ levels.

Example 176 (Triangulations)**.** The brick polytope of the sorting network $\mathcal{B}^1_{n+2}$ (obtained from $\mathcal{B}_{n+2}$ by erasing the top and bottom levels), is a translate of Loday's associahedron.

Example 177 (Multitriangulations)**.** The f-vectors of the brick polytopes $\Omega(\mathcal{B}^2_7)$, $\Omega(\mathcal{B}^2_8)$, $\Omega(\mathcal{B}^2_9)$ and $\Omega(\mathcal{B}^2_{10})$ are $(6,6)$, $(22,33,13)$, $(92,185,118,25)$ and $(420,1062,945,346,45)$ respectively. We have represented $\Omega(\mathcal{B}^2_8)$ and $\Omega(\mathcal{B}^2_9)$ in Figures 60 and 61. The polytopes $\Omega(\mathcal{B}^2_7)$ and $\Omega(\mathcal{B}^2_8)$ are simple while the polytope $\Omega(\mathcal{B}^2_9)$ has two non-simple vertices (which are contained in the projection facet of the Schlegel diagram on the right of Figure 61) and the polytope $\Omega(\mathcal{B}^2_{10})$ has 24 non-simple vertices.

Exercice 178. Consider a reduced network $\mathcal{N}$ with n levels and $\binom{n}{2}$ commutators. For any distinct $i,j \in [n]$, we labeled by $\{i,j\}$ the commutator of $\mathcal{N}$ where the ith and jth pseudolines of the unique pseudoline arrangement supported by $\mathcal{N}$ cross. Let Γ be a connected graph on $[n]$. We define $\mathcal{Z}(\Gamma)$ to be the network with n levels and $m = \binom{n}{2} + |\Gamma|$ commutators obtained from $\mathcal{N}$ by duplicating the commutators labeled by the edges of Γ. We say that $\mathcal{Z}(\Gamma)$ is a *duplicated network*.

(1) Describe the pseudoline arrangements supported by $\mathcal{Z}(\Gamma)$ as well as their contact graphs
(2) What is the simplicial complex $\Delta(\mathcal{Z}(\Gamma))$ and the flip graph on pseudoline arrangements supported by $\mathcal{Z}(\Gamma)$?
(3) Describe the brick polytope of $\mathcal{Z}(\Gamma)$.
(4) When does the brick polytope $\Omega(\mathcal{Z}(\Gamma))$ realize the simplicial complex $\Delta(\mathcal{Z}(\Gamma))$?

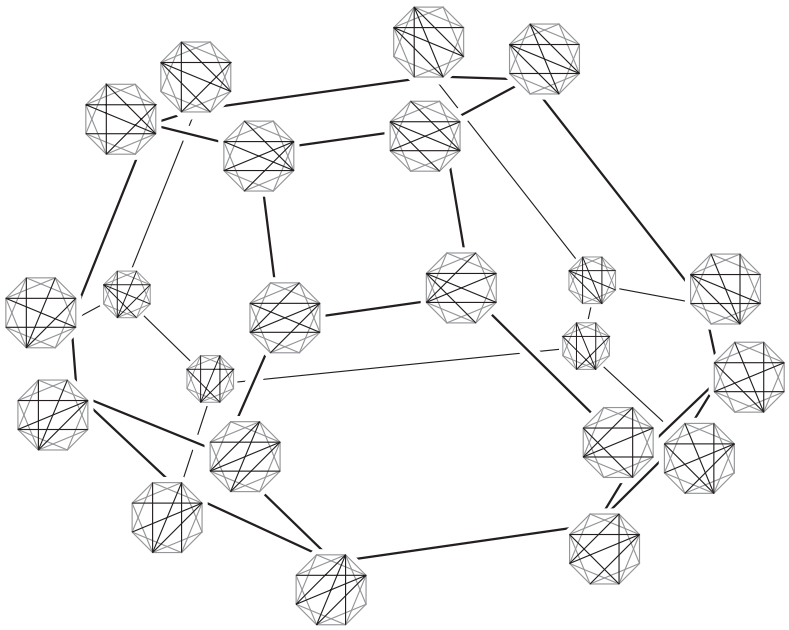

FIGURE 60. The 3-dimensional polytope $\Omega(\mathcal{B}_8^2)$. Only 22 of the 84 2-triangulations of the octagon appear as vertices.

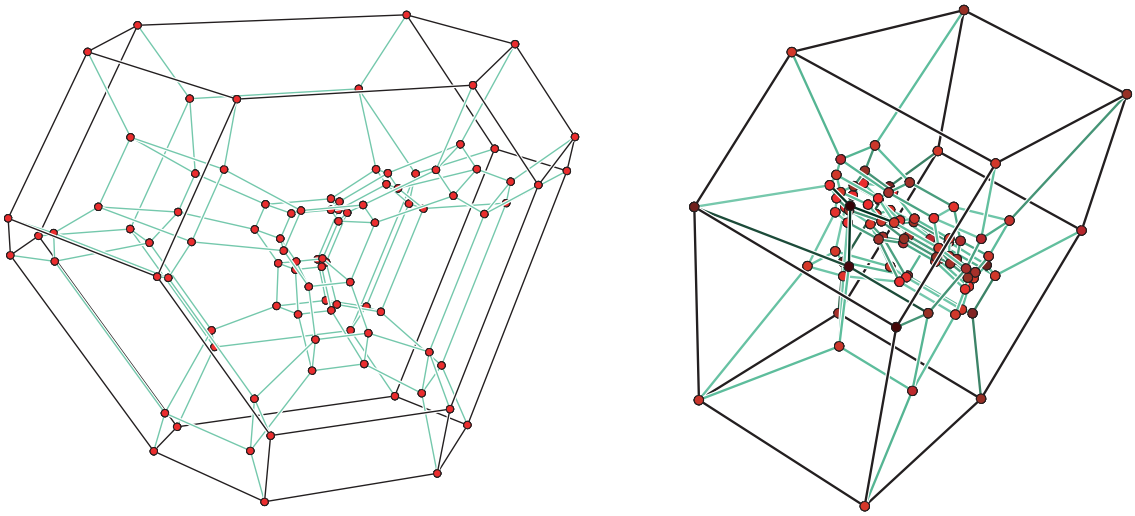

FIGURE 61. Two Schlegel diagrams of the 4-dimensional polytope $\Omega(\mathcal{B}_9^2)$. On the second one, the two leftmost vertices of the projection facet are non-simple vertices.

References

[Bal61] Michel L. Balinski. On the graph structure of convex polyhedra in n-space. *Pacific J. Math.*, 11:431–434, 1961.

[Bar67] David Barnette. A necessary condition for d-polyhedrality. *Pacific J. Math.*, 23:435–440, 1967.

[Bar73] David Barnette. A proof of the lower bound conjecture for convex polytopes. *Pacific J. Math.*, 46:349–354, 1973.

[Bar74] D. Barnette. An upper bound for the diameter of a polytope. *Discrete Math.*, 10:9–13, 1974.

[BDL+11] Prosenjit Bose, Luc Devroye, Maarten Löffler, Jack Snoeyink, and Vishal Verma. Almost all Delaunay triangulations have stretch factor greater than $\pi/2$. *Comput. Geom.*, 44(2):121–127, 2011.

[BGHP10] Nicolas Bonichon, Cyril Gavoille, Nicolas Hanusse, and Ljubomir Perković. Plane spanners of maximum degree six. In *Automata, languages and programming. Part I*, volume 6198 of *Lecture Notes in Comput. Sci.*, pages 19–30. Springer, Berlin, 2010.

[BML87] Roswitha Blind and Peter Mani-Levitska. Puzzles and polytope isomorphisms. *Aequationes Math.*, 34(2-3):287–297, 1987.

[Che89] L. Paul Chew. There are planar graphs almost as good as the complete graph. *J. Comput. System Sci.*, 39(2):205–219, 1989. Computational geometry.

[CP92] Vasilis Capoyleas and János Pach. A Turán-type theorem on chords of a convex polygon. *J. Combin. Theory Ser. B*, 56(1):9–15, 1992.

[DBTV99] G. Di Battista, R. Tamassia, and L. Vismara. Output-sensitive reporting of disjoint paths. *Algorithmica*, 23(4):302–340, 1999. Second Annual International Computing and Combinatorics Conference (Hong Kong, 1996).

[dFdMR94] Hubert de Fraysseix, Patrice Ossona de Mendez, and Pierre Rosenstiehl. On triangle contact graphs. *Combin. Probab. Comput.*, 3(2):233–246, 1994.

[DRS10] Jesus A. De Loera, Jörg Rambau, and Francisco Santos. *Triangulations: Structures for Algorithms and Applications*, volume 25 of *Algorithms and Computation in Mathematics*. Springer Verlag, 2010.

[EG73] P. Erdős and R. K. Guy. Crossing number problems. *Amer. Math. Monthly*, 80:52–58, 1973.

[Fel04] Stefan Felsner. *Geometric graphs and arrangements*. Advanced Lectures in Mathematics. Friedr. Vieweg & Sohn, Wiesbaden, 2004. Some chapters from combinatorial geometry.

[Fri09] Eric J. Friedman. Finding a simple polytope from its graph in polynomial time. *Discrete Comput. Geom.*, 41(2):249–256, 2009.

[GKZ94] Israel M. Gel′fand, Mikhail M. Kapranov, and Andrei V. Zelevinsky. *Discriminants, resultants, and multidimensional determinants*. Mathematics: Theory & Applications. Birkhäuser Boston Inc., Boston, MA, 1994.

[Guy60] Richard K. Guy. A combinatorial problem. *Nabla*, 7:68–72, 1960.

[HL07] Christophe Hohlweg and Carsten Lange. Realizations of the associahedron and cyclohedron. *Discrete Comput. Geom.*, 37(4):517–543, 2007.

[Hum90] James E. Humphreys. *Reflection groups and Coxeter groups*, volume 29 of *Cambridge Studies in Advanced Mathematics*. Cambridge University Press, Cambridge, 1990.

[Kal88] Gil Kalai. A simple way to tell a simple polytope from its graph. *J. Combin. Theory Ser. A*, 49(2):381–383, 1988.

[Kan96] Goos Kant. Drawing planar graphs using the canonical ordering. *Algorithmica*, 16(1):4–32, 1996.

[KG92] J. Mark Keil and Carl A. Gutwin. Classes of graphs which approximate the complete Euclidean graph. *Discrete Comput. Geom.*, 7(1):13–28, 1992.

[KK92] G. Kalai and D. Kleitman. A quasi-polynomial bound for the diameter of graphs of polyhedra. *Bull. Amer. Math. Soc. (N.S.)*, 26(2):315–316, 1992.

[Kle64] Victor Klee. A property of d-polyhedral graphs. *J. Math. Mech.*, 13:1039–1042, 1964.

[Kur30] Kazimierz Kuratowski. Sur le problème des courbes gauches en topologie. *Fund. Math.*, 15:271–283, 1930.

[Lar70] D. Larman. Paths of polytopes. *Proc. London Math. Soc. (3)*, 20:161–178, 1970.

[Lod04] Jean-Louis Loday. Realization of the Stasheff polytope. *Arch. Math. (Basel)*, 83(3):267–278, 2004.

[LP13] Carsten Lange and Vincent Pilaud. Using spines to revisit a construction of the associahedron. Preprint, `arXiv:1307.4391`, 2013.

[LVWW04] László Lovász, Katalin Vesztergombi, Uli Wagner, and Emo Welzl. Convex quadrilaterals and k-sets. In *Towards a theory of geometric graphs*, volume 342 of *Contemp. Math.*, pages 139–148. Amer. Math. Soc., Providence, RI, 2004.

[Mat02] Jiří Matoušek. *Lectures on discrete geometry*, volume 212 of *Graduate Texts in Mathematics*. Springer-Verlag, New York, 2002.

[McM70] Peter McMullen. The maximum numbers of faces of a convex polytope. *Mathematika*, 17:179–184, 1970.

[Mil02] Ezra Miller. Planar graphs as minimal resolutions of trivariate monomial ideals. *Doc. Math.*, 7:43–90, 2002.

[Pou14] Lionel Pournin. The diameter of associahedra. *Adv. in Math.*, 259:13–42, 2014.

[PP12] Vincent Pilaud and Michel Pocchiola. Multitriangulations, pseudotriangulations and primitive sorting networks. *Discrete Comput. Geom.*, 48(1):142–191, 2012.

[PS09] Vincent Pilaud and Francisco Santos. Multitriangulations as complexes of star polygons. *Discrete Comput. Geom.*, 41(2):284–317, 2009.

[PS12] Vincent Pilaud and Francisco Santos. The brick polytope of a sorting network. *European J. Combin.*, 33(4):632–662, 2012.

[PT97] János Pach and Géza Tóth. Graphs drawn with few crossings per edge. *Combinatorica*, 17(3):427–439, 1997.

[RG96] Jürgen Richter-Gebert. *Realization spaces of polytopes*, volume 1643 of *Lecture Notes in Mathematics*. Springer-Verlag, Berlin, 1996.

[RSS03] Günter Rote, Francisco Santos, and Ileana Streinu. Expansive motions and the polytope of pointed pseudo-triangulations. In *Discrete and computational geometry*, volume 25 of *Algorithms Combin.*, pages 699–736. Springer, Berlin, 2003.

[RSS08] Günter Rote, Francisco Santos, and Ileana Streinu. Pseudo-triangulations — a survey. In *Surveys on discrete and computational geometry*, volume 453 of *Contemp. Math.*, pages 343–410. Amer. Math. Soc., Providence, RI, 2008.

[RSST97] Neil Robertson, Daniel Sanders, Paul Seymour, and Robin Thomas. The four-colour theorem. *J. Combin. Theory Ser. B*, 70(1):2–44, 1997.

[San00] Francisco Santos. A point set whose space of triangulations is disconnected. *J. Amer. Math. Soc.*, 13(3):611–637 (electronic), 2000.

[San12] F. Santos. A counter-example to the Hirsch conjecture. *Ann. of Math. (2)*, 176:383–412, 2012.

[Sch89] Walter Schnyder. Planar graphs and poset dimension. *Order*, 5(4):323–343, 1989.

[ST83] Endre Szemerédi and William T. Trotter, Jr. Extremal problems in discrete geometry. *Combinatorica*, 3(3-4):381–392, 1983.

[Sta63] Jim Stasheff. Homotopy associativity of H-spaces I, II. *Trans. Amer. Math. Soc.*, 108(2):293–312, 1963.

[Sta12] Richard P. Stanley. *Enumerative combinatorics. Volume 1*, volume 49 of *Cambridge Studies in Advanced Mathematics*. Cambridge University Press, Cambridge, second edition, 2012.

[Ste22] Ernst Steinitz. Polyeder und Raumeinteilungen. In *Encyclopädie der mathematischen Wissenschaften, Band 3 (Geometrie), Teil 3AB12*, pages 1–139. 1922.

[Szé97] László A. Székely. Crossing numbers and hard Erdős problems in discrete geometry. *Combin. Probab. Comput.*, 6(3):353–358, 1997.

[Whi32] Hassler Whitney. Non-separable and planar graphs. *Trans. Amer. Math. Soc.*, 34(2):339–362, 1932.

[Xia13] Ge Xia. The stretch factor of the Delaunay triangulation is less than 1.998. *SIAM J. Comput.*, 42(4):1620–1659, 2013.

[Zie95] Günter M. Ziegler. *Lectures on polytopes*, volume 152 of *Graduate Texts in Mathematics*. Springer-Verlag, New York, 1995.

CNRS & LIX, École Polytechnique, Palaiseau
Email address: vincent.pilaud@lix.polytechnique.fr
URL: http://www.lix.polytechnique.fr/~pilaud/